

**AC SYSTEM STABILITY ANALYSIS AND ASSESSMENT FOR
SHIPBOARD POWER SYSTEMS**

A Dissertation

by

LI QI

Submitted to the Office of Graduate Studies of
Texas A&M University
in partial fulfillment of the requirements for the degree of
DOCTOR OF PHILOSOPHY

December 2004

Major Subject: Electrical Engineering

**AC SYSTEM STABILITY ANALYSIS AND ASSESSMENT FOR
SHIPBOARD POWER SYSTEMS**

A Dissertation

by

LI QI

Submitted to Texas A&M University
in partial fulfillment of the requirements
for the degree of

DOCTOR OF PHILOSOPHY

Approved as to style and content by:

Karen L. Butler-Purry
(Chair of Committee)

Mehrdad Ehsani
(Member)

Alexander G. Parlos
(Member)

Karan L. Watson
(Member)

Chanan Singh
(Head of Department)

December 2004

Major Subject: Electrical Engineering

ABSTRACT

AC System Stability Analysis and Assessment for Shipboard Power Systems.

(December 2004)

Li Qi, B.E., Xi'an Jiaotong University;

M.Sc., Zhejiang University

Chair of Advisory Committee: Dr. Karen L. Butler-Purry

The electric power systems in U.S. Navy ships supply energy to sophisticated systems for weapons, communications, navigation and operation. The reliability and survivability of a Shipboard Power System (SPS) are critical to the mission of a Navy ship, especially under battle conditions. When a weapon hits the ship in the event of battle, it can cause severe damage to the electrical systems on the ship. Researchers in the Power System Automation Laboratory (PSAL) at Texas A&M University have developed methods for performing reconfiguration of SPS before or after a weapon hit to reduce the damage to SPS. Reconfiguration operations change the topology of an SPS. When a system is stressed, these topology changes and induced dynamics of equipment due to reconfiguration might cause voltage instability, such as progressive voltage decreases or voltage oscillations. SPS stability thus should be assessed to ensure the stable operation of a system during reconfiguration.

In this dissertation, time frames of SPS dynamics are presented. Stability problems during SPS reconfiguration are classified as long-term stability problems. Since angle stability is strongly maintained in SPS, voltage stability is studied in this dissertation for SPS stability during reconfiguration. A test SPS computer model, whose simulation results were used for stability studies, is presented in this dissertation. The model used a new generalized methodology for modeling and simulating ungrounded stiffly grounded power systems.

This dissertation presents two new indices, a static voltage stability index ($SVSI_{Lji}$) and a dynamic voltage stability index (DVSI), for assessing the voltage stability in static and dynamic analysis. $SVSI_{Lji}$ assesses system stability by all lines in SPS. DVSI detects local bifurcations in SPS. $SVSI_{Lji}$ was found to be a better index in comparison with some indices in the literature for a study on a two-bus power system. Also, results of DVSI were similar to the results of conventional bifurcation analysis software when applied to a small power system. Using $SVSI_{Lji}$ and DVSI on the test SPS computer model, three of four factors affection voltage stability during SPS reconfiguration were verified. During reconfiguration, $SVSI_{Lji}$ and DVSI are used together to assess SPS stability.

DEDICATION

my father, mother and brother.

Thank you for everything you have given me.

ACKNOWLEDGMENTS

I thank my parents and my brother for their constant support and love. I especially thank them for their sacrifice in supporting my Ph.D. study. “Ba”, “Ma” and “GeGe”: thank you for giving me the confidence to succeed, supporting me in my entire education. You always trust me in all my endeavors and motivate me to do my best. Your love without end is always the source of my strength.

I thank my advisor, Dr. Karen Butler-Purry, for her patience, guidance and support. I thank you for encouraging me at difficult times and believing in me all the time. Thank you for all the work you put into to provide my assistantship throughout my Ph.D. study. I have learned a lot from you not only about academics but also about life. I can not thank you enough for all you have done for me.

I thank Dr. Alexander Parlos, Dr. Mehrdad Ehsani, Dr. Karan Watson, and Dr. Mi Lu for investing their time on my committee. I especially thank Dr. Parlos in mechanical engineering for his help to solve problems in my research.

I thank my fellow students within the Power System Automation Laboratory for their friendship and support in my research. I have seen many lab members come and go. I thank you all for the help you gave to me, especially the discussions about power system stability problems. I also thank you for all the laughs you gave to me. I wish all of you have a successful life.

TABLE OF CONTENTS

	Page
ABSTRACT.....	iii
DEDICATION.....	v
ACKNOWLEDGMENTS.....	vi
TABLE OF CONTENTS.....	vii
LIST OF TABLES.....	ix
LIST OF FIGURES.....	x
 CHAPTER	
I INTRODUCTION.....	1
1.1 Introduction.....	1
1.2 Organization.....	4
II LITERATURE REVIEW AND BACKGROUND.....	6
2.1 Introduction.....	6
2.2 Power System Stability.....	6
2.3 Shipboard Power System Stability.....	15
2.4 Chapter Summary.....	19
III PROBLEM FORMULATION.....	21
3.1 Introduction.....	21
3.2 Time Frame Analysis of SPS Dynamics.....	25
3.3 SPS Salient Features.....	29
3.4 Stability Issues in SPS.....	32
3.5 Chapter Summary.....	68
IV MODELING AND SIMULATION OF SHIPBOARD POWER SYSTEMS.....	70
4.1 Introduction.....	70
4.2 Ungrounded Stiffly Connected SPS.....	71
4.3 Component Models.....	72
4.4 Component Interconnections.....	85

CHAPTER	Page
4.5 Case Study.....	88
4.6 A Test Shipboard Power System.....	93
4.7 Chapter Summary.....	102
V STATIC VOLTAGE STABILITY ANALYSIS.....	104
5.1 Introduction.....	104
5.2 Static Voltage Stability Index.....	104
5.3 Comparison of Static Voltage Stability Indices.....	110
5.4 Case Study.....	115
5.5 Chapter Summary.....	124
VI DYNAMIC VOLTAGE STABILITY ANALYSIS.....	126
6.1 Introduction.....	126
6.2 Eigenvalue Decomposition and Singular Value Decomposition.....	126
6.3 Dynamic Voltage Stability Index.....	128
6.4 Comparison of Bifurcation Detection.....	132
6.5 Comparison of QSS and Simulation.....	141
6.6 Case Studies	144
6.7 Chapter Summary.....	154
VII CONCLUSIONS AND FUTURE WORK.....	156
7.1 Summary.....	156
7.2 Conclusions.....	159
7.3 Future Work.....	161
REFERENCES.....	163
APPENDIX A PARAMETERS OF A REDUCED SPS.....	171
APPENDIX B PARAMETERS AND MODELS OF A TWO-GENERATOR-ONE-MOTOR POWER SYSTEM.....	173
B.1 Parameters.....	173
B.2 Mathematical Models.....	174
VITA.....	176

LIST OF TABLES

TABLE	Page
4.1 Components for Test SPS for Stability Study.....	95
4.2 Three Phase Power of Induction Motor Loads.....	96
4.3 Three Phase Power of Static Loads.....	96
5.1 Line Impedance.....	111
5.2 Load Power Factors.....	112
5.3 $SVSI_{Lji}$ Values of Cables at Normal Operation.....	118
5.4 $SVSI_{Lji}$ Values of Cables When Loads Are on Alternate Paths.....	120
5.5 $SVSI_{Lji}$ Values When $P_{L312}=3.02$ p.u.....	123
6.1 AUTO Results.....	138

LIST OF FIGURES

FIGURE	Page
3.1 A Typical AC Radial SPS [49]	23
3.2 Time Frames for Dynamics of AC Shipboard Power Systems.....	27
3.3 Illustration of Parallel Operation of Generators in Figure 3.1.....	34
3.4 Illustration of Saddle Node Bifurcation.....	42
3.5 PV Curve Analysis for Saddle Node Bifurcation.....	43
3.6 PV Curve Analysis for Losing Equilibrium of Fast Dynamics.....	45
3.7 Illustration of Subcritical Hopf Bifurcation.....	47
3.8 Illustration of Supercritical Hopf Bifurcation.....	47
3.9 PV Curve Analysis for Hopf Bifurcation.....	48
3.10 PV Curve Analysis for Losing Attraction of Fast Dynamics.....	49
3.11 A Reduced AC Radial SPS.....	51
3.12 The Cable between Switchboard 3 and Load Center 2 in Figure 3.11.....	52
3.13 PV Curves with Different Load Factors.....	52
3.14 IEEE Type II AVR.....	54
3.15 IEEE Type II AVR with Excitation Limit Reached.....	55
3.16 PV Curves With and Without Excitation Limit Reached.....	57
3.17 Some Typical Torque Speed Curves of Induction Motors.....	58
3.18 One Line Diagram of a Single-Generator-Single-Load System.....	62
4.1 Transformation Between the Reference Frame dq0 and abc.....	73

FIGURE	Page
4.2 Transformation between Reference Frames.....	75
4.3 A Three-Phase Connecting Line Model.....	81
4.4 A Single Phase Linear Transformer Model.....	82
4.5 Interconnection on a Reference Generator Bus.....	86
4.6 Interconnection on a Typical Inductor or Resistor Bus.....	87
4.7 A Reduced SPS.....	88
4.8 Block Diagram of a Governor with Gas Turbine.....	89
4.9 Phase AB Voltage of Generator 2.....	90
4.10 Phase BC Voltage of Generator 2.....	91
4.11 Phase AB Current of Static Load 5.....	91
4.12 Phase BC Current of Load 5.....	92
4.13 Phase AB Current of Induction Motor 1.....	92
4.14 A Test SPS for Stability Study.....	98
4.15 Phase AB Voltage of Generator 1.....	100
4.16 Phase BC Voltage on Switchboard 3.....	100
4.17 Phase A Current of Motor Load L11.....	101
4.18 Rotor Angular Speed of Motor Load L11.....	101
4.19 Phase A Current of Static Load L14.....	102
5.1 A Two-Bus Power System.....	105
5.2 One-line Diagram of a Line in a Power System.....	109

FIGURE	Page
5.3 Performance Comparison of Various Static Voltage Stability Indices with SL and HPF.....	113
5.4 Performance Comparison of Various Static Voltage Stability Indices with SL and LPF.....	114
5.5 Performance Comparison of Various Static Voltage Stability Indices with LL and HPF.....	114
5.6 Performance Comparison of Various Static Voltage Stability Indices with LL and LPF.....	115
5.7 The Relationship between $SVSI_{C312}$ and P_{L312}	122
6.1 A Two-Generator-One-Motor Power System.....	133
6.2 Motor Speed with Change of K.....	134
6.3 Voltage on Bus 3 with Change of K.....	135
6.4 DVSI with Change of K.....	136
6.5 DVSI1 with Change of K.....	136
6.6 Complete Bifurcation Diagram from AUTO.....	139
6.7 Root Locus of the Power System in Figure 6.1 for Stability Study.....	140
6.8 Enlarged Root Locus of Area A in Figure 6.7.....	141
6.9 Results of Comparison between Simulation and QSS.....	142
6.10 Results of Comparison between Simulation and QSS ($K=1.0118\sim 1.0228$).....	143
6.11 Results of Comparison between Simulation and QSS ($K=2.03\sim 2.102$).....	143
6.12 Voltage V_{L312} with Change of K for Various Load Torques.....	147
6.13 Motor Speed W_{L312} with Change of K for Various Load Torques.....	147
6.14 DVSI and DVSI1 with Constant Mechanical Torque.....	149

FIGURE	Page
6.15 DVSI and DVSI1 with Linear Mechanical Torque.....	149
6.16 DVSI and DVSI1 with Quadratic Mechanical Torque.....	150
6.17 Terminal Voltage $V_{t_{g1}}$ with Change of System Load Level K_L	152
6.18 Terminal Voltage $V_{t_{g1}}$ with Change of System Load Level K_L ($K_L=1.3\sim 2.3$)..	152
6.19 DVSI and DVSI1 with Change of System Load Level K_L	154

CHAPTER I

INTRODUCTION

1.1 INTRODUCTION

The electric power systems in U.S. Navy ships supply energy to sophisticated systems for weapons, communications, navigation, and operation. The reliability and survivability of a Shipboard Power System (SPS) are critical to the mission of a Navy ship, especially under battle conditions. In the event of battle, various weapons might attack a ship. When a weapon hits the ship, it can cause severe damage to the electrical systems on the ship. This damage can lead to de-energization of critical loads on a ship that can eventually decrease a ship's ability to survive the attack. Researchers in the Power System Automation Laboratory (PSAL) at Texas A&M University have developed methods for performing reconfiguration of SPS. Reconfiguration operations change the status of open/close of switches in an SPS. These operations are performed before or after a weapon hit to reduce the damage to SPS.

Stability is one critical aspect of system reliability, and stable operations must be maintained during reconfiguration. Power system stability is maintained by real and reactive power supplied from sources, normally generators. Power systems are stressed if the margin of real and reactive power between the supply and the consumption is small. Reconfiguration operations change the topology of an SPS and induce the dynamics of equipments. When the stability margin is small, the topology changes and the dynamics of equipments due to reconfiguration might cause voltage instability, such as progressive voltage fall or voltage oscillations. SPS stability should thus be assessed to ensure the stable operation of a system during reconfiguration. In the literature, one methodology is found for angle stability studies for SPS [1], and no methodology was

found for voltage stability analysis and assessment for Alternate Current (AC) radial SPS. Therefore, there is a need to develop new methods that can perform such a task.

To analyze and assess SPS stability, understanding SPS is important and the first thing to be done. This dissertation presents the time frames of dynamics of SPS. With appropriate categorization of stability problems due to time frames, we can emphasize key elements affecting the stability under study. SPS are special power systems, which have the features of being isolated, ungrounded, and stiffly connected. The salient features of SPS are discussed. These salient features affect SPS stability and contribute to the determination of factors involved in SPS stability analysis.

An effective stability assessment methodology can only be developed based on the study of dynamics during SPS reconfiguration. A “computer model” test system representing an AC SPS was designed and developed for stability studies. A special modeling methodology is required to efficiently model and simulate the dynamics of SPS. Due to the feature of stiff connection, inductor and resistor buses emerge. All component models on inductor and resistor buses are voltage-in-current-out models and the voltage inputs can not be derived from any component model, which creates interconnection incompatibility on inductor or resistor buses. The voltage inputs on inductor or resistor buses can be generated in artificial ways. In this dissertation, a new generalized methodology is presented to model and simulate ungrounded stiffly connected power systems such as SPS. Dynamic simulations are performed on the test SPS to investigate the dynamic behavior of an SPS during reconfiguration and simulation results are used in voltage stability and assessment.

Power system stability studies whether a system can regain equilibrium after being subjected to disturbances. The nature of a stability problem is reflected by synchronism between synchronous generators or voltages at buses, which belongs to the study areas of angle stability and voltage stability, respectively. Due to the parallel operations of generators and the stiff connection of SPS, the synchronism between generators is strongly maintained in SPS. Hence, voltage stability is the concern of the stability study in this dissertation. Voltage instability occurs in a stressed system, where reactive power

margin is small. When a disturbance occurs, voltages in a system can decrease below a certain level or oscillate. Bifurcations are detected when voltage instability occurs.

In this dissertation, two new voltage stability indices are presented to assess voltage stability during SPS reconfiguration. The two indices are a static voltage stability index (SVSI_{L_{ji}}) for static voltage stability analysis and a dynamic voltage stability index (DVSI) for dynamic stability analysis. SVSI_{L_{ji}} and DVSI are used together to assess SPS stability during reconfiguration. SVSI_{L_{ji}} is deduced based on the power flow equations at steady state. In static analysis, instability is detected if SVSI_{L_{ji}} is equal to one. As the value of SVSI_{L_{ji}} gets closer to one, the system is more prone to be unstable. DVSI is deduced from eigenvalue decomposition and singular value decomposition. DVSI detects bifurcations in a dynamic system and thus identifies voltage instability. The dynamic index is evaluated with dynamic simulations, which are performed with the generalized modeling and simulation method. A zero value of DVSI indicates the occurrence of bifurcations and voltage instability. The system is prone to be unstable if DVSI is closer to zero. Case studies were performed for SVSI_{L_{ji}} and DVSI indices on the test SPS. Case studies show that SVSI_{L_{ji}} and DVSI are effective voltage stability indices in static and dynamic voltage stability analysis.

The major contributions of this dissertation are in six areas. First, the time frames of dynamic phenomenon were studied for shipboard power systems. The time frames classify dynamics in SPS into different types of stability. With proper classifications, stability studies concentrate on important factors affecting SPS stability. Secondly, a new methodology for modeling and simulating ungrounded stiffly connected power systems was developed. The obstacles to utilizing conventional power system simulation methods for ungrounded stiffly connected power systems are discussed. This new modeling methodology was successfully applied on ungrounded shipboard power systems. Thirdly, a study of factors affecting shipboard voltage stability during reconfiguration was conducted and four factors were identified as affecting voltage stability. The effects of the four factors, loading condition, motor stalling, windup limit

in voltage controllers, and interaction between loads and voltage controllers on SPS voltage stability, are discussed and analyzed.

Fourthly, approach to assess SPS stability during reconfiguration was developed. The approach includes two new indices, $SVSI_{Lji}$ and DVSI, for static and dynamic voltage analysis. A new static voltage stability index ($SVSI_{Lji}$) was developed. The deduction of this new index was made from the mathematical formulations of power flows. The performance of this new index in static voltage stability analysis and assessment was compared with that of three existing static voltage stability indices found in the literature. The new index performed better than the three indices. $SVSI_{Lji}$ was applied on the test shipboard power system computer model for stability studies. The test system for stability studies was developed from a reduced shipboard power system model previously designed in the Power System Automation Lab. The stability studies performed on the test SPS consider factors affecting SPS stability. A new dynamic voltage stability index (DVSI) was developed to detect bifurcations in dynamic voltage stability analysis. Local bifurcations, including both saddle node bifurcation and Hopf bifurcation, can be detected by the DVSI. The new index was derived with the techniques of eigenvalue decomposition and singular value decomposition. In a study on a two-generator-one-motor power system, the bifurcations detected by this new index agree with those detected on a conventional bifurcation analysis software package called AUTO. This new index was implemented on the test SPS for stability analysis. The results show that the bifurcations occurring during dynamic processes of the test system can be detected by this new DVSI.

1.2 ORGANIZATION

This dissertation consists of seven chapters. In Chapter I, an introduction to this work and the organization of the dissertation are given. In Chapter II, the literature on stability studies for conventional utility power systems and shipboard power systems (SPS) will be reviewed. In Chapter III, stability problems during reconfiguration will be formulated. This dissertation will discuss stability problems in SPS and study voltage

stability during SPS reconfiguration. Bifurcations will be introduced as causes of voltage instability. Steady state and dynamic analysis for voltage stability will be presented as different ways to analyze voltage instability. Factors affecting voltage stability in SPS during reconfiguration will be described and analyzed. In Chapter IV, a new generalized methodology for modeling and simulating ungrounded stiffly power systems will be presented. A test shipboard power system for stability studies will be constructed in this chapter. The new modeling and simulating methodology will be implemented on the test SPS. In Chapter V, a new static voltage stability index ($SVSI_{Lji}$) for static stability analysis will be deduced. Comparisons of the new index and some indices in the literature will be made. The new $SVSI_{Lji}$ will be illustrated with the test SPS. In Chapter VI, a new dynamic voltage stability index (DVSI) for dynamic stability analysis will be deduced. The bifurcation analysis results of a small power system by DVSI will be compared with those by AUTO, a conventional bifurcation analysis software. The effectiveness of the new DVSI will be illustrated on the test SPS. In Chapter VII, conclusions will be drawn and some remarks about future work will be given.

CHAPTER II

LITERATURE REVIEW AND BACKGROUND

2.1 INTRODUCTION

In this chapter, the literature on stability and analysis methods will be reviewed and summarized. Power system stability is an important factor in power system studies. Shipboard power systems (SPS) are special power systems. Stability analysis and assessment for AC SPS are the topic of this dissertation.

Appropriate mathematical models of power systems are necessary as the first step for power system stability analysis and assessment. In this chapter, work on the stability of utility power systems will be presented first. Work on the stability of SPS will then be discussed.

2.2 POWER SYSTEM STABILITY

Power System Stability is the ability of an electric power system, for a given initial operating condition, to regain a state of operating equilibrium after being subjected to a physical disturbance, with system variables bounded so that system integrity is preserved [2]. According to the time frames of dynamics, power system stability can be divided into steady-state, dynamic, or small signal and transient and long-term stability. The main physical nature of instability in power systems could be angle or voltage.

In this section, modeling work on power systems will be described first. A literature review of different categories of stability and various analysis methods for utility power systems will then be presented.

2.2.1 Power System Modeling

Any power system can be represented by a set of differential algebraic equations (DAE) shown as (2.1) and (2.2) [2].

$$\dot{\mathbf{x}} = \mathbf{f}(\mathbf{x}, \mathbf{y}) \quad (2.1)$$

$$\mathbf{0} = \mathbf{g}(\mathbf{x}, \mathbf{y}) \quad (2.2)$$

where \mathbf{x} is a vector of state variables and describes the dynamics of power systems, such as the dynamics of exciter control systems. \mathbf{x} could also include specific system configurations and operating conditions, such as loads, generation, voltage setting points, etc. \mathbf{y} is a vector of algebraic variables and satisfies algebraic constraints, such as power flow equations, which is implicitly assumed to have an instantaneously converging transient.

The conventional methods for modeling and simulating power systems can be classified into two main categories: 1) nodal admittance matrix based circuit simulation methods, such as implemented by EMTP/ATP [3] (The Electromagnetic Transients Program/Alternative Transient Program), and 2) differential algebraic equation solver based methods, such as implemented in SimPowerSystems Toolbox by Matlab/Simulink [4][5]. The essence of nodal admittance matrix based methods is that a power system can be represented by an electric circuit of mixed constant impedance and voltage source at each time step. For differential algebraic equation solvers based methods, the differential equations and algebraic equations are partitioned and solved by explicit numerical methods or simultaneously solved by implicit numerical methods. Due to the salient features of SPS, the modeling and simulation of SPS could then be different from the modeling and simulation of utility power systems, and this will be discussed later.

2.2.2 Steady State Stability

The stability of an electric power system is a property of the system motion around an equilibrium set, i.e., the initial operating condition [2]. Steady-state analysis consists of assessing the existence of the steady-state operating points of a power system. At steady state, time derivatives of state variables are assumed to be zero. Consequently, the overall DAE equations describing the system are reduced to pure algebraic equations. No solution for the algebraic equations means that the system cannot operate under

specific conditions. One solution means that a unique operating point exists. Multiple solutions means that further investigation is required to study the characteristics of each solution and find the stable solution. Conventionally, power flow equations are applied to conduct the steady state analysis. In the past, voltage stability was studied by steady state analysis methods.

2.2.3 Dynamic Stability

Dynamic stability or small signal stability exists when a system is subjected to small aperiodic disturbances [2]. The time frame of dynamics in small signal stability is up to one second. Initially the operating point of a system is x_i . After a disturbance, the operating point moves to $x_i + \Delta x_i$, where Δx_i is the deviation of the operating point. In dynamic stability, the deviation Δx_i is so small that its effects to the system can be linearized, which is the theory basis for small signal stability analysis. The linear system depends not only on the physical characteristics of the system but also on the equilibrium point about which the linearization is performed. The locations of the eigenvalues of a system are checked for dynamic stability. The imaginary parts of the eigenvalues represent the potential frequencies of the oscillation modes. The real parts of the eigenvalues represent the damping factors of the corresponding frequencies. If all the real parts of the eigenvalues are negative, then the system is stable.

The nonlinear behavior of the system can be approximated by the behavior of its linear system within a small proximity to the system equilibrium points. The linear system is almost equivalent to the nonlinear system in a small neighborhood of the equilibrium point. Within the small neighborhood of the equilibrium point, the qualitative stability characteristics of the linear system are thus the same as the qualitative stability characteristics of the nonlinear system. This approximation is the theoretical basis for the application of local bifurcation analysis for dynamic voltage stability analysis [6].

2.2.4 Transient Stability

Transient stability exists when a system is subjected to large aperiodic disturbances [2]. The time frame of transient stability is up to ten seconds. For transient stability analysis, the deviation Δx_i of state variables is large and the nonlinear system model can not be linearized. In the study of power systems, without specification, transient stability is normally referred to as angle stability. Angle stability is concerned with the ability of interconnected synchronous machines in a power system to remain in synchronism after being subjected to a disturbance from a given initial operating condition [2]. The electromechanical energy conversion in rotating machines is studied for angle stability.

Indirect and direct methods are used in the study of angle stability. Indirect methods are time domain simulation methods. Time domain simulations compute the solution trajectories of the state variables from dynamic equations and algebraic equations. The stability is observed from the solution trajectories. Indirect methods are reliable and accurate, but the computation results can not indicate the stability margin and the computation speed is slow for stability assessment [2][7][8].

Direct methods are suggested in many papers for their speed of computation and efficiency in stability assessment. Good summarization on various direct methods is made in [7][8]. Basically, Lyapunov functions, usually the energy functions of a system, are constructed in direct methods to evaluate stability. However, Lyapunov theorem gives only a sufficient but not a necessary *and* sufficient condition for the determination of stability regions. As a result, the stability regions calculated from direct methods are conservative or smaller than real stability regions. In addition, it is difficult to construct a Lyapunov function for a system with detailed component models included. Most of the direct methods are restricted to use with classical second order generator models and constant impedance load models. In [8], a third order flux decay generator model (a more detailed generator model) was considered for formulating Lyapunov functions.

Various direct methods use different characteristics of the stability boundary to determine the stability region. These methods include Unstable equilibrium point (UEP), controlling UEP, Potential energy boundary surface (PEBS), and Equal area criterion

(EAC). In the UEP method, the stability boundary is on an unstable equilibrium point resulting in the lowest value of the Lyapunov function among all the unstable equilibrium points. In the controlling UEP method, the stability boundary is on a relevant or controlling unstable equilibrium point or the unstable equilibrium point closest to the point where the disturbed trajectory exits the stability region. In the PEBS method, the stability boundary is on the points where the maximum value of the potential energy occurs along disturbance-on trajectory. The EAC method uses the same boundary condition as the PEBS method. However, the characteristics of the maximum potential energy are described in a different way. In EAC, the boundary of the region of attraction is when the accelerated energy during disturbance-on trajectory is equal to the decelerated energy after disturbances are removed.

2.2.5 Long-Term Stability

Long-term stability is defined as the ability of a power system to reach an acceptable state of operating equilibrium following a severe disturbance that may or may not have resulted in the system being divided into subsystems [2]. Long-term stability problems are usually concerned with system response to major disturbances that involve contingencies beyond normal system design criteria. The disturbances are either so severe or long lasting that they evoke the actions of slow response equipment. Therefore, long-term stability studies require that the system model include slow response component models, which are normally considered unnecessary in transient and dynamic stability studies.

For long-term stability studies, time domain simulations are the only way to evaluate stability [9]-[11]. In long-term stability studies, different time scales (fast and slow) are modeled and simulated simultaneously. Long-term stability studies thus could be time consuming. At present, several specially designed simulation packages, such as LOTDYS (Long-Term DYnamic Simulation), ETMSP (ExTended Mid-term Simulation Program) and EUROSTAG (STAlilite Generalisée, in French), can be used to simulate long-term dynamics. LOTDYS assumes uniform system frequency and neglects fast

transients [12]. ETMSP is a better simulation program for including fast transients, but it assumes constant frequency in long-term time frames, which is unacceptable when it is used for investigating long-term dynamics involving large excursions in system frequency [13]. EUROSTAG uses the Gear type implicit integration algorithm, in which time step size varies automatically due to the truncation error of the former step [14]-[17]. EUROSTAG allows the simulation of all dynamics with one invariant complete model except for fast electromagnetic transients [14]. In many situations in voltage stability studies, slow acting equipment will be involved. Long-term voltage stability could be studied by software packages designed for the study of long-term stability.

The three commercial long-term simulation tools mentioned earlier were developed to simulate long-term dynamics in bulk power systems, where transmission systems are significant. If a power system is stiffly connected, due to the small shunt capacitances of the short lines, the line time constants are small. Therefore, small time steps will be introduced into the simulation to guarantee a stable integration algorithm even though the small capacitances have little effect on the overall system performance [18][19]. The small steps decrease the speed of computation significantly. Consequently, the earlier mentioned software packages for long-term stability studies are not applicable in stiffly connected power systems.

2.2.6 Voltage Stability

Voltage stability is the ability of a power system to maintain steady acceptable voltages at all buses in the system under normal operating conditions and after being subjected to a disturbance [2]. Voltage stability is not new to the study of power systems but is now receiving more and more attention as a result of heavier loading in developed power networks. In recent years, voltage instability has been responsible for several major network collapses [2]. Voltage instability occurs when a power system is stressed [2][6][20].

Recently, nonlinear bifurcation theory was applied in a power system voltage stability study [6]. The bifurcation points are the thresholds where instability occurs. Some

typical types of bifurcation occurring in power systems are saddle node bifurcation (SNB), Hopf bifurcation (HB), and singular induced bifurcation (SIB). These bifurcations are local bifurcations. SNB has been linked to voltage collapse [6]. HB is associated with oscillatory voltage instability [6]. SNB and HB are generic local bifurcations [6]. Researchers are unclear as to whether SIB does exist in power systems or whether it is just a mathematical concept [6].

In voltage stability analysis, load characteristics could be critical. In section 2.2.6.1, work on loading modeling for voltage stability will be described and discussed. Voltage stability can be analyzed by static and dynamic analysis methods. In section 2.2.6.2, the literature on these two analysis methods will be reviewed.

2.2.6.1 Load Modeling

Voltage is maintained by reactive power in power systems. After a system is subjected to a disturbance, power of loads tries to be restored to the levels before being disturbed. The restored loads increase reactive power consumption after being disturbed and can cause voltage instability in stressed power systems. Voltage stability is thus closely related to load characteristics [2][6][21][22]. The importance of load modeling in voltage stability studies, especially in the location of the bifurcation points and the corresponding system dynamic response has been addressed in the literature. Various load models have been proposed to capture the basic dynamic voltage response of the loads in a power system.

In [23], the authors examine the characteristics of power systems where induction motors constitute a main portion of the load. In their study, a first order induction motor model was used and three different induction motor load models were considered. The load torques were modeled as constant, linear, and quadratic functions of the induction motor rotor speed. Static loads were also included in the system model allowing for the examination of the effect of changing the proportion of the total load, which was composed of static elements. Fixed voltage and constant generator models were used with no generator dynamics considered. Different types of load torque on induction

motors can have different effects on voltage stability. The study found that for constant load models, saddle node bifurcations occurred at higher voltage levels and at higher speeds as compared to the speed dependent mechanical load models. The percentage of the total load composed of induction motor load did not affect the nature of bifurcations, but it did influence the value of induction motor loading at which the bifurcations occurred. The effect on voltage collapse of combined induction motor and impedance loads by means of lab measurements and computer simulations using reduced order load models is studied in [24]. The study focused on the ability of switching capacitors to prevent voltage collapse in heavily loaded systems and the operation of induction motors on the lower portion Power Voltage (PV) curves.

In most voltage stability analysis, studies concentrate on simplified induction motor models, and little attention has been placed on the interaction of the different power system components. A Hopf bifurcation was detected along with typical saddle node bifurcations with a simple two-bus-single-generator system in [25]. The loads in the system were modeled as a third order induction motor model and lumped impedance elements. The generator was modeled using a dynamic two axis model with an IEEE type I exciter. The interaction between the induction motor loads and voltage controllers on generators was studied in [26]. It was found that the dynamics of induction motors can delay the response of voltage controllers. Voltage oscillatory instability thus could be caused by the interaction between voltage controllers and induction motors.

2.2.6.2 Voltage Stability Analysis

At its earlier development stage, voltage stability used to be analyzed by static analysis methods, such as power flows. However, as understanding of voltage stability developed, more and more researchers came to believe that voltage stability is dynamic stability and dynamic analysis should be applied.

Static analysis methods could be used to analyze voltage stability problems approximately. The equivalence of the occurrence of saddle node bifurcation of the algebraic equations to the reduced differential equation modeled by a set of DAE is

shown in [27]. Many static studies have been done on voltage stability in transmission systems, but hardly any work has been done on voltage stability in distribution systems. Several voltage stability indices derived from static power flow analysis were proposed for utility power systems. The values of the indices were calculated for each distribution line based on load flow results. The line with the largest value was taken as the weakest line in a system and received special attention to maintain voltage stability. A voltage stability index LQP that neglected line resistance was proposed by Mohamed [28]. A fast voltage stability index FVSI was derived in [29] by Musirin. The fast index neglected the angle difference between the voltages at both ends of a line. A voltage index was represented by the power injected by the load on a local bus and the power injected from the other buses in a system in [30]. In [31][32], a voltage stability index for distribution systems was derived with the whole distribution network represented by a single line equivalent. However, the equivalent index is only valid at the operating point at which it is derived and is not adequate for assessing stability when a large change of load is involved [32].

As described earlier, various long-term simulation packages mentioned in section 2.2.5 could be used for dynamic voltage stability analysis. Voltage magnitudes at critical buses are observed during simulations to determine if voltages are stable. With differential equations of fast dynamics approximated by algebraic equations, voltage stability can be analyzed and assessed by successive static analysis methods, such as Quasi Steady State (QSS) analysis [2]. In time domain simulations, differential and algebraic equations are partitioned and solved explicitly, or integrated and solved implicitly. In QSS, approximated algebraic equations are solved to calculate equilibrium points successively. Numerical algorithms, such as the Newton-Raphson algorithm, are applied in QSS for incrementally changing the value of parameters. It has been suggested that the most effective approach for studying voltage stability is to make complementary use of QSS and time domain simulations [2][6]. QSS derives the trajectory approximately. Time domain simulations derive the detailed trajectory between the equilibrium points derived from QSS analysis when a system is close to

bifurcations. The bifurcation points can thus be identified along the trajectory by bifurcation detection techniques, such as eigenvalue decomposition (ED) and singular value decomposition (SVD) [6]. The minimum singular value can be used to detect bifurcations for voltage collapse [6]. However, in a real power system, several small singular values could mask the critical singular value, and a method is suggested in [33] to unmask the critical singular value. In many long-term stability studies, successive static analysis is thus applied for determining long-term stability margins and identifying factors influencing long-term stability [2][6][34]. However, numerical difficulties can arise as the solution of steady state equations approaches a singular point caused by saddle node bifurcation.

Continuation methods overcome the singular problem by reformulating the differential algebraic equations so that they will remain well-conditioned at all possible loading conditions. Continuation techniques are generally composed of two or three steps. The first step is a predictor step, the second is a corrector step, and the last step is a parameterization routine. At the predictor step, a predictor step of state variables and the change of parameters are determined. From the new point, a corrector routine is used to calculate the new equilibrium point. A parameterization is used to ensure that the Jacobian matrix used in the continuation method does not become singular at saddle node bifurcations. UWPFLOW, a publicly available QSS, uses a continuation method to detect the voltage stability limit of a power system [34]. Another public program AUTO [35] is also mentioned in the literature. AUTO applies a continuation method to solve the differential algebraic equations of the system. AUTO has been used for theoretical studies of bifurcations in small power systems [6][36].

2.3 SHIPBOARD POWER SYSTEM STABILITY

The stability analysis for SPS is different from stability analysis for conventional utility power systems. Little research work has been found in the literature in the area of shipboard power system stability.

In this section, shipboard power system modeling will first be reviewed. Secondly, a method found in the literature for SPS stability analysis and assessment will be discussed.

2.3.1 Shipboard Power System Modeling

Shipboard power systems are isolated finite inertia power systems. References [37]-[43] presented modeling and simulation studies of versatile isolated finite inertia power systems from different perspectives. Ross, Concordia and O'Sullivan [37]-[39] modeled isolated power systems for designing frequency controllers. Kariniotakis and Stavrakakis [40] neglected machine stator transients and network transients. Their methods thus derived incorrect simulation results when the transients were large. The objective of Sharma [41] was to consider transients in the first five seconds, so detailed models were not applied. Fahmi and Johnson [42] divided an isolated power system into several subsystems, with phase co-ordinate models then adopted for analysis of each subsystem. Limited controller models were included, which would not be appropriate in long-term stability studies. Murray, Graham and Halsall [43] concentrated on the modeling of synchronous motor drives and the simulation of waveform distortion due to motor drives in an isolated power system.

A test ungrounded delta connected SPS was developed in the Power System Automation Lab based on a U.S. Navy combatant ship [44]. The modeling and simulations of the test SPS were conducted with Alternative Transient Program (ATP). The test SPS comprised various components, including generators, load centers, numerous cables, induction motor loads, constant impedance loads, transformers, and different types of protective devices. The test SPS provided a platform for studying the behavior of SPS. The test system was simulated to aid the development of automated failure assessment and restoration for SPS.

With small shunt capacitance neglected in SPS, there emerges incompatibility when the components models are interconnected. The incompatibility problem caused by neglecting the capacitances in modeling SPS could be solved by the traditional method

of adding auxiliary resistance in systems [8]. Two methods for modeling and simulating SPS were proposed in [18][19] to solve the modeling incompatibility. In [18], at each inductor bus one component model is reformulated. The reformulated component is a nonroot generator or motor. The original physical models of the reformulated components are kept, while reformulation changes the mathematical formulation of the reformulated component models to facilitate the derivation of bus voltages. The method in [19] keeps the original mathematical format of equations and derived bus voltages by solving algebraic constraints with an algebraic solver; as a result, the speed of computation improved greatly.

The methods in [18] and [19] used ACSL (Advanced Continuous Simulation Language) as the simulation tool. In Mayer's method [18], the inductor buses in a stiffly connected system are first categorized; the standard model of one machine connected to each inductor bus is then reformulated to facilitate the deduction of the inductor bus voltages. Mayer's method requires that at least one machine be connected to each inductor bus and certain procedures are required to solve the voltages of each inductor bus on the basis of the reformulated state space equations of root and nonroot machines. Ciezki's method [19] relies greatly on the simulation language, more specifically, the accuracy of the algebraic solver in ACSL.

2.3.2 Shipboard Power System Stability Analysis

A stability analysis and assessment method for composite systems was discussed and proposed for SPS by Amy [1]. A composite system was modeled as (2.3) and (2.4) [1].

$$\dot{x}_i = f_i(x_i, t) + D_i u_i \quad (2.3)$$

$$y_i = H_i x_i \quad (2.4)$$

where x_i is the states of the i^{th} subsystem, u_i is the inputs of the i^{th} subsystem, and y_i represents the outputs of the i^{th} subsystem. G_i and H_i are system parameters. The representation of interconnection of subsystems was given by (2.5) [1].

$$u_i = \sum_{j=1}^m B_{ij} y_j + G_i u \quad (2.5)$$

where B_{ij} describes the interconnections between the inputs of i^{th} subsystem and the outputs of the other subsystems. u is the global inputs to the composite system. G represents the parameters associated with the global inputs. A Lyapunov function was constructed from the composite model (2.3)- (2.5) to assess system stability [1].

Amy considered SPS as a composite system, and each component was taken as a subsystem in the composite system [1]. However, the close proximity and tight coupling of SPS components increase the order of models to capture dynamics. Further, it was difficult to construct a Lyapunov function for a detailed system model. Co-energy was used by Amy to construct Lyapunov functions for detailed generator models in SPS [1]. He assumed each generator was a lossless “coupling field” where the mechanical and electrical interaction takes place. The energy contained within the “coupling field” was co-energy. Amy then used the instantaneous co-energy stored in a generator and its rate of change for stability analysis and assessment during the transient process [1]. At steady state, the co-energy was stationary and the mechanical energy injected into the field was extracted as electric power. Co-energy within the field did not directly participate in electromechanical energy conversion at steady state. When the system was disturbed, co-energy in generators increased. After the disturbance, if the excess co-energy stored in the coupling field was extracted and converted into the electrical system, the system was stable. Otherwise, the system was unstable.

Co-energy in a three-phase synchronous machine in dq0 variables was written as (2.6) by Amy in [1].

$$W'_{mdq} = \frac{1}{2} \begin{bmatrix} I_{dq}^T & I_R^T \end{bmatrix} L_{DQ} \begin{bmatrix} I_{dq} \\ I_R \end{bmatrix} \quad (2.6)$$

where I_{dq} is the stator currents and I_R is the rotor currents. L_{DQ} is the stator and rotor inductance of the generator. A co-energy based Lyapunov function including kinetic energy $K.E.$ as (2.7) was then developed by Amy for detailed SPS generator models [1].

$$V'_m = W'_{mdq} + K.E. = \frac{1}{2} \begin{bmatrix} I_{dq}^T & I_R^T \end{bmatrix} L_{DQ} \begin{bmatrix} I_{dq} \\ I_R \end{bmatrix} + \frac{1}{2} J \omega_m^2 \quad (2.7)$$

where J and ω are the inertia and rotor speed of the generator. Four other Lyapunov functions with different scaling factors on co-energy and kinetic energy were also presented [1]. Since a SPS is a composite system, Amy used the summation of the Lyapunov function of each individual generator as the system Lyapunov function of a SPS [1]. If the derivative of the system Lyapunov was positive, then the system was determined unstable. Otherwise, the system was determined as stable. The co-energy based Lyapunov function was applied by Amy to analyze stability of a simple two-generator SPS [1]. In the system, one generator was a super-conducting generator and the other was a conventional generator. A short circuit fault was applied at the terminal of the super-conducting generator. The critical clearing time for the faults was determined as the time instant when the derivative of the system Lyapunov was equal to zero.

The concept of a co-energy based Lyapunov function needs some improvement to be feasible in real SPS. In order to assess system stability, Amy believed each relevant component in a system should have its own “co-energy based” Lyapunov function [1]. However, the implementation of the co-energy concept on components other than synchronous generators needs further research work. In addition, because the co-energy in generators is normally small, weighting factors were used by him to enlarge the co-energy in the total energy [1]. These weighting factors are important for assessing stability accurately. An efficient way to select the weighting factors is necessary for the co-energy based Lyapunov function to be used in stability analysis.

2.4 CHAPTER SUMMARY

This chapter addressed the literature on stability. Stability and its analysis methods for conventional utility power systems were presented. Different methods of modeling and simulations of SPS were reviewed. A stability study method developed for shipboard power systems was described and discussed.

Chapter III will formulate the stability problems studied in this dissertation.

CHAPTER III

PROBLEM FORMULATION

3.1 INTRODUCTION

The electric power systems in U.S. Navy ships supply energy to sophisticated systems for weapons, communications, navigation and operation. At present, there are many forms of system configuration for electric power systems in U.S. Navy ships or SPS, such as AC radial, AC zonal, and integrated power systems (IPS) [45]-[47]. Some AC shipboard power systems (SPS) are ungrounded, having no permanent, low-resistant connections between the power system and the structure of the ship [45]. An ungrounded power system is used for AC radial SPS to survive the most frequently occurring single-line-to-hull fault. Figure 3.1 shows the one-line diagram of a typical AC radial SPS [48].

In SPS, some generators are in normal operation, and some are back-up or standby generators that provide generation in emergencies. In Figure 3.1, four generators are in service and two are emergency generators that provide back up power. Typical voltage output from the generators is 450 volts AC at 60 Hz. To further enhance survivability of an SPS under attack, main switchboards are connected with bus-tie cables in a ring configuration. In emergencies, the ring connection provides power supply from the generators to the main switchboards through alternate paths. To avoid total generation loss under attack, the generators are located in different places on shipboard.

Circuits downstream of the main switchboards are in radial configuration. The load centers are downstream of the main switchboards; while the power panels are downstream of the main switchboards or load centers. Loads directly connect to the main switchboards, load centers, or power panels. Single-phase loads connect to power panels through power transformers. Transformer banks are three, single-phase delta connected transformers that reduce the voltage to supply single-phase loads. Transformers convert the supply voltage of the distribution system from 450 volts to 120 volts. Therefore, an SPS could operate under unbalanced conditions. Loads operate at

440 or 115 volts at 60 Hz or 400 Hz. 400 Hz loads are usually part of the weapons systems and aircraft and aviation equipment.

Generally, generators, main switchboards, and load center feeders are equipped with circuit breakers (CBs), while power panel feeders are equipped with switches or fuses [45]. Switchboard protection devices, including an under-frequency module relay, an over-power relay, a reverse power relay, and an under-voltage relay protect its associated generator/switchboard set [49]. Low voltage protective devices (LVs), such as low voltage protection (LVP) and low voltage release (LVR), are installed to protect induction motors. LVPs and LVRs isolate the protected motor if the terminal voltage is below the drop out voltage. If the terminal voltage is restored to a value above the pick up voltage, the LVR switches the load back into the system. LVPs require manual operator action to switch the load back into the system.

There are two categories of loads in the system: non-vital loads and vital loads. Non-vital loads have one path (normal path) to achieve power supply; while vital loads have an extra path (alternate path) to enhance survivability in emergencies. Two kinds of bus transfer units (BTs), automatic bus transfer (ABT) units and manual bus transfer (MBT) units, are employed to perform this protection function. The switches of a bus transfer unit on the normal path of the load are normally closed, while the switches on the alternate path are normally open. An ABT automatically switches the load to its alternate path if the voltage on the normal path is below the drop out voltage, and returns to its normal path when the voltage returns to a value above the pick up voltage. An MBT needs manual interaction to change the path of the protected load.

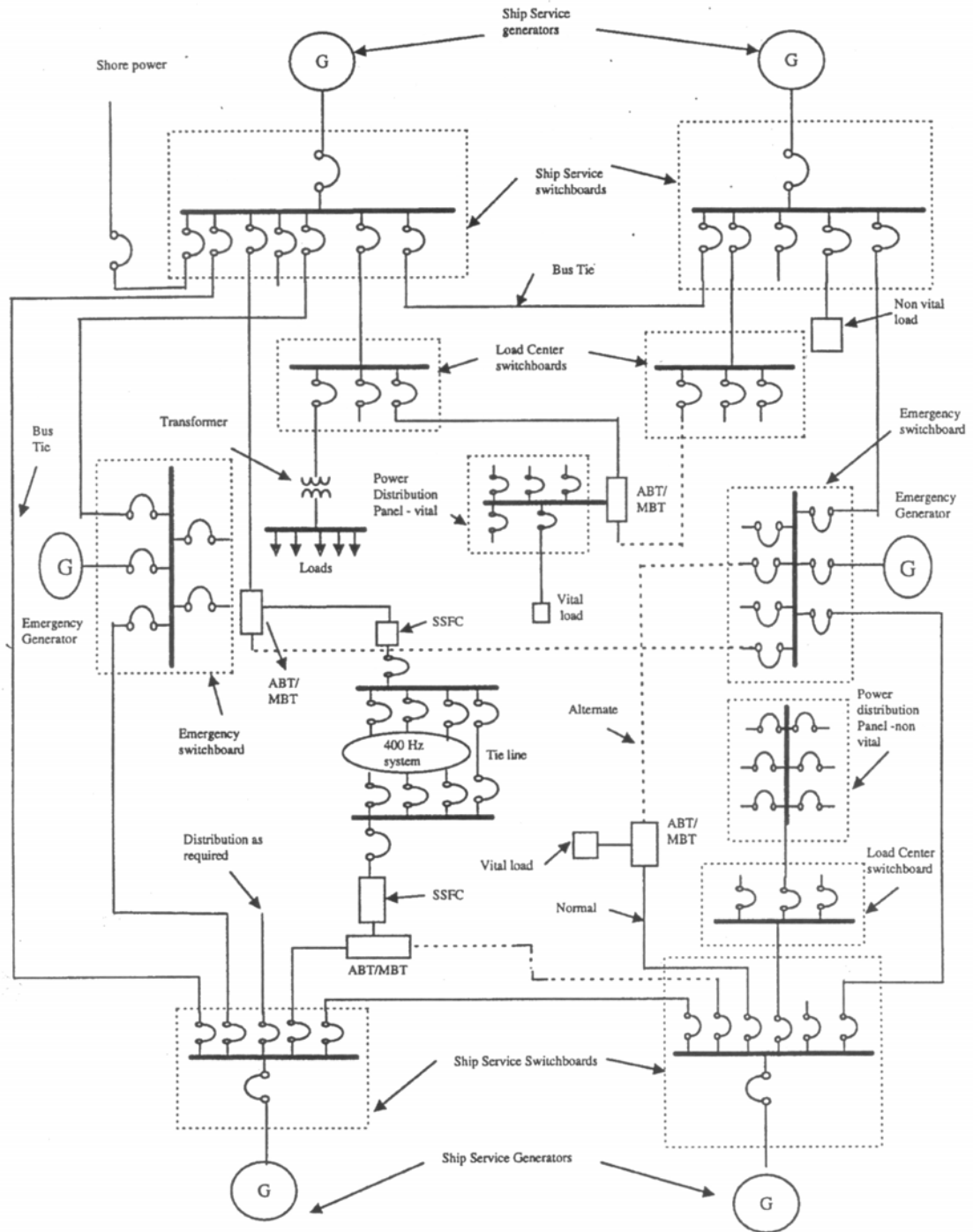


Figure 3.1 A Typical AC Radial SPS [48]

The reconfiguration phenomenon in SPS is divided into three types. They are static reconfiguration, mission reconfiguration, and dynamic reconfiguration. Static reconfiguration implies the choosing of the actual shipboard power architecture but also includes platform performance upgrades by means of software and open architecture based upgrades [50]. Mission reconfiguration means a change in platform state in response to varying readiness conditions such as cruise, on-station, anchor, battle, etc [50]. Dynamic reconfiguration is a platform response to assure electric power to vital loads during damage or failure [50]. Dynamic reconfiguration commonly occurs during rapidly changing conditions such as battle. Dynamic reconfiguration is the type of reconfiguration that was studied in this dissertation.

In the event of battle, various weapons might attack the ship. When a weapon hits a ship, it can cause damage to the electrical system on the ship. The effects of damage to the SPS comprise open and short circuits from damage to equipment [48]. Two types of dynamic reconfiguration are being studied by researchers in the Power System Automation Lab (PSAL). They are restorative reconfiguration and predicative reconfiguration. Reconfiguration operations change the open/closing status of circuit breakers, bus transfers, and low voltage protective devices. The multiple closing/opening of switches and protective devices changes system configuration and reduces the system loss caused by damage.

For power systems, the process of a system being disturbed can be subdivided into three stages: pre-disturbance, disturbed, and post-disturbance [2]. A power system is initially operating at an operating point. After being subjected to disturbances, the system could regain or lose a state of operating equilibrium. For dynamic reconfiguration of SPS, disturbances include the effects of damage, such as open circuits and short circuits, and reconfiguration operations. The pre-disturbance stage during SPS reconfiguration is up to the instant when the first disturbance occurs. The post-disturbance stage during SPS reconfiguration is from the instant when the last disturbance occurs. The disturbed stage during SPS reconfiguration is the transient process after the pre-disturbance stage and before the post-disturbance stage.

Stability is an important condition for the success of reconfiguration. During SPS reconfiguration, an SPS starts from steady state at the pre-disturbance stage, experiences the transient process at the disturbed stage and finally settles down to steady state at post-disturbance stage. Stability during reconfiguration studies if a SPS will settle down to a state of operating equilibrium at the post-disturbance stage. If instability occurs during reconfiguration, a SPS would move to some unknown state. Instability is undesirable during the operation of a SPS. Therefore, SPS stability should be analyzed and assessed before any reconfiguration operation is undertaken.

In this section, shipboard power systems and reconfiguration are introduced. This dissertation concentrates on stability during dynamic reconfiguration. The complexity of a system model and analysis methods for stability studies depends on the type of a stability problem and the characteristics of the system studied. In section 3.2, SPS dynamics will be categorized according to the results of time frame analysis. In section 3.3, some salient features of SPS will be presented. The effects of the features on stability will be discussed. Based on the classification of SPS dynamics and the features of SPS, the stability problems during SPS reconfiguration will be formulated in section 3.4. Two types of stability issues in SPS, angle stability and voltage stability, will be analyzed. Voltage stability problems will be shown to be the main stability problems. Four factors affecting voltage stability during reconfiguration in SPS will be analyzed. Static and dynamic analysis can be applied for voltage stability analysis. Considering static or dynamic effect on voltage stability, the four factors affecting voltage stability can be analyzed in static or dynamic analysis.

3.2 TIME FRAME ANALYSIS OF SPS DYNAMICS

With appropriate categorization of stability problems, we can emphasize key elements that affect stability studies. Time spans or time frames of dynamics can be used to classify stability problems. Time frames of power system stability problems for conventional utility power systems are given in and [51]. Detailed time frames of voltage stability problems for conventional utility power systems can be found in [20].

Classifications of stability problems for conventional systems can be found in [2]. The larger a disturbance, the longer the duration of the dynamics due to the disturbance. Due to different time frames, stability problems can be classified into small signal or dynamic stability, transient stability, or long-term stability. Small signal and transient stability can be grouped under short-term stability [2]. The time frame of small signal stability or dynamic stability is up to one second, the time frame of transient stability is from one to ten seconds, and the time frame of long-term stability is from ten seconds to tens of minutes.

Figure 3.2 shows the time frames of relevant dynamics in AC SPS. Electronic transients are defined as the sudden turn-ons of an electronic type load such as radar high voltage direct current power supplies or the sudden turn-offs of a radar system by its protective device [52]. Military specification requires that the voltage at the terminals of the electronic loads recover and stay within the steady state regulation band within 0.02 second after application of the loads. In the design of a future generation of shipboard power system PEBB (Power Electronic Building Blocks), it is suggested that switching frequencies of Pulse Width Modulator (PWM) used for a wide range of inverter and rectifier applications reduces as power rating of the associated load increases [53]. The switching frequencies should be 200HZ, 2KHZ, and 20KHZ with different power ratings. The time frame of switching surges of PWM is from 0.005s to 50us. The stability of transients of electronic loads and switching surges thus belongs to dynamic stability. The time frames of the dynamics caused by machines, fast controllers, protective devices, faults and generator removal last no more than ten seconds. The corresponding stability problems thus fall into the categories of dynamic and transient stability. The time frames of the dynamics caused by slow controllers, nonlinear limits, load shedding and incremental loading for restoration could be several minutes. The time frames of load increasing on ships are in a ship's lifetime. The stability of dynamics caused by load shedding, incremental loading for restoration, slow controllers, nonlinear excitation limits, and load increasing thus belongs to long-term stability.

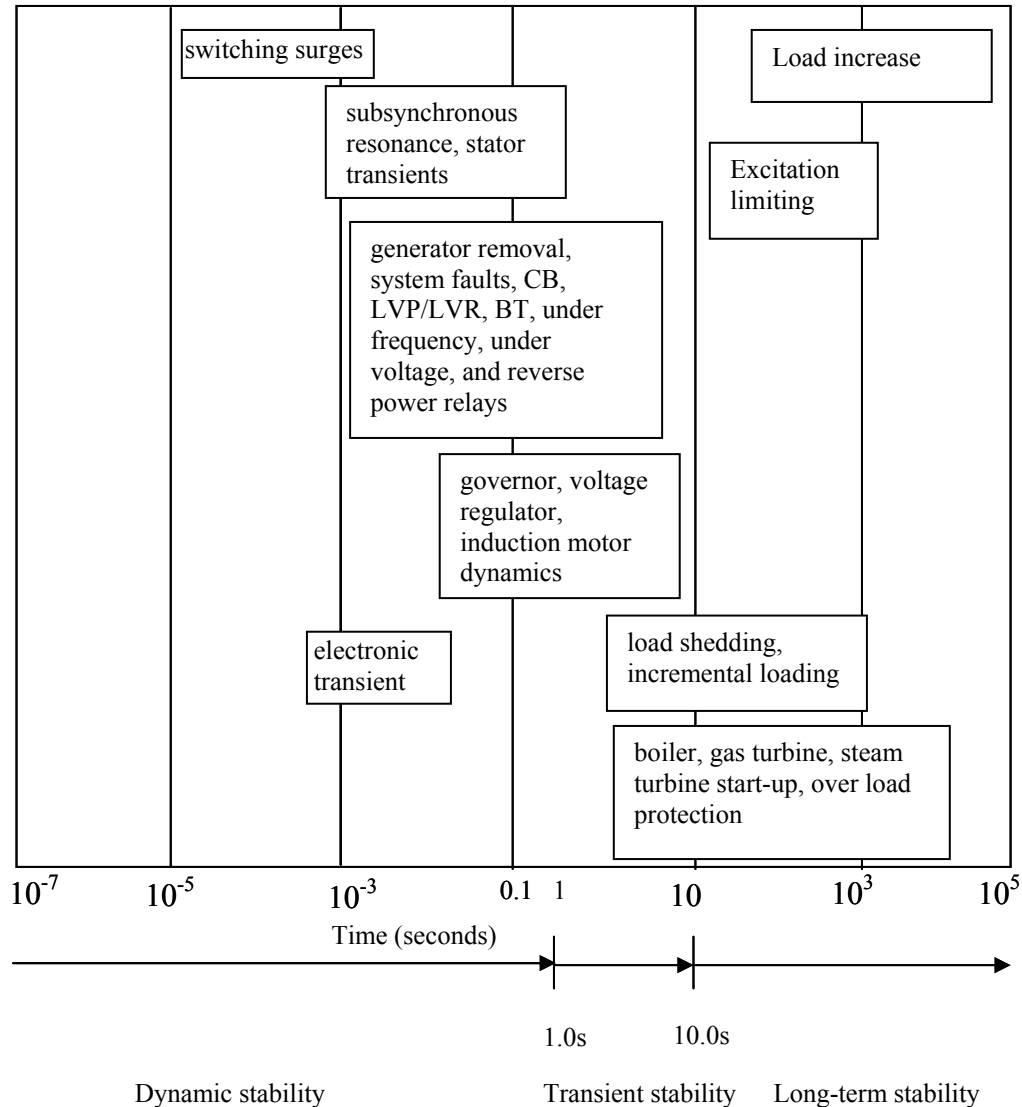


Figure 3.2 Time Frames for Dynamics of AC Shipboard Power Systems

Time constants of stators and rotors of machines in SPS, including generators and induction motors, determine the time frames of machine dynamics. Similarly, time constants of controllers in SPS determine the time frames due to controller dynamics. The response of some controllers in SPS, such as governors and automatic voltage regulators (AVR) take several seconds. These controllers are fast controllers. The response of some other controllers in SPS, such as prime movers, including boilers and

gas turbines, could normally take several minutes. These controllers are slow controllers. If a voltage controller has nonlinear excitation limits, the response of the limits may take several minutes or even longer.

The response time of protective devices in SPS, including CBs, LVs and BTs, determine the time frames of dynamics caused by protective devices. To derive the time frame of these dynamics, a two-generator system was modeled. The two generators were connected by one line. Simplified component models for generators and lines were then used for the analysis for faults and generator removal. Response time curves for faults given in [54] were applied to derive the time frames of line-to-line faults, double line-to-ground faults, and three-phase ground faults, respectively. Response time curves for generator removal given in [54] were used to obtain the time frame of generator removal.

The process of some operations determines the time frame of the dynamics caused by these operations. Load shedding in SPS due to overloaded generators can be divided into several stages. It may take several minutes to complete the whole process. Reconfiguration operations for restoration bring de-energized loads back on line. The incremental loading due to restoration could last for minutes or hours. On a Navy ship, the load profile increases continuously over a ship's lifetime. Historically, loading could increase twenty percent during the lifetime of a ship [1].

Comparing the time frames given in [2] and [20], most SPS dynamics have the same time frames as utility power systems. However, the time frame of subsynchronous resonance of SPS is different from that of utility power systems. To determine the time frame for subsynchronous resonance, a one-generator system was modeled. The simplified mechanical and electrical systems of the generator in the system were used. The frequency range of subsynchronous resonance of SPS was derived following the approaches in [55]-[58]. Due to the low inertia of generators in SPS, the derived frequency range of SPS was smaller than the frequency range of utility power systems. Therefore, the time frame of subsynchronous resonance in SPS is longer than that in utility power systems.

Reconfiguration comprises a set of control actions to change the system configuration and transfer loads. Reconfiguration operations could cause dynamics in SPS, such as the dynamics of generators, loads, controllers, and protective devices. As seen in Figure 3.2, these dynamics occurring during reconfiguration could fall within the areas of dynamic stability, or transient stability. During dynamic reconfiguration, SPS may need to respond to major disturbances, such as a hit by weapons. Under this condition, the slow dynamics of equipment in SPS, such as start up of generators, may be taken into consideration. Some reconfiguration, such as reconfiguration for restoration, could be undertaken in several stages. The corresponding reconfiguration operations are thus taken sequentially in the long-term. Consequently, the time frames of individual dynamics involved in reconfiguration could be short-term (including dynamic or transient periods). However, considering the longest possible dynamic response during the process of reconfiguration, the stability study during reconfiguration thus falls into the category of long-term stability. The stability study occurring during reconfiguration extends beyond the time frame of transient stability to include, in addition to fast dynamics in short-term periods, the effects of slow dynamics in the long-term.

3.3 SPS SALIENT FEATURES

SPS are special power systems. Generally, an SPS is a small isolated or island electric power system, relatively small and isolated from neighboring power systems electrically. Features of isolated and island power systems can be found in studies [1][37][43]-[48][59]-[62]. Some salient features of SPS and their effects on SPS stability studies are discussed as follows:

--- The generation of SPS has limited capacity and inertia, and lacks support from neighboring power systems. Being small and isolated from other power systems makes SPS susceptible to disturbances. Deviations of bus voltages and system frequency from nominal values due to disturbances could be large.

Due to this feature, some common sense experience used in utility power system stability analysis would not apply in SPS. In utility power systems, the inertia of a

critical generator is much smaller than the total inertia of the rest of the machines of the system. An infinite bus thus is able to represent the rest of the system in angle stability analysis. The number of machines in SPS is limited. The finite inertia amount of one generator is comparable to the total inertia of the other machines in SPS. Thereby, the concept of infinite bus is not applicable for SPS stability analysis.

--- Connecting cables are short in length and transmission is thus not as significant as for utility power systems. Shunt capacitance on cables is small. Cables thus have small electrical time constants, and electrical transients on cables are short. Due to the short cable, the electric transients on networks of SPS are very short and can be neglected [18].

Due to the short connecting cables between components, SPS is tightly coupled. The generators on ships are strongly synchronized. Due to the tight coupling, interactions between types of equipments (for example, interactions between controllers and induction motors) are strong. The strong interactions would affect controller dynamics and may even cause instability. To observe complete interactions in such a tightly connected power system, detailed component models should be employed in SPS stability analysis.

--- Induction motors are predominant in SPS. In utility power systems, motors take approximately fifty-seven percent of consumed power, and ninety percent of motors are induction motors [20]. On ships, induction motors make up approximately seventy-eighty percent of total loads [1]. In SPS, it is possible that generators may be connected to several paralleled large induction motors. With a large amount of induction motors loads, SPS stability analysis and assessment require careful consideration of the characteristics of induction motors.

Induction motors increase nonlinearity in system models and could have adverse effects on controller dynamics. The response speeds of induction motors, determined by a motor's inertia and rotor flux time constant, are comparable to the speed of response of voltage controllers. The motor dynamics may thus affect the functions of voltage controllers adversely. For example, the negative damping of induction motors may

induce unstable oscillatory voltage stability in power systems [26]. In such a tightly coupled system as SPS, the interactions between motors and controllers are thus greater. Higher order models of induction motors may be required to determine the detailed effects of dynamic loads on SPS stability.

If the load torque of a motor exceeds the electrical torque, the motor decelerates. If the load torque exceeds the maximum electrical torque of a motor, the motor could stall or become unstable. Motor instability belongs to the study of voltage instability [2][6][20]. In SPS, due to the small inertia, the speed reduction of motors is large. The greatly reduced motor speed would impose large, low power factor “starting currents” on the network after the causes of deceleration are removed and motors reaccelerate. The more motor speeds are reduced, the larger the reaccelerating currents. The reaccelerating currents are the largest when Black Start starts to occur. If the network is not strong enough to reaccelerate the motors, system voltage would be depressed and motor speeds would continue to decay. The large amount of current drawn by stalled motors would reduce system voltage even further and cause motor stalling elsewhere in the system, thereby giving rise to cascaded motor stalling [63][64]. The stalling of large induction motors and cascaded motor stalling may induce system wide voltage collapse.

--- An SPS has fast controllers to maintain system frequency and voltage. The fast controllers could pull voltages and frequency in a disturbed system back within the allowable ranges quickly. For fast controllers, the overshoot of a controller would be sacrificed to achieve the prompt control. In SPS, negative damping generated by fast response controllers could cause oscillatory instability.

Basically, an SPS is a system susceptible to disturbances and includes a predominant number of induction motor loads. The salient features of SPS should be considered for modeling SPS appropriately. These salient features are important for the stability analysis and assessment of AC SPS.

3.4 STABILITY ISSUES IN SPS

According to the physical nature of stability problems, they belong to two types: angle stability and voltage stability. In this section, both of these types of stability problems will be discussed as they apply to AC SPS.

3.4.1 Angle Stability

Angle stability is the ability of a power system to maintain synchronism when subjected to disturbances [2]. If the angular separation between the synchronous generators in a system remains within certain bounds, the system maintains synchronism. Any instability that may result occurs in the form of increasing angular swings of some generators, leading to their loss of synchronism with other generators. The angle stability problem is one of holding disturbed generators in synchronism with the remaining generators.

Angle stability studies the electromechanical oscillations inherent in power systems. The electromechanical equation of a synchronous generator can be described by (3.1).

$$\frac{d^2 \delta}{dt^2} = \frac{1}{2H} (P_M - P_E) \quad (3.1)$$

where δ is the rotor angle, ω is rotor speed. P_M is the mechanical power, and P_E is the electrical power. H is the inertia constant. The electrical power P_E is a function of bus voltages and admittance between buses. Based on (3.1), for a power system having two finite generators, the angle difference between the two finite generators could be solved by (3.2) [65]. Subscripts 1 and 2 indicate variables associated with generators 1 and 2.

$$\frac{H_1 H_2}{H_1 + H_2} \frac{d^2 \delta_{12}}{dt^2} = \frac{H_2 P_{M1} - H_1 P_{M2}}{H_1 + H_2} - \frac{H_2 P_{E1} - H_1 P_{E2}}{H_1 + H_2} \quad (3.2)$$

$$\delta_{12} = \delta_1 - \delta_2 \quad (3.3)$$

The mechanical power of each generator is determined by the load assigned to the generator and normally assumed to be constant during a transient angle stability study. When a generator is disturbed, the electrical power would increase or decrease, and the

generator would decelerate or accelerate correspondingly. The angle difference between accelerating generators and decelerating generators could increase. If the angle difference is over a certain limit, the system becomes unstable. From (3.1), it can be seen that angle stability is the ability to maintain or restore equilibrium between electromagnetic torque and mechanical torque of each synchronous generator in a system.

All ship designs are provided with multiple ship service generators, designed to be operated either in split or parallel modes. Parallel operation is emphasized during normal operation to provide for continuity of power while minimizing the magnitude of system voltage and frequency variations [45]. Split operation is used when maximum reliability of ship service power is required and is normally used during battle conditions to avoid cascading failures of the entire electric plant [45]. Split plant operation has generators operating independently, with each generator serving different groups of electrical loads [45]. Since generators operate independently in split operation, angle stability is only of concern for generators in parallel operation. Angle stability studies the synchronism between multiple generators. Parallel operation of the AC generators in Figure 3.1 is illustrated in Figure 3.3. The generators are considered to be paralleled by the associated switchboards.

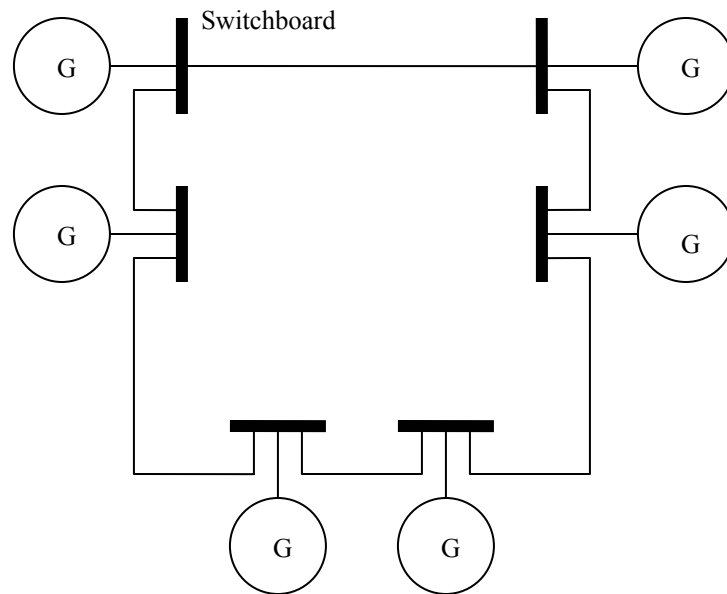


Figure 3.3 Illustration of Parallel Operation of Generators in Figure 3.1

As described earlier, the generators of SPS have finite inertia. An SPS with two generators can thus be analyzed by (3.2). From (3.2), it can be seen that the mechanical and electrical power determines the angle difference between generators. For generators in SPS, governors are installed to adjust steam or fuel to prime movers. Using governors, paralleled generators divide the total load between the various units installed according to the capacities of the generators [65]. Generators in SPS are designed to have the same capacity. Loads are thus divided equally between the generators. Due to the equal load sharing in SPS, the mechanical power of the paralleled generators is equal. (3.2) thus can be rewritten as (3.4). Constant H represents the same inertia of the two finite generators.

$$\frac{d^2 \delta_{12}}{dt^2} = -\frac{1}{2H} (P_{E1} - P_{E2}) \quad (3.4)$$

As described earlier, the electrical power of a generator is the function of the voltage at buses and admittance between buses. The generators are considered to be paralleled at their switchboards and thus have the same terminal voltages. Due to limited space, the

lengths of cables between buses to the paralleled generators are of the same order of magnitude. Any disturbance downstream in the generator switchboards affects each generator almost equally. Therefore, the electrical power difference $P_{E1} - P_{E2}$ in (3.4) is very small.

Power tending to bring the generators into synchronism is termed synchronizing power. If generators operating in parallel get out of synchronism, there is a circulating current between the paralleled generators. The circulating current flows between the armatures of the paralleled generators. Because the armature reactance of generators is larger than the armature resistance, the circulating current is in phase with the leading or accelerating generators. The leading generators then pump electrical power into the lagging generators. The accelerating generators tend to slow down while the decelerating generators tend to speed up. The circulating current thus tends to pull the out of synchronism generators in parallel operation back into synchronism. It is concluded that the synchronizing power between paralleled generators is strong [66]. The disturbances in SPS thus have little tendency to make the paralleled generators lose synchronism.

From the analysis earlier, it was found that the most severe disturbances from the standpoint of angle stability analysis are the disturbances that make load distribution unevenly or occur closely to one generator. In SPS, load distributions are even between generators, and any disturbance downstream of the generator switchboards has similar closeness to the generators. Angle stability of SPS then could be affected by relatively more severe disturbances, such as short circuits upstream of the generators. However, when the disturbance occurs at the terminal of a generator, the voltage and frequency excursions of generators in SPS are large. In SPS, large excursion of voltage and frequency could trip the breakers on switchboards and split generators. For example, the Synch Monitor would prevent the paralleling of generators unless the frequency deviation is less than two percent, the voltage deviation is less than five percent, and the angle difference is less than 30 degrees [49]. The system would go into split operation before it becomes unstable.

In summary, synchronism between generators in tightly coupled SPS is strong. The synchronism is further strengthened by the parallel operation of the generators. Angle stability is thus not the main concern for SPS stability.

3.4.2 Voltage Stability

In this section, we will focus on the other type of stability problem: voltage stability in SPS. First, the concept and classification of voltage stability will be described. Bifurcation in voltage stability analysis then will be discussed. Finally, the factors affecting voltage stability in SPS will be analyzed.

3.4.2.1 Definition and Classification of Voltage Stability

Voltage stability is the ability of a power system to maintain steady acceptable voltages at all buses in the system under normal operating conditions and after being subjected to a disturbance [2][20]. A power system in a given operating state and subject to a given disturbance is voltage stable if voltages near loads approach post disturbance equilibrium values. The main factor causing voltage instability is the inability of the power system to meet the demand for reactive power in the stressed systems in order to keep desired voltages [2][20]. Voltage instability occurs if a power system is stressed or the consumed reactive power is too large to be compensated by supplied reactive power.

A power system becomes unstable when voltages decrease below a certain level. Voltage instability stems from the attempt of load dynamics to restore power consumption beyond the capability of the combined transmission and generation system [20]. Two types of voltage stability problems can be observed in power systems. These are voltage collapse and unstable voltage oscillation. A power system in a given operating state and subject to a given disturbance undergoes voltage collapse if post-disturbance equilibrium voltages are below acceptable limits [20]. Voltage collapse is usually the result of a sequence of events leading to a low-voltage profile in a significant

part of the power system [2]. Unstable voltage oscillation is often associated with the interactions of controllers and equipment in a power system [2].

For the purpose of analysis, voltage stability can also be classified into small and large disturbance types [2]. Small disturbance voltage stability considers the ability of a power system to control voltage after small disturbances [2]. The power system can be linearized around an operating point and system stability is analyzed based on the linear system. Large disturbance voltage stability analyzes the response of the power system to large disturbances such as system faults, loss of generation, or circuit contingencies [2]. Determination of large-disturbance voltage stability requires the examination of the nonlinear response of the power system over a period of time sufficient to capture the performance and interactions of loads and devices such as induction motors, generator excitation limiters, and voltage controllers. Large disturbance voltage stability can be studied by using nonlinear time domain simulations in short-term periods and static analysis in the long-term [6]. The study period of large disturbance voltage stability may extend from a few seconds to tens of minutes.

According to the time frames of the dynamics of interest, the time frames of voltage stability problems may vary from a few seconds to tens of minutes. Voltage stability problems can thus be separated into short-term and long-term problems [2]. As described in section 3.2, stability problems can be classified into small signal, transient, and long-term problems. Short-term voltage stability comprises small signal and transient stability, such as the stability of the dynamics of induction motors and interactions between components. The study period of short-term voltage stability is in the order of several seconds. Long-term stability involves long-term dynamics, such as dynamics due to generator excitation limit and load increase. The study period of long-term voltage stability may extend to several minutes.

3.4.2.2 Time Scale Decomposition

As described earlier, the process of a system going from being reconfigured to settling down to a steady state or becoming unstable could be a long one. In SPS,

reconfiguration operations change system configurations and cause dynamics. The changes of configuration of SPS are abrupt and are represented by algebraic equations. All dynamics caused by reconfiguration operations can be modeled by differential equations. In contrast to the fast variables of the algebraic equations, the state variables of the differential equations can not change abruptly and constitute relatively slower variables.

The dynamics caused by reconfiguration operations can thus be decomposed into fast and slow dynamics based on time scales of short-term and long-term modes. Short-term voltage stability includes small signal and transient voltage stability. In Figure 3.2, short-term voltage stability is featured by components, such as induction motors and the voltage controllers of synchronous generators. The study period of interest is in the order of several seconds. When short-term dynamics have died out some time after disturbances, the system enters a slower time frame. As seen in Figure 3.2, long-term voltage stability involves slower dynamics such as load increase and excitation limiting. The study period of interest may extend to several minutes.

As described in Chapter II, any power system can be modeled by a set of nonlinear Differential-Algebraic-Equations (DAE). In DAE, dynamics are modeled by differential equations. For a system with two time scales, dynamics in the system can be decomposed into fast and slow dynamics and the corresponding state variables can be decomposed into fast and slow variables [6][67]. The differential equation shown as (2.1) is thus decomposed into (3.5) and (3.6), which describe the fast state variables \mathbf{x}_f and the slow state variables \mathbf{x}_s , respectively.

$$\dot{\mathbf{x}}_s = \mathbf{f}_s(\mathbf{x}_f, \mathbf{x}_s, \mathbf{y}) \quad (3.5)$$

$$\varepsilon \dot{\mathbf{x}}_f = \mathbf{f}_f(\mathbf{x}_f, \mathbf{x}_s, \mathbf{y}) \quad (3.6)$$

where \mathbf{x}_s is the slow state vector and \mathbf{x}_f is the fast state vector. ε is a very small number. (3.6) is the singular perturbation for fast state variables \mathbf{x}_f .

When ε is close to zero, differential equation (3.6) can be approximated by the algebraic equation shown as (3.7). The system modeled by (2.1) and (2.2) can then be approximated by (3.7)-(3.9).

$$\dot{\mathbf{x}}_s = \mathbf{f}_s(\mathbf{x}_f, \mathbf{x}_s, \mathbf{y}) \quad (3.7)$$

$$\mathbf{0} = \mathbf{f}_f(\mathbf{x}_f, \mathbf{x}_s, \mathbf{y}) \quad (3.8)$$

$$\mathbf{0} = \mathbf{g}(\mathbf{x}_f, \mathbf{x}_s, \mathbf{y}) \quad (3.9)$$

Equations (3.7)-(3.9) are thus the Quasi-Steady-State (QSS) representations of a system having two differential time scales. QSS captures the snapshots of system conditions at slow time frames along the time-domain trajectory [2].

3.4.3 Bifurcation for Voltage Stability Study

Power systems are basically nonlinear systems. It is thus natural that nonlinear analysis techniques such as bifurcation theory are used to study power system voltage stability. With system variables decomposed into fast and slow variables, bifurcation analysis assumes slowly varying variables as parameters, and it describes qualitative changes of stability with changes of parameters [6]. It is noted that an assumption for bifurcation theory is that parameters should change slowly. Along a trajectory of a system moving with parameters, voltage instability occurs at bifurcation points. In this section, the application of bifurcation theory on voltage stability will be discussed. Power Voltage (PV) curves are useful for conceptually analyzing and understanding voltage stability, and will aid the illustration of the application of bifurcation theory to voltage stability.

3.4.3.1 Power System Models for Bifurcation

According to time scale decomposition shown in section 3.4.2.2, (2.1) and (2.2) can be rewritten as (3.7)-(3.9). If the slowly changing variables \mathbf{x}_s are considered as

parameters \mathbf{p} , a set of parameter dependent DAE shown as (3.10) and (3.11) can be used to model the system dynamics for voltage stability analysis [6].

$$\dot{\mathbf{x}} = \mathbf{f}(\mathbf{x}, \mathbf{y}, \mathbf{p}) \quad (3.10)$$

$$\mathbf{g}(\mathbf{x}, \mathbf{y}, \mathbf{p}) = 0 \quad (3.11)$$

where \mathbf{x} is a vector of state variables, \mathbf{y} is a vector of algebraic variables, and \mathbf{p} is a vector of parameters. The equilibrium points for a system modeled by (3.10) and (3.11) should satisfy (3.12) and (3.13).

$$\mathbf{0} = \mathbf{f}(\mathbf{x}_e, \mathbf{y}_e, \mathbf{p}_e) \quad (3.12)$$

$$\mathbf{g}(\mathbf{x}_e, \mathbf{y}_e, \mathbf{p}_e) = \mathbf{0} \quad (3.13)$$

In power systems, solving DAE shown as (3.10) and (3.11) is complicated. First, the algebraic variable \mathbf{y} should be solved from (3.11) in the form of state variable \mathbf{x} and parameter \mathbf{p} and substituted into (3.10). After the algebraic variable \mathbf{y} has been eliminated from (3.10), the set of DAE is reduced to the differential equation shown as (3.14).

$$\dot{\mathbf{x}} = \mathbf{F}(\mathbf{x}, \mathbf{p}) \quad (3.14)$$

Bifurcation analysis for the nonlinear system should be done on (3.14). However, it is normally quite difficult in power system analysis to derive the reduced differential equations from a set of DAE. This is because the order of differential equations in power systems is normally quite high. In the analysis of nonlinear system dynamics for power systems, linearization is therefore used to get a local picture of dynamic behaviors around an equilibrium point in a nonlinear system [6]. Local bifurcations are detected from the linear system.

At each equilibrium, the nonlinear system modeled by (3.10) and (3.11) can be approximated by a system linearized around an equilibrium point. The linearized model is shown as (3.15).

$$\begin{bmatrix} \dot{\Delta \mathbf{x}} \\ \mathbf{0} \end{bmatrix} = \mathbf{J} \cdot \begin{bmatrix} \Delta \mathbf{x} \\ \Delta \mathbf{y} \end{bmatrix} \quad (3.15)$$

$$\mathbf{J}_u = \begin{bmatrix} \mathbf{f}_x & \mathbf{f}_y \\ \mathbf{g}_x & \mathbf{g}_y \end{bmatrix} = \begin{bmatrix} \frac{\partial \mathbf{f}}{\partial \mathbf{x}} & \frac{\partial \mathbf{f}}{\partial \mathbf{y}} \\ \frac{\partial \mathbf{g}}{\partial \mathbf{x}} & \frac{\partial \mathbf{g}}{\partial \mathbf{y}} \end{bmatrix} \quad (3.16)$$

The matrix \mathbf{J}_u is the unreduced Jacobian matrix of the DAE. If \mathbf{g}_y is nonsingular, we can eliminate $\Delta \mathbf{y}$ to get the reduced model as (3.17).

$$\Delta \dot{\mathbf{x}} = \mathbf{J}_r \Delta \mathbf{x} \quad (3.17)$$

$$\mathbf{J}_r = [\mathbf{f}_x - \mathbf{f}_y \mathbf{g}_y^{-1} \mathbf{g}_x] \quad (3.18)$$

In power system analysis, the matrix \mathbf{J}_r is called the reduced Jacobian matrix of the DAE. As the parameter variable p changes slowly, the system equilibrium points can be solved successively. A reduced Jacobian matrix can be built for each equilibrium point. The dynamic behaviors of a system around equilibrium points can then be analyzed through the reduced Jacobian \mathbf{J}_r evaluated at each equilibrium point. A reduced Jacobian matrix can be derived analytically or numerically. The analytical form of a reduced Jacobian matrix is difficult for large systems. In this dissertation work, numerical differentiation is used for the derivation of reduced Jacobian matrices. In the numerical differentiation method, small perturbations are applied to state variables around equilibrium points to derive reduced Jacobian matrices.

Local bifurcations may occur at any point along the path where the parameters change. At bifurcations, different trajectories of equilibrium points intersect each other, and thus either bifurcate or disappear [68]. The qualitative structure of the system (3.10)-(3.11) changes drastically through small perturbations of parameters at a bifurcation point [6]. Local bifurcation points are thus critical for dynamic stability analysis of nonlinear systems, which deal with local properties such as the dynamic stability of equilibrium points under small variations of parameters [68].

Different types of local bifurcations exist in power systems. Normally, Saddle-Node Bifurcation (SNB) and Hopf Bifurcation (HB) are studied for voltage stability. In the following sections, the theory of the SNB and HB and their applications on voltage stability analysis will be discussed.

3.4.3.2 Saddle Node Bifurcation

An SNB is a point where a pair of equilibrium points meets and disappears with a zero eigenvalue [69] as the parameters of a system are changing. One of the two equilibrium points is stable (node) while the other is unstable (saddle). The particular point is referred to as a saddle-node bifurcation. At an SNB, two equilibrium points (one with a real positive and the other a real negative eigenvalue) coalesce and disappear. There is at least one zero eigenvalue at an SNB [69].

Figure 3.4 shows how an SNB occurs with the change of a parameter in a nonlinear system. The arrow of the horizontal line shows the direction in which the parameter moves. Each plane in the figure represents a snapshot of the system along a time domain trajectory, and the parameter is constant at each snapshot. At point A, saddle node bifurcation occurs. Before point A, the system is stable. If the system is disturbed, the disturbed system goes back to the stable equilibrium point $(\mathbf{x}^s, \mathbf{y}^s)$ eventually. The stable equilibrium disappears from point A. After point A, if the system is disturbed, it would become unstable.

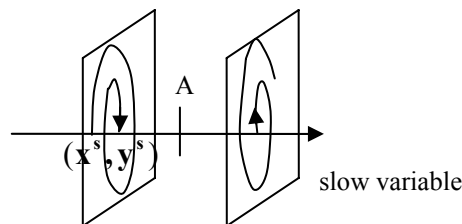


Figure 3.4 Illustration of Saddle Node Bifurcation

PV curves in Figure 3.5 conceptually explain the application of SNB for voltage stability analysis. V is the voltage at a critical or representative bus and P is the real

power at the bus. There are two PV curves for the selected bus. They are the PV curve obtained from the source and the PV curve obtained from the load. The intersections of the two PV curves are the system equilibrium points. The load power is constant in the long-term and assumed to be the slowly changing parameter for the system. P_2 is the maximum power of the source PV curve. If the load is less than P_2 , there are always two equilibrium points in the system. When the load is equal to P_1 , the two equilibrium points are S_1 and U_1 . The stable equilibrium point is S_1 and the unstable equilibrium point is U_1 . If the load increases to P_2 , the stable equilibrium and unstable equilibrium points coalesce at point X. The system at P_2 in Figure 3.5 corresponds to the system at point A in Figure 3.4 where an SNB is detected. If the load increases continuously after reaching P_2 , the system is unstable. The voltage corresponding to point X is the voltage stability limit. Detection of SNB thus could detect the voltage stability limit. It is noted that in this situation, voltage stability limit agrees with the maximum transfer limit of the system.

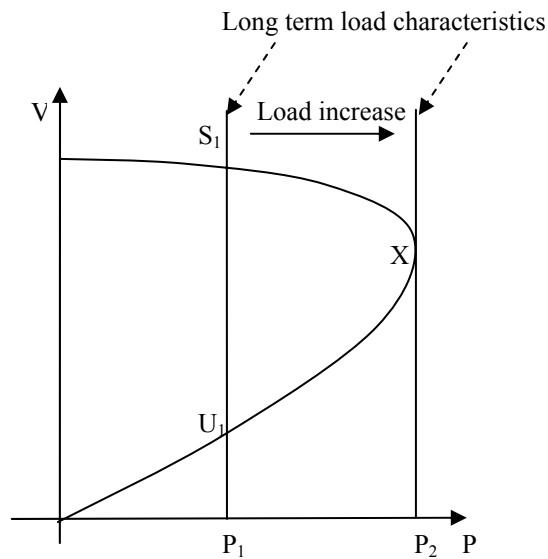


Figure 3.5 PV Curve Analysis for Saddle Node Bifurcation

In the previous example, a power system is assumed to move from one equilibrium point to another along the direction of change in the slow variables. At bifurcation points, the system becomes unstable. Between the equilibrium points, the system is assumed to be stable. Slow dynamics is thus the cause of voltage instability, and fast dynamics are assumed to die out before the system moves to the next state of the slow variable. However, between equilibrium points, fast dynamics could become unstable and cause system voltage instability before the system moves to the next equilibrium point. Fast dynamics, instead of slow dynamics, thus become the cause of voltage instability.

Figure 3.6 conceptually explains how instability could be caused by losing transient equilibrium in fast dynamics. The load power is constant in long-term and assumed to change slowly. The transient load characteristic curves are shown by dotted lines and represent fast dynamics. The straight line of long-term load characteristic has two intersections with the source PV curve. S is the stable equilibrium and U_L is the unstable equilibrium. At S, the transient load curve is $P(t)$. There are two transient equilibrium points. S is the stable transient equilibrium point, and U_S is the unstable transient equilibrium point. During the transient process, the transient load characteristic curve changes with time and the system moves along the source PV curve $P(t_1)$. If the transient process is long and the transient load characteristic curve moves to $P(t_1)$, the two transient equilibrium points coalesce at point X where the transient load characteristic curve $P(t_1)$ and the source PV curve touch. The system becomes unstable during the transient process. The voltage corresponding to the touching point X defines the voltage stability limit.

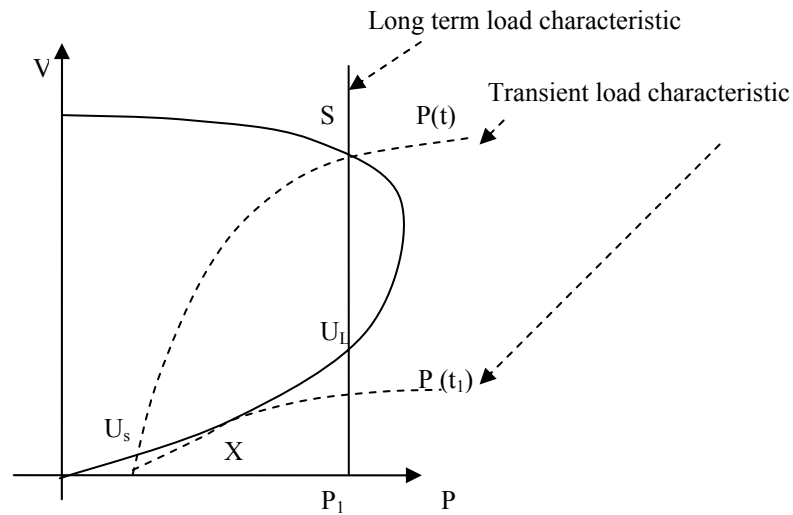


Figure 3.6 PV Curve Analysis for Losing Equilibrium of Fast Dynamics

3.4.3.3 Hopf Bifurcation

From the definition of saddle node bifurcation, an SNB is characterized by a zero eigenvalue at the origin of the complex plane. A system can become unstable following parameter variation that forces a pair of complex eigenvalues to cross the imaginary axis in the complex plane [69]. The point where a pair of complex eigenvalues crosses the imaginary axis in the complex plane is called Hopf bifurcation. At a Hopf bifurcation, the system Jacobian has a pair of eigenvalues on the imaginary axis with nonzero frequency.

At a Hopf bifurcation, the stable equilibrium becomes unstable by interacting with a periodic orbit or a limit cycle. A periodic orbit means that each state trajectory with respect to time is a periodic waveform with the same period and the state vector traverses a closed loop in the state space once every period. A periodic orbit is thus a steady state oscillation in a nonlinear system. When Hopf bifurcation occurs, a power system initially operating at a stable equilibrium typically starts oscillating. It is expected that in the vicinity of Hopf bifurcation, either stable or unstable limit cycles exist. Due to

the nature of the interaction between the stable equilibrium and the limit cycles, there are two types of Hopf bifurcation: subcritical and supercritical.

At a subcritical Hopf bifurcation, an unstable limit cycle existing prior to the bifurcation shrinks and eventually disappears as it coalesces with a stable equilibrium point at the bifurcation [69]. Figure 3.7 illustrates subcritical Hopf bifurcation in a system. In Figure 3.7, at each snapshot before point A, there is an unstable limit cycle around a stable equilibrium point $(\mathbf{x}^s, \mathbf{y}^s)$. If the disturbed system moves only within the unstable limit cycle, the system could eventually be attracted back to the stable equilibrium point and be stable. The unstable limit cycle shrinks as the system moves towards point A. At point A, the unstable limit cycle shrinks to zero and the stable equilibrium point $(\mathbf{x}^s, \mathbf{y}^s)$ becomes unstable. Any disturbance to the system would lead to oscillatory divergence of the variables in the system.

At a supercritical Hopf bifurcation, a stable limit cycle is generated at the bifurcation, and a stable equilibrium point becomes unstable with increasing amplitude oscillations, which are eventually attracted by the stable limit cycle [69]. In Figure 3.8, at point A, a stable limit cycle is generated and remains in the system after point A. After the supercritical Hopf bifurcation, the equilibrium point becomes unstable, resulting in growing oscillations toward the stable limit cycle. The voltages of the system appear stable and oscillatory. In power systems, the subcritical bifurcation is considered to be unstable as voltage oscillations are not allowed.

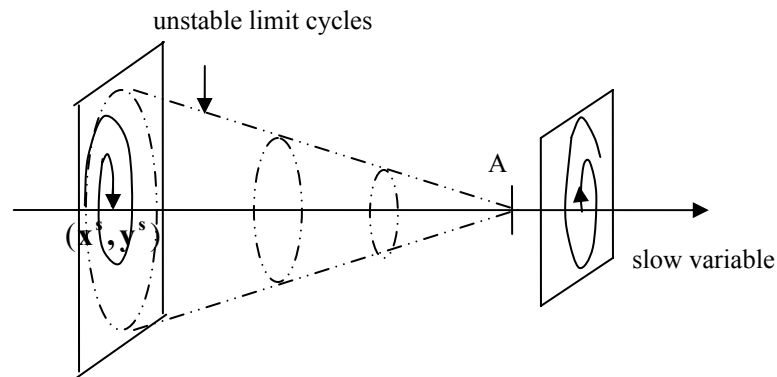


Figure 3.7 Illustration of Subcritical Hopf Bifurcation

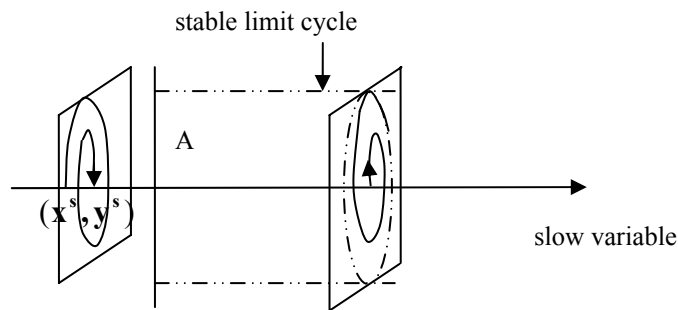


Figure 3.8 Illustration of Supercritical Hopf Bifurcation

PV curves in Figure 3.9 conceptually explain the application of Hopf bifurcation for voltage stability analysis. At each point on the PV curve, the eigenvalues of the reduced Jacobian matrix are calculated. The long-term load characteristic is constant power. When the constant load increases to P_2 , the imaginary parts of a pair of complex eigenvalues become positive. The system at S_2 in Figure 3.9 corresponds to point A in Figure 3.7 or Figure 3.8 where Hopf bifurcation occurs. The voltage corresponding to S_2 is the voltage stability limit. Hopf bifurcation can thus detect the voltage stability limit during a dynamic process. It should be noted that Hopf bifurcation normally occurs earlier than saddle node bifurcation [6]. In other words, the stability limit defined by

Hopf bifurcation is often reached earlier than the limit defined by saddle node bifurcation.

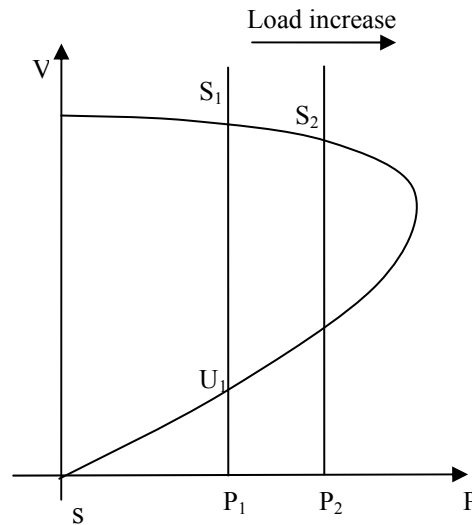


Figure 3.9 PV Curve Analysis for Hopf Bifurcation

As described earlier, instability could be caused by fast dynamics. A stability boundary exists around a stable equilibrium. Unstable limit cycles in Figure 3.7 can be explained as the stability boundaries of a system. The region within the boundary is the region of attraction where the disturbed system can be attracted back to the stable equilibrium point. In Figure 3.7, at any point before point A, there is a region of attraction around the stable equilibrium point $(\mathbf{x}^s, \mathbf{y}^s)$. If a disturbed system moves out of the stability boundary, it can not be attracted back to the stable equilibrium and becomes unstable. The system thus loses its stability before the slow variable moves to the next state.

Figure 3.6 explains how instability can be caused by losing transient equilibrium in fast dynamics. Figure 3.10 conceptually explains how instability can be caused by losing the attraction of fast dynamics. There are two intersections between source PV and long-

term load characteristic P_1 . S is the stable equilibrium. The PV curve above unstable equilibrium U is the region of attraction. If a disturbance occurs, any point above point U can draw the system back to S . During the transient process, the transient load characteristic curve can move to $P(t_1)$. If the transient process is longer, the transient load curve moves to $P(t_2)$. In Figure 3.6, the intersections of PV curve with the transient load curve $P(t_1)$ is above point U , while the intersections of PV curve with $P(t_2)$ is below U . With the transient load characteristics shown as $P(t_1)$, the disturbed system could go back to the stable operating point S . However, with the transient load characteristics shown as $P(t_2)$, the system moves out of the region of attraction and can not move back to S . The system thus loses stability due to losing the attraction of fast dynamics. A typical example of this transient instability is motor stalling after losing power exceeding its allowable time. The voltage corresponding to point U defines the voltage stability limit.

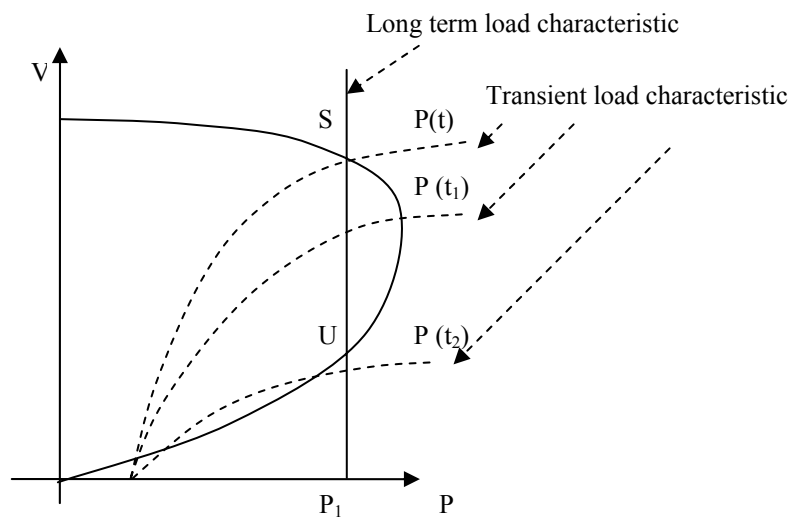


Figure 3.10 PV Curve Analysis for Losing Attraction of Fast Dynamics

As shown in Figure 3.7, when a system moves closer to HB, the stability boundary is reduced [6]. The degree of ability of a disturbance to move the system out of the stability boundary can be large at first. Gradually, the degree of disturbance becomes smaller and smaller. The instability caused by fast dynamics occurs more and more easily.

3.4.4 Factors to Affect Voltage Stability in SPS

Loads increase slowly on a ship during its lifetime. This long-term load increase can deteriorate voltage stability in SPS. System voltages may fall with load increase. The reactive power consumed by constant impedance load is less when the supplied voltage is lower. However, the reactive power consumption by induction motors increases after voltage decreases below a certain level. SPS thus become stressed as loads increase and reactive power margin reduces. During reconfiguration, the status of switches is changed to transfer loads between different paths. As described earlier, the dynamics of different magnitude and time frames could be caused by reconfiguration operations. After reconfiguration operations, a system tries to operate on a new stable equilibrium point. If the system can not operate on a stable equilibrium point, it becomes unstable.

In this section, some factors affecting SPS voltage stability for reconfiguration will be listed. The factors are loading condition, windup limit, motor stalling, and interactions between controllers and loads. The effects of these factors on voltage stability when SPS is stressed will be discussed. PV curves will be used for the conceptual analysis of voltage stability. Torque speed curves will be used for analysis where induction motors are involved.

3.4.4.1 Loading Condition

The loading conditions at buses, including load level and load factor, can change during reconfiguration. The loading condition in the post-disturbance system can be different from the loading condition in the pre-disturbance system. The static limit of

voltage stability of the post-disturbance system can be reached if the loading level increases or the load factor decreases.

The change of loading condition by reconfiguration can be illustrated in a reduced SPS shown as Figure 3.11. In Figure 3.11, a bus transfer is upstream of load1. The normal path of load1 is connected to main switchboard1 and the alternate path is connected to load center2. If a reconfiguration action transfers load1 from its normal path to the alternate path, the load level and load factor on load center2 change. The load level and load factor at the switchboard1 and load center2 change too.

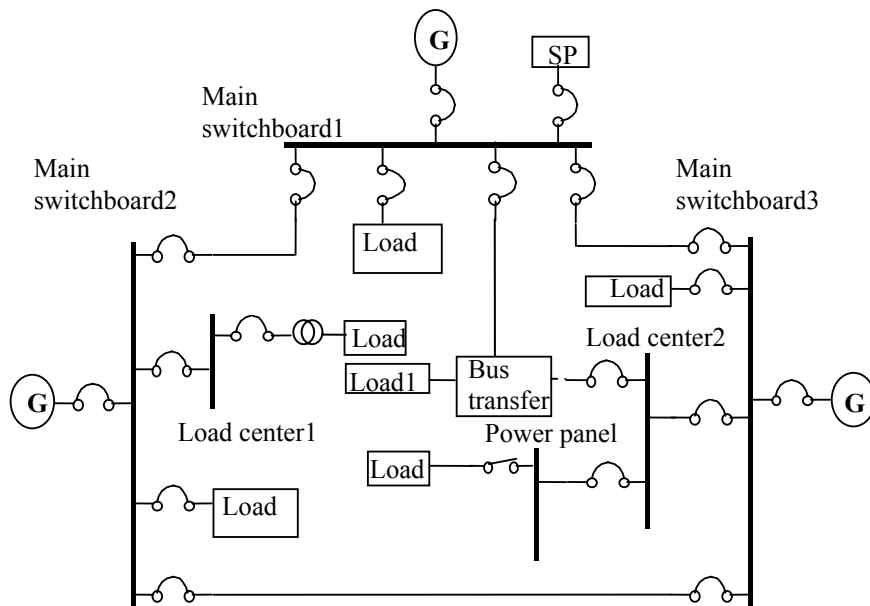


Figure 3.11 A Reduced AC Radial SPS

Figure 3.12 shows the cable between switchboard 3 and load center 2. Bus 1 corresponds to switchboard 3 and bus 2 corresponds to load center 2. The load on bus 2 is $P_2 + jQ_2$, where the real power and reactive power are P_2 and Q_2 , respectively. The resistance and reactance of the cable is R and X .

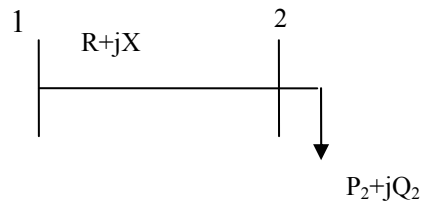


Figure 3.12 The Cable between Switchboard 3 and Load Center 2 in Figure 3.11

Figure 3.13 illustrates the voltage stability analysis when the load condition at load bus 2 in Figure 3.12 is changed. The source and load PV curves at the load bus 2 are shown in the figure. The load is assumed to be a constant power load. The source PV curve is kept the same in pre-disturbance and post-disturbance systems or can shrink from curve 1 to 2 due to a decrease in the load factor. As described earlier, detection of SNB can detect the maximum power occurring on the source PV curve.

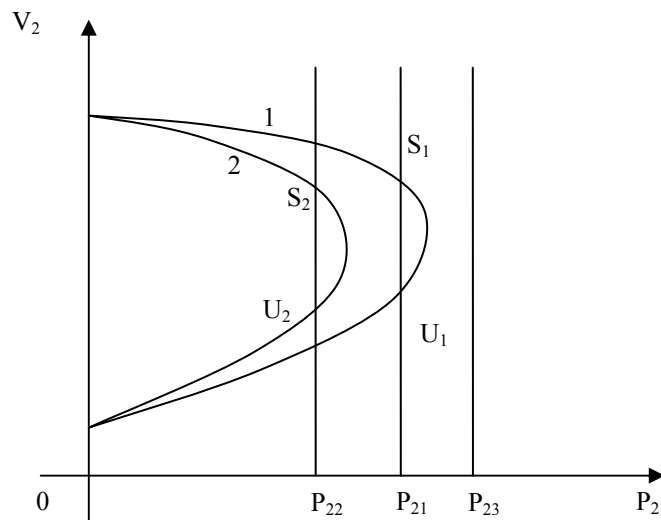


Figure 3.13 PV Curves with Different Load Factors

In the pre-disturbance system, the source PV curve is curve 1 and the load power is equal to P_{21} . The constant power load characteristic thus has two intersections to PV curve 1. Intersection S_1 represents a stable equilibrium point, while the other intersection U_1 is the unstable equilibrium point. If the load is increased to P_{23} after reconfiguration operations and the source PV curve is kept the same, there are no equilibrium points in the system. When the load power is increased to its maximum value, the two equilibrium points coalesce and saddle node bifurcation occurs. Voltage stability thus is lost at SNB.

If the load factor on bus 2 decreases, the source PV curve of the post-reconfiguration system shrinks and static limit is reduced. Some reconfiguration operations involve load shedding. If the PV curve of the post-disturbance system shrinks to curve 2 due to change in the loading factor and the constant power at bus 2 is reduced from P_{21} to P_{22} at the same time, there are equilibrium points S_2 and U_2 in the post-disturbance system. If the load level does not change, then there is no intersection between PV curve 2 and the constant power load characteristic. Saddle node bifurcation thus occurs and the system thus loses its voltage stability.

3.4.4.2 Windup Limit in AVR

Synchronous generators are the main reactive power suppliers on ships. The terminal voltage magnitudes of the generators are determined by the field excitation voltage provided by the excitation systems of the generators. In SPS, automatic voltage regulators (AVRs) are installed on generators. AVRs on generators sense the terminal voltage of generators and adjust the excitation fields of generators. However, there are some nonlinear limiters in AVRs, and the excitation fields of the generators are limited by these limiters.

The diagram of an IEEE type II AVR is illustrated in Figure 3.14 [18] and [19]. A nonlinear windup limiter exists in the regulator to limit the output variable V_R . If the value of V_R is larger than the upper limit $V_{R_{max}}$, the output of the windup limit is equal

to $V_{R\max}$. If the value of V_R is lower than the lower limit $V_{R\min}$, the output of the windup limit is equal to $V_{R\min}$.

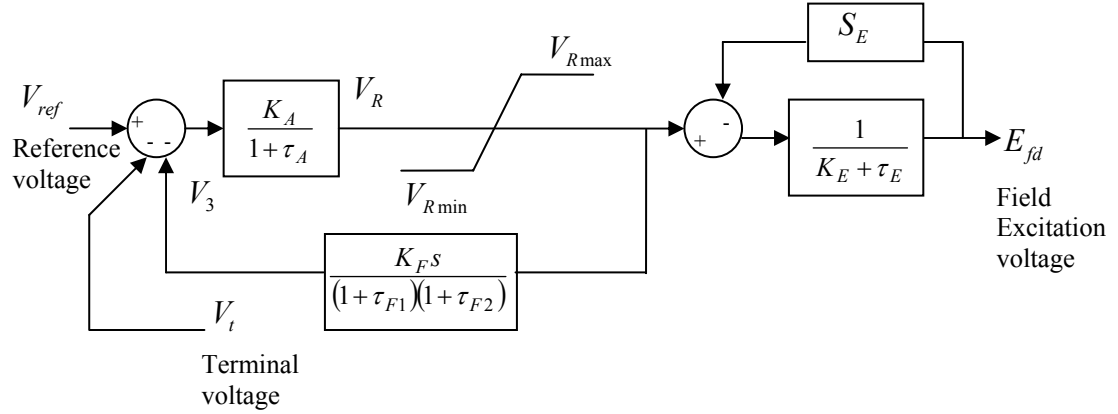


Figure 3.14 IEEE Type II AVR

The mathematical representation of the AVR in Figure 3.14 is shown as (3.19)-(3.22). S_E is the saturation function and can be approximated by a constant [70]. For sufficiently small E_{fd} , the excitation field is linear, and S_E is assumed to be zero.

$$\dot{V}_R = \frac{K_A}{\tau_A} (V_{ref} - V_1 - V_3) - \frac{1}{\tau_A} V_R \quad (3.19)$$

$$\dot{E}_{fd} = \frac{1}{\tau_E} V_R - \frac{K_E + S_E}{\tau_E} E_{fd} \quad (3.20)$$

$$\ddot{V}_3 = \frac{K_F K_A}{\tau_{f1} \tau_{f2} \tau_A} (V_{ref} - V_1 - V_3) - \frac{K_F}{\tau_{f1} \tau_{f2} \tau_A} V_R - \frac{\tau_{f1} + \tau_{f2}}{\tau_{f1} \tau_{f2}} \dot{V}_3 - \frac{1}{\tau_{f1} \tau_{f2}} V_3 \quad (3.21)$$

$$\dot{V}_3 = \dot{V}_3 \quad (3.22)$$

When the upper limit of the windup limit in Figure 3.14 is reached, V_R becomes a constant. The diagram of the regulator when $V_{R\max}$ is hit is shown in Figure 3.15. In

Figure 3.14, the magnitude of terminal voltage V_t is measured and adjusted to be a constant as close to V_{ref} as possible. However, in Figure 3.14, with V_R as a constant, the function blocks adjusting V_t in the AVR disappear, and the constant terminal voltage of generators can no longer be maintained.

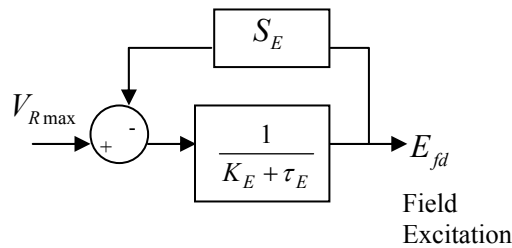


Figure 3.15 IEEE Type II AVR with Excitation Limit Reached

The mathematical representation of the AVR in Figure 3.15 can be written as (3.23). At steady state, the excitation field voltage E_{fd} is solved as (3.24), which is also the maximum excitation field voltage. Similarly, when the lower limit $V_{R\min}$ is reached, the excitation field voltage is the minimum shown as (3.25). It is shown from (3.24) and (3.25) that a constraint exists between the maximum values of $E_{fd\max}$ and $V_{R\max}$ or the minimum values of $E_{fd\min}$ and $V_{R\min}$.

$$\dot{E}_{fd} = \frac{1}{\tau_E} V_{R\max} - \frac{K_E + S_E}{\tau_E} E_{fd} \quad (3.23)$$

$$E_{fd\max} = \frac{V_{R\max}}{K_E + S_E} \quad (3.24)$$

$$E_{fd\min} = \frac{V_{R\min}}{K_E + S_E} \quad (3.25)$$

In the earlier analysis, it was shown that reactive power limits of generators are related to windup limits in voltage controllers. When system voltages decrease as loads

increase or faults occur in the system, generators produce more reactive power to maintain terminal voltages on the generators. When the limits of these controllers are encountered as the generator reactive output increases, the terminal voltages of the generators are no longer constant and the inner voltage of the generators becomes constant. The inner reactance of the generators becomes a part of network reactance and thus consumes reactive power from the generators. A part of reactive power from generators is consumed by generator reactance. The reactive power supply to systems is reduced and the shortage of reactive power may thus cause voltage instability.

Figure 3.16 conceptually illustrates the analysis of voltage stability when excitation limits are encountered. PV curves before and after excitation limits are shown in this figure. Before the excitation limits are encountered, there is one stable equilibrium point S and one unstable equilibrium point U in the system. The limits in the excitation systems of generators can cause a non-smooth change in a system. When excitation limits are encountered, the PV curve changes from the curve before windup limit to the curve after windup limit. The static limit of PV curves thus decreases. The equilibrium points of the system disappear discretely after the excitation limit is reached. SNB can be detected for the disappearance of equilibrium points, and the system becomes unstable after the excitation limit is hit.

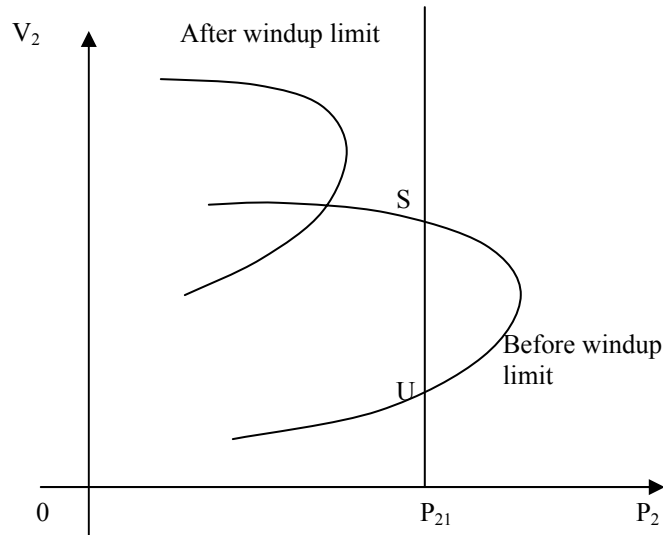


Figure 3.16 PV Curves With and Without Excitation Limit Reached

3.4.4.3 Motor Stalling

The mathematical representation of the first order model of an induction motor is described as (3.26).

$$\frac{d\omega_m}{dt} = \frac{1}{2H}(T_E - T_M) \quad (3.26)$$

where T_E is the electrical torque, ω_m is the rotor angular speed for the mechanical system, T_M is the mechanical torque, and H is the motor inertia. Motors decelerate when electromagnetic torques are less than load torques. Figure 3.17 shows some typical torque speed curves in induction motors at different voltage levels. When there is a disturbance in a system, if the load torque exceeds the maximum electromagnetic torque, either due to the increase of load torque or low system voltage, motor instability occurs. As described earlier, due to low inertia, induction motors are prone to stall.

Figure 3.17 illustrates how motor instability can occur after a motor is disturbed. The load torque T_M is assumed to be constant. If system voltages are reduced, the electrical torque decreases from T_{E1} to T_{E2} or T_{E3} . The intersections of the load torque and electrical torque curves indicate the motor equilibrium points. A stable equilibrium point

corresponds to a high speed, and an unstable equilibrium point corresponds to a low speed. A motor originally operates at the stable equilibrium point S_1 with a high rotor speed. If the electrical torque is reduced to T_{E2} , the region of attraction of motor speed is from the highest speed to the speed corresponding to the unstable equilibrium point U_2 . For motors following a large disturbance, the motor speed must be higher than U_2 to be attracted back to the stable equilibrium point S_2 . If the disturbed motor is operated under low voltage for long, the motor can decelerate to a speed lower than the speed at U_2 . Motor speeds will continue to decay and eventually the motors will stall. The lack of attraction to the stable region would cause motor instability. If the transient process is long and the voltages are reduced such that the electrical torque curve shrinks to T_{E3} , there is no equilibrium in the motor. SNB can be detected and the motor will stall eventually.

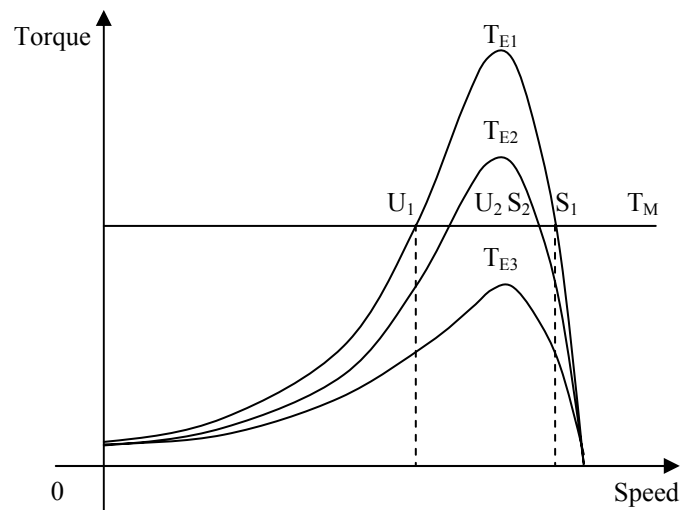


Figure 3.17 Some Typical Torque Speed Curves of Induction Motors

As analyzed earlier, motors can decelerate when disturbances occur in a system. After the causes of deceleration are removed, motors reaccelerate. Motor reaccelerating currents are large. If motor reaccelerating fails, motors would eventually stall or motor

instability occurs. As described in section 3.3, motor instability is related to voltage instability, and could induce system wide voltage instability. The motor reaccelerating currents become larger if motor speeds are reduced further. The reduction of motor speeds is determined by the time duration of motors decelerating or the time duration of motors being disturbed. The time duration of motors being exposed to unfavorable operating conditions thus basically determines whether motor instability will occur.

The time duration of motors being disturbed is determined by the response time of protective devices in SPS. Low voltage at motor terminals is the main reason why motor instability occurs. In many situations, low voltage is caused by faults close to induction motors. Protective devices upstream of induction motors, including circuit breakers (CBs), motor protections (LVRs and LVPs) and bus transfers (ABTs and MBTs), will trip due to low voltage and over current. The tripping time of these protective devices basically determines the time duration of motors being under low voltages. The longer the tripping time is, the more likely motor instability will occur.

The tripping time of circuit breakers is decided by the level of over currents. For fault currents, the settings of time delays in circuit breakers are instantaneous, short time, or long time. The larger the fault currents, the faster the circuit breakers will trip. SPS is a tightly connected power system. Low voltages caused by short circuit faults will be felt by multiple motors at many locations in SPS. It is more difficult for motors to be reaccelerated at multiple locations. Faults in SPS could thus cause multiple motor stalling or even system-wide cascaded voltage collapse.

In SPS, motor low voltage protections and bus transfers are installed closer to motors than are circuit breakers. Low voltage protections and bus transfers are set with short time delays, and will thus trip rapidly if voltages are under low voltage thresholds. The low voltage thresholds of low voltage protections are higher than the thresholds of bus transfers. If low voltages occur in a system, then the low voltage protective devices will trip earlier than bus transfers. It should be noticed that a time delay is experienced in the transfer operation of ABTs and MBTs, which increases the time duration of motors being under low voltage. An ABT can take from 60 to 500 milliseconds to complete the

transfer, whereas an MBT may take at least 20 seconds since it depends on operator actions [45]. Motor instability can thus occur more easily during the transfer operations of MBT.

In SPS, there are some combinations of low voltage protection and bus transfers for motors, including LVR and ABT, LVP and ABT, and LVP and MBT. The motors with LVR and ABT installed have the shortest time durations operating under low voltage for the automatic reclosing ability of LVR and ABT. The motors with LVP or MBT installed are exposed to low voltages for a longer time because manual intervention for reclosing or switching is needed. Some motors in SPS, such as high pressure air compressors, have no low voltage protection devices or bus transfers associated with them. If system voltages are low, these motors are exposed to low voltages for the longest time. However, motors without any protective devices are normally small in capacity and thus have relatively smaller effects on SPS stability. From the analysis of operation time for the combinations of low voltage protections and bus transfers, the motors with LVRs and ABTs thus have the smallest effects on voltage stability. The motors with LVPs and MBTs have larger effects on voltage stability because their response time is longer.

Further the possibility of motor stalling could increase greatly in SPS in special situations. When a casualty occurs, a ship's personnel are pressured to get the combat system back on line as soon as possible [45]. Some steps in the restoration procedures may be missed due to the emergency. Additionally, no perfect procedures exist because attempting to cover all circumstances in advance is impossible. Two types of power applications, soft start and unstable start, can occur in special situations [45]. Soft start occurs when power is applied to several parallel connected loads at one time [45]. Soft start occurs most often when energizing equipment with several cabinets (for power supplies and cooling fans) all connected in parallel. Unstable start occurs when very large motors, such as hydraulic pumps and air conditioning units, are inadvertently left on line after a casualty. Soft start and unstable start in electric motors can induce large reaccelerating currents for long durations and hold system voltages down for several

seconds. The combination of line loss, generator regulation, and even failure tripping of circuit breakers during soft or unstable start can cause system-wide voltage instability.

A motor loses its ability to be attracted back to stable equilibrium points as a result of being exposed to low voltages or other undesirable conditions for a long time. Motor instability is voltage instability, and it may induce system-wide voltage instability. The analysis of this voltage instability involves the transient behavior of induction motors, and the evolution of motor instability should be analyzed carefully. Dynamic analysis is thus required for voltage instability caused by motors.

3.4.4.4 Interaction of Loads and Voltage Controllers

Voltage controllers on ships, such as automatic voltage regulators (AVR) on synchronous generators, are designed by system engineers to adjust voltages within certain limits. The parameters of the controllers are set according to expected loading condition. However, after ships have been designed and built, other engineers add more equipment and thus may ruin the calculations of system engineers [45]. In this situation, the same parameter settings of voltage controllers can be inappropriate for loading conditions in the future. When an SPS is under reconfiguration, the loading condition in the system is potentially continuously changing. The interaction thus changes under different loading conditions. In some situations, the interaction may be harmful to the system. The interaction of loads and voltage controllers may contribute to unstable oscillatory voltage in power systems. This interaction between loads and voltage controllers is especially important in SPS because there are many induction motors. The dynamics of induction motors have a similar time frame to that of voltage controllers and could have adverse effects on SPS stability.

A simple single-generator-single-load system shown in Figure 3.18 is used to analyze the interaction between a load and voltage regulator. Similar analysis can be applied to large power systems with multiple loads and multiple voltage controllers. There are two buses in the system in Figure 3.18. The generator is connected to bus1 and the load is connected to bus2. The load can be dynamic or static. The generator is modeled by a

voltage source behind reactance. x_d and x_d' are the reactance and transient reactance of the generator. E' is the magnitude of the voltage source. The load on bus2 is $P_2 + jQ_2$, where the real power and reactive power are P_2 and Q_2 , respectively.

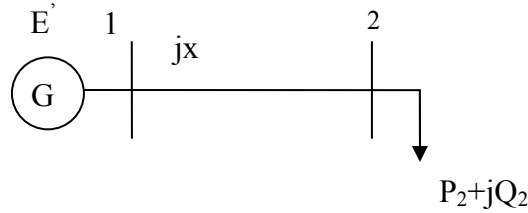


Figure 3.18 One Line Diagram of a Single-Generator-Single-Load System

A simplified first order excitation system is shown as (3.27) [71], and the generator and network equation are shown as (3.28)-(3.29) [71]. Reactance x' is equal to $x + x_d'$. The state variable vector is $[E_{fd} \ E']$, and the algebraic variable vector is $[V_2]$. As described in 3.4.3.1, the Jacobian matrix is studied for bifurcations. If we assume a constant power load on bus 2, then the unreduced Jacobian matrix \mathbf{J} of the system in Figure 3.18 is (3.30).

$$\dot{E}_{fd} = \frac{1}{T_E} (- (E_{fd} - E_{fd}(0)) - K_E \left(\frac{\sqrt{x^2 P_2^2 + (x Q_2 + V_2)^2}}{V_2} - 1 \right)) \quad (3.27)$$

$$\dot{E}' = \frac{1}{T_{d0}} \left(- \frac{x + x_d}{x'} E' + \frac{x_d - x_d'}{x'} \frac{V_2^2 + (x + x_d') Q_2}{E'} + E_{fd} \right) \quad (3.28)$$

$$0 = E'^2 V_2^2 - (x' P_2)^2 - (x' Q_2 + V_2^2)^2 \quad (3.29)$$

$$\mathbf{J} = \begin{bmatrix} \frac{1}{T_E} & 0 & J_{13} \\ -\frac{1}{T_{d0}'} & J_{22} & \frac{1}{T_{d0}'} \left(\frac{x_d - x_d'}{x'} \frac{2V_2}{E'} \right) \\ 0 & 2E'V_2^2 & 2E'^2V_2 - 4(x'Q_2 + V_2^2)V_2^2 \end{bmatrix} \quad (3.30)$$

$$J_{13} = \frac{K_E}{T_E} \left(\frac{\sqrt{x^2P_2^2 + (xQ_2 + V_2)^2}}{V_2^2} - \frac{xQ_2 + V_2}{V_2 \sqrt{x^2P_2^2 + (xQ_2 + V_2)^2}} \right) \quad (3.31)$$

$$J_{22} = \frac{1}{T_{d0}'} \left(-\frac{x + x_d}{x'} - \frac{x_d - x_d'}{x'} \frac{V_2^2 + (x + x_d')Q_2}{E'^2} \right) \quad (3.32)$$

With the reactance of the generator and line fixed, the Jacobian matrix shown as (3.30) is determined by the real and reactive power of the load on bus 2. The eigenvalues of the Jacobian matrix is thus determined by P_2 and Q_2 on bus 2. If the real parts of all eigenvalues of the Jacobian matrix are negative, voltage stability in the system is maintained. If the loading condition at bus 2 is changed but the parameters of the voltage controller are unchanged, the real parts of the eigenvalues of the Jacobian matrix can change from negative to positive, and the system becomes unstable. During the change of eigenvalues from negative to positive, Hopf bifurcation can be detected.

This interaction between loads and voltage controllers is more complex if dynamic loads, such as induction motors, are involved. If the load on bus 2 is an induction motor, the system Jacobian matrix is more complex. A simplified first order differential equation shown as (3.33) is applied to model induction motors. The order of the differential equations of the motor could be as high as the fifth because of the requirement of detail modeling of induction motors in SPS modeling. The state variable of the dynamic load, motor slip s_m , is added into the state variable vector. Real power P_m and reactive power Q_m drawn by the motor are shown as (3.34) and (3.35).

$$\frac{ds_m}{dt} = \frac{1}{2H} (T_M - T_E) \quad (3.33)$$

$$P_m = \frac{R_{2m}/s_m}{(R_{1m} + R_{2m}/s_m)^2 + (X_{1m} + X_{2m})^2} (V_2^2) \quad (3.34)$$

$$Q_m = \frac{X_{1m} + X_{2m}}{(R_{1m} + R_{2m}/s_m)^2 + (X_{1m} + X_{2m})^2} (V_2^2) \quad (3.35)$$

Where R and X are the resistance and reactance of motors. The subscripts 1 and 2 represent the variables associated with the stator and rotor windings of the motor, respectively. T_M and T_E are the mechanical and electrical torque of the motor. In the per unit system, electrical torque T_E is equal to the real power drawn by motor load P_m .

The differential and algebraic equations of the dynamic motor loads should be included to derive the Jacobian matrix of the system. From (3.34) and (3.35), the real and reactive power of the dynamic load are the function of state variables s_m and algebraic variable V_2 . The unreduced Jacobian matrix of the system with a dynamic load is shown as (3.36).

$$J = \begin{bmatrix} \frac{1}{T_E} & 0 & J_{13} & J_{14} \\ -\frac{1}{T_{d0}'} & J_{22} & J_{23} & J_{24} \\ 0 & 0 & \frac{1}{2H} \left(\frac{\partial P_2}{\partial s_m} - \frac{\partial T_M}{\partial s_m} \right) & \frac{1}{2H} \frac{\partial P_2}{\partial V_2} \\ 0 & 2V_2^2 E' & J_{43} & J_{44} \end{bmatrix} \quad (3.36)$$

$$J_{13} = -\frac{K_E}{T_E} \frac{x^2 P_2 \frac{\partial P_2}{\partial s_m} + (xQ_2 + V_2) \frac{\partial Q_2}{\partial s_m}}{\sqrt{x^2 P_2^2 + (xQ_2 + V_2)^2}} \quad (3.37)$$

$$J_{14} = \frac{K_E}{T_E} \left(\frac{\sqrt{x^2 P_2^2 + (xQ_2 + V_2)^2}}{V_2^2} - \frac{x^2 P_2 \frac{\partial P_2}{\partial V_2} + (xQ_2 + V_2) \left(x \frac{\partial Q_2}{\partial V_2} + 1 \right)}{V_2 \sqrt{x^2 P_2^2 + (xQ_2 + V_2)^2}} \right) \quad (3.38)$$

$$J_{22} = \frac{1}{T_{d0}'} \left(-\frac{x + x_d}{x'} - \frac{x_d - x_d'}{x'} \frac{V_2^2 + (x + x_d') Q_2}{E'^2} \right) \quad (3.39)$$

$$J_{23} = \frac{1}{T_{d0}'} \frac{x_d - x_d'}{x'} \frac{x + x_d'}{E'^2} \frac{\partial Q_2}{\partial s_m} \quad (3.40)$$

$$J_{24} = \frac{1}{T_{d0}'} \frac{x_d - x_d'}{x'} \frac{2V_2 + (x + x_d')}{E'} \frac{\partial Q_2}{\partial V_2} \quad (3.41)$$

$$J_{43} = -2x'^2 P_2 \frac{\partial P_2}{\partial s_m} - 2(x' Q_2 + V_2^2) x' \frac{\partial Q_2}{\partial s_m} \quad (3.42)$$

$$J_{44} = 2E'^2 V_2 - 2x' P_2 \frac{\partial P_2}{\partial V_2} - 2(x' Q_2 + V_2^2) (x' \frac{\partial Q_2}{\partial V_2} + 2V_2) \quad (3.43)$$

During the dynamic process, the dynamics of induction motors interact with the dynamics of voltage controllers. Unstable oscillatory voltages may thus occur because the controllers can not provide effective voltage adjustment. From (3.36), the characteristics of induction motors are included in the Jacobian matrix. With the equilibrium points of the system changing during a dynamic process, the eigenvalues of the Jacobian matrix (3.36) change. If the eigenvalues can change from positive to negative during the dynamic process, HB can be detected for the unstable oscillations in the system. Dynamic analysis is thus required for voltage instability caused by interactions in component models.

3.4.5 Voltage Stability Analysis

Traditionally, there are two types of analysis methods for voltage stability study: static analysis and dynamic analysis. Static analysis involves only the solution of algebraic equations and is computationally more efficient than dynamic analysis. Dynamic analysis requires the solution of both differential and algebraic equations. Dynamic analysis provides more accurate results in voltage stability studies. According to the effect of each factor on voltage stability during SPS reconfiguration, the four factors to affect voltage stability discussed in the last section will be analyzed in static or dynamic voltage analysis.

3.4.5.1 *Static Analysis*

Static analysis studies the existence of steady state solutions for a system. With a system modeled by a set of DAE as (2.1) and (2.2), the differential equations are neglected and only the steady state solution of the algebraic equation is studied in static voltage analysis for power systems. In power system analysis, the algebraic equations normally adopt load flow equations. The steady state solution of the algebraic equations can be found by solving (3.44). The existence of steady state solutions of (3.44) indicates that there are equilibrium points for the modeled system and that static voltage stability is satisfied.

$$\mathbf{0} = \mathbf{g}(\mathbf{x}, \mathbf{y}) \quad (3.44)$$

As described earlier, a saddle node bifurcation is the disappearance of a system equilibrium point. In power systems, saddle node bifurcation is important especially when a stable equilibrium point where the power system operates disappears. In some situations, the appearance of a saddle node bifurcation of load flow equations can meet the same condition where a saddle node bifurcation of DAE occurs [27]. The disappearance of steady state solutions of (3.44) thus could meet the same condition at which a saddle node bifurcation occurs.

Static analysis can analyze and assess voltage stability approximately. Static analysis has been largely applied in voltage stability analysis and is ideal for studies where voltage stability limits for many cases must be determined [6].

3.4.5.2 *Dynamic Analysis*

As understanding of voltage stability developed, more and more dynamics are found related with voltage stability. Dynamic analysis is used for voltage stability studies on these dynamics. Voltage stability assessment results are more accurate with dynamic analysis than static analysis. In dynamic analysis, differential-algebraic equations (2.1) and (2.2) are solved explicitly or implicitly at each time step. Local bifurcation could be detected for voltage instability during the dynamic process. As described earlier, in some

situations, saddle node bifurcations of a system modeled by a set of DAE can be detected by solving the algebraic equations in DAE. Another type of bifurcation, Hopf bifurcation, can also cause voltage instability. Normally, Hopf bifurcation occurs earlier than saddle node bifurcation [6]. Hopf bifurcation is more complex and more often caused by interactions between equipments. Complete detection of saddle node bifurcation and Hopf bifurcation thus requires the detailed modeling of a system, with differential equations for various components included. However, dynamic analysis with detailed component models would be time consuming in terms of computation and engineering required for analysis of results [6].

As described in section 3.4.2.2, the dynamics of a power system can be decomposed into slow and fast dynamics, and a power system thus can be represented by its quasi-steady-state (QSS) equations (3.7)-(3.9). In QSS analysis, a system is assumed to move from one equilibrium point to another successively. QSS analysis captures snapshots of system conditions at each equilibrium point along a time domain trajectory given with change in slow dynamics. It is assumed that the slow variables are constants at each steady state. At each equilibrium point, the steady state solution of the system can be derived from (3.45)-(3.47). The results from QSS analysis can be considered as the approximate replication of time domain simulation.

$$\mathbf{x}_s = \text{constant} \quad (3.45)$$

$$\mathbf{0} = \mathbf{f}_s(\mathbf{x}_f, \mathbf{x}_s) \quad (3.46)$$

$$\mathbf{0} = \mathbf{g}(\mathbf{x}_f, \mathbf{x}_s, \mathbf{y}) \quad (3.47)$$

Dynamic analysis, including time domain simulations or simplified QSS modeling, permits more accurate assessment of voltage stability problems than is possible with static analysis [6]. The results from time domain and QSS simulations can not readily provide further information about stability, such as degree of stability. The other analytical approaches, such as approaches for detection of bifurcations, should be applied on the simulation results to provide further information about stability.

3.4.5.3 Analysis Methods of Factors to Affect Voltage Stability

Four factors to affect voltage stability were discussed in section 3.4.4. The first factor, loading condition including load level and load factor, involves only static change of loads caused by SPS reconfiguration. The effect of these static changes during SPS reconfiguration on voltage stability should be considered in voltage stability analysis. The first factor, loading condition, thus will be studied in static voltage stability analysis.

The other three factors, motor stalling, interactions between loads and voltage controllers, and windup limits, involve dynamics during SPS reconfiguration. The effect of the dynamics on voltage stability should be considered in voltage stability analysis. Since dynamics can not be modeled in static analysis, static analysis is not applicable for analyzing voltage instability caused by dynamics. The three factors, motor stalling, interactions between loads and voltage controllers, and windup limits, thus should be studied in dynamic voltage stability analysis.

3.5 CHAPTER SUMMARY

In this chapter, the stability problems of AC SPS were discussed. The time frames of dynamics in SPS were discussed and were used to categorize stability problems in AC SPS. Due to the parallel operation of generators in tightly coupled SPS, voltage stability was considered as the main concern of AC SPS stability analysis and assessment. Bifurcation theory and its application on voltage stability were discussed in this chapter. Possible voltage stability problems during reconfiguration in SPS were investigated. Four factors to affect voltage stability were described and analyzed by bifurcation theory. Two voltage stability analysis methods, static analysis and dynamic analysis, were discussed and presented. The four factors to affect voltage stability can be studied in the static and dynamic voltage stability analysis. Among the four factors, three factors can be analyzed and assessed by two new voltage stability indices presented later.

In the next chapter, a test SPS that was modeled and simulated to study stability during reconfiguration will be discussed. The modeling and simulation strategies for

stiffly connected ungrounded SPS will be introduced. The time domain simulation results will be applied to static and dynamic voltage stability analysis.

CHAPTER IV

MODELING AND SIMULATION OF SHIPBOARD POWER SYSTEMS

4.1 INTRODUCTION

Time domain simulations provide valuable information for stability studies. In conventional stability studies, stator and network transients are neglected. In these studies, reduced order models only provide an approximation for actual dynamics. However, in ungrounded stiffly connected systems, various components are strongly coupled through short transmission lines. Due to the strong interactions, simulation results neglecting stator and network transients can cause large errors in transient stability analysis. Therefore, detailed models should be adopted to simulate the accurate dynamics of ungrounded stiffly connected systems such as SPS.

In this chapter, a new generalized modeling methodology for ungrounded SPS will be presented. The methodology will be applied to a reduced SPS. The test SPS will be developed and will be used in stability studies in Chapters V and VI. In section 4.2, the problems of modeling and simulating ungrounded stiffly connected shipboard power systems will be described. In sections 4.3 and 4.4, the new generalized modeling methodology, including the detailed component models and the interconnection strategy, will be presented. In section 4.5, a reduced SPS modeled and simulated with the new modeling methodology will be presented. The results will show that the new methodology is an efficient way to model and simulate SPS. In section 4.6, a test system will be described. In section 4.6.2, some representative simulation results of the test system at normal operation will be presented.

4.2 UNGROUNDED STIFFLY CONNECTED SPS

Shipboard power systems studied in this dissertation are ungrounded power systems. Due to size of ships, the cables between equipment on ships are short and components are tightly coupled. The short cables thus make SPS stiffly connected systems. Due to small shunt and mutual capacitances of short cables, the natural frequencies of short electric lines are very large. The time constants of the short cables are small. Small integration time steps are required to derive stable and accurate simulation results of SPS and normally stiff integration algorithms are needed. The speed of the simulations of stiffly connected power systems is reduced significantly due to the stable small integration time steps.

One way to improve the simulation speed is to neglect the small line capacitances. The capacitances of short electric lines are so small that they have little effect on system dynamics [18]. However, without capacitances, the tie lines are modeled with pure resistances and inductances. Ungrounded stiffly connected systems are completely isolated from the ground. Inductor and resistor buses emerge in the systems.

An inductor or resistor bus is a kind of bus where only inductive or resistive components are connected [18]. Inductor and resistor buses induce difficulties in modeling ungrounded power systems. With naturally interconnected grounded components, such as grounded capacitances, the input voltages of inductor and resistor buses can be established by grounded components. However, incompatibility occurs when only voltage-in current-out inductive or resistive models are interconnected. The input voltages of inductor and resistor buses need to be established in artificial ways. Traditionally, reformulated current-in voltage-out resistor models have been used to derive the input voltages of resistor buses. The derivation of the input voltages of inductor buses is more complex. An auxiliary resistor can be paralleled with the inductance [57]. An inductor bus is thus changed into a resistor bus and the inductor bus voltage can be solved in the same way as a resistor bus.

As described earlier, conventional nodal admittance matrix based circuit simulation methods such as EMTP/ATP [3] and differential algebraic equation solver based

methods such as SimPowerSystems [4] are able to model and simulate power systems. Without shunt capacitances in an ungrounded system, EMTP/ATP is no longer applicable because of the singularity of the system nodal admittance matrix. In SimPowerSystems, connecting a current source or nonlinear element in series with an inductance is not allowed [4]. Therefore, the inductive lines can not be connected in series with synchronous and asynchronous machines. As described earlier, the voltages on resistor and inductor buses can be obtained by reformulating the auxiliary resistor model. The size of the resistor is the key to achieving a good trade off between simulation speed and accuracy. However, it is usually difficult to select one robust resistor value for various dynamic simulations.

This dissertation proposes a new generalized strategy for modeling detailed ungrounded stiffly connected power systems. In the new method, the resistor and inductor buses are solved in the usual ways. Voltage-in flux-out reformulated reference generator models and voltage-current-in voltage-out reformulated line models are used. The input voltages of ungrounded stiffly connected systems are derived on the basis of the reformulated reference generator and line models. The interconnection procedures involve applying Kirchoff Current Law (KCL) on each bus and a set of interconnection equations on the reference generator bus. The new generalized method was realized in the environment of Matlab/Simulink [5]. Matlab/Simulink is an equation solver program that can simulate dynamic systems by solving user-defined mathematical equations with given integration rules.

4.3 COMPONENT MODELS

Any power system can be modeled by a set of nonlinear differential-algebraic-equations (DAE) as (2.1)-(2.2). The nonlinear differential equations can be rewritten as (4.1).

$$\dot{\mathbf{x}} = \mathbf{A}(\mathbf{x}, t)\mathbf{x} + \mathbf{B}\mathbf{u} \quad (4.1)$$

where \mathbf{A} and \mathbf{B} are the parameter matrices of the nonlinear equations. The standard models can be found in [72] and rewritten into the format of (4.1). With \mathbf{x} , \mathbf{u} , \mathbf{A} , and \mathbf{B} given, each set of differential equations can be realized in Matlab Simulink [5].

4.3.1 Park Transformation

Figure 4.1 shows the relationship between the reference frame d (direct axis) q (quadrature axis) 0 and abc. Park Transformation, shown as (4.2) is used to transform all electrical quantities from phases a, b, and c into new variables, 0, d and q [72] as (4.3). ω is the relative angular speed of the reference frame dq0 to abc and θ is the angle between reference frame abc and dq0. Inverse park transformation transforms variables from reference frame 0dq to abc. The transformation shown as (4.2-4.3) is applied to transform the voltage, current, and flux variables of different components into the common system reference frame.

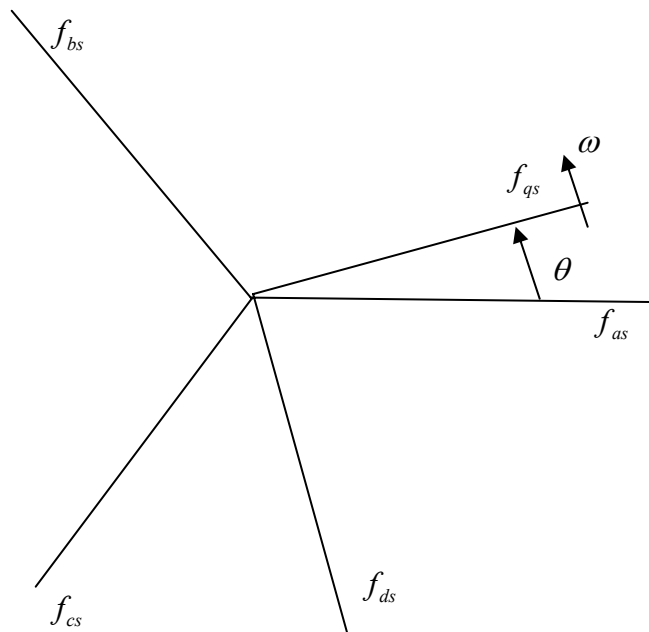


Figure 4.1 Transformation Between the Reference Frame dq0 and abc

$$\mathbf{P} = \frac{2}{3} \begin{bmatrix} \frac{1}{2} & \frac{1}{2} & \frac{1}{2} \\ \sin \theta & \sin(\theta - \frac{2\pi}{3}) & \sin(\theta + \frac{2\pi}{3}) \\ \cos \theta & \cos(\theta - \frac{2\pi}{3}) & \cos(\theta + \frac{2\pi}{3}) \end{bmatrix} \quad (4.2)$$

$$\mathbf{f}_{qd0} = \mathbf{P}\mathbf{f}_{abc} \quad (4.3)$$

where $\theta = \int_0^t \omega(\xi) d\xi + \theta(0)$. \mathbf{f} can represent either voltage, current, flux linkage, or electric charge.

In the new modeling strategy, the 0dq reference frame rotating with the rotor of the reference generator is selected as the system reference frame. This selection will reduce complexity of computation in low-level computers. Because the reference frame of generators are in their own rotors, it is necessary to relate variables in one reference frame to variables in another reference frame. The transformation can be done directly without involving the abc variables in the transformation. The relationship between reference frame 1 from which the variables are being transformed and reference frame 2 to which the variables are being transformed is shown in Figure 4.2. The transformation from reference frame 1 to reference frame 2 is shown as (4.4)-(4.5) [72].

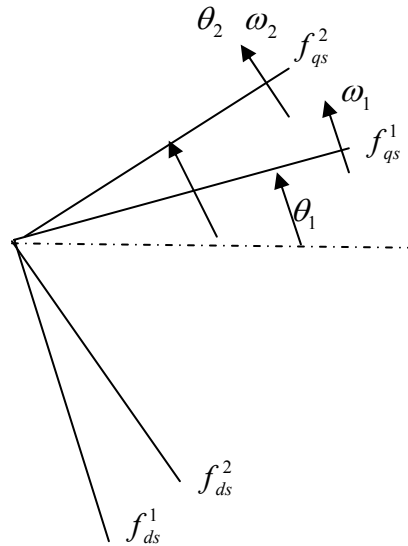


Figure 4.2 Transformation between Reference Frames

$$\mathbf{P}_{12} = \begin{bmatrix} \cos(\theta_2 - \theta_1) & -\sin(\theta_2 - \theta_1) & 0 \\ \sin(\theta_2 - \theta_1) & \cos(\theta_2 - \theta_1) & 0 \\ 0 & 0 & 1 \end{bmatrix} \quad (4.4)$$

$$\mathbf{f}_{qd0}^2 = \mathbf{P}_{12} \mathbf{f}_{qd0}^1 \quad (4.5)$$

4.3.2 Standard Component Models

In the new modeling method, three types of standard component models, standard synchronous generator models, standard induction motor models, and standard static load were used.

4.3.2.1 Standard Synchronous Generator Model

Standard generators use voltages as inputs and currents as outputs. \mathbf{x} , \mathbf{u} , \mathbf{A} and \mathbf{B} of the full order standard synchronous generators in the form of (4.1) are shown as (4.6)-(4.9) [72].

$$\mathbf{x} = [i_o \quad i_d \quad i_F \quad i_D \quad i_q \quad i_Q]^T \quad (4.6)$$

$$\mathbf{u} = [v_o \quad v_d \quad v_F \quad v_D \quad v_q \quad v_Q]^T \quad (4.7)$$

$$\mathbf{A} = -\mathbf{L}_G^{-1}(\mathbf{R}_G + \omega \mathbf{N}_G \mathbf{L}_G^{-1}) \quad (4.8)$$

$$\mathbf{B} = \mathbf{L}_G^{-1} \quad (4.9)$$

$$\mathbf{L}_G = \begin{bmatrix} -L_0 & 0 & 0 & 0 & 0 & 0 \\ 0 & -L_d & L_{mD} & L_{mD} & 0 & 0 \\ 0 & -L_{mD} & L_F & L_{mR} & 0 & 0 \\ 0 & -L_{mD} & L_{mR} & L_D & 0 & 0 \\ 0 & 0 & 0 & 0 & -L_q & L_{mQ} \\ 0 & 0 & 0 & 0 & -L_{mQ} & L_Q \end{bmatrix} \quad (4.10)$$

$$\mathbf{R}_G = \text{diag}(-r_s, -r_s, r_F, r_D, -r_s, r_Q) \quad (4.11)$$

$$\omega \mathbf{N}_G = \begin{bmatrix} 0 & 0 & 0 & 0 & 0 & 0 \\ 0 & 0 & 0 & 0 & \omega_r L_q & -\omega_r L_{mQ} \\ 0 & 0 & 0 & 0 & 0 & 0 \\ 0 & 0 & 0 & 0 & 0 & 0 \\ 0 & -\omega_r L_d & \omega_r L_{mR} & \omega_r L_{mD} & 0 & 0 \\ 0 & 0 & 0 & 0 & 0 & 0 \end{bmatrix} \quad (4.12)$$

where r_s is the resistance on stator windings, r_F , r_D and r_Q are the resistance on rotor windings, L_0 , L_d and L_q are the self inductance on stator windings, L_F , L_D and L_Q are the self inductance on rotor windings, L_{mD} is the mutual inductance between rotor windings d and D, L_{mR} is the mutual inductance between rotor windings F and D, and L_{mQ} is the mutual inductance between rotor windings q and Q.

The mechanical system of the generator can be represented by (4.13)-(4.14) [72].

$$\frac{\dot{\omega}_r}{\omega_b} = \frac{1}{2H} (T_M - T_E) \quad (4.13)$$

$$\dot{\delta} = \frac{\omega_r}{\omega_b} - 1 \quad (4.14)$$

$$T_E = \lambda_d i_q - \lambda_q i_d \quad (4.15)$$

$$\lambda_d = -L_d i_d + L_{mR} i_F + L_{mD} i_D \quad (4.16)$$

$$\lambda_q = -L_q i_q + L_{mQ} i_Q \quad (4.17)$$

where ω_b is the system base rotation angular speed, H is the rotor inertia in seconds, T_M is the mechanical torque, T_E is the electromagnetic torque, i_0 , i_d and i_q are the currents on stator windings, and i_F , i_D , i_Q are the currents on rotor windings. Each generator is modeled in its own 0dq reference frame.

4.3.2.2 Standard Induction Motor Model

Standard induction motor models have voltages as inputs and currents as outputs. \mathbf{x} , \mathbf{u} , \mathbf{A} and \mathbf{B} of the full-order induction machine model in the form of (4.1) can be expressed as (4.18)-(4.21) [72].

$$\mathbf{x} = [i_0 \quad i_d \quad i_F \quad i_D \quad i_q \quad i_Q]^T \quad (4.18)$$

$$\mathbf{u} = [v_0 \quad v_d \quad v_F \quad v_D \quad v_q \quad v_Q]^T \quad (4.19)$$

$$\mathbf{A} = -\mathbf{L}_M^{-1} (\mathbf{R}_M + \omega \mathbf{N}_M \mathbf{L}_M) \quad (4.20)$$

$$\mathbf{B} = \mathbf{L}_M^{-1} \quad (4.21)$$

$$\mathbf{L}_M = \begin{bmatrix} L_0 & 0 & 0 & 0 & 0 & 0 \\ 0 & L_d & L_{mD} & 0 & 0 & 0 \\ 0 & L_{mD} & L_D & 0 & 0 & 0 \\ 0 & 0 & 0 & L_q & L_{mQ} & 0 \\ 0 & 0 & 0 & L_{mQ} & L_Q & 0 \end{bmatrix} \quad (4.22)$$

$$\mathbf{R}_M = \text{diag}(r_s, r_s, r_D, r_s, r_Q) \quad (4.23)$$

$$\omega \mathbf{N}_M = \begin{bmatrix} 0 & 0 & 0 & 0 & 0 \\ 0 & 0 & 0 & -L_q \omega & -L_{mQ} \omega \\ 0 & 0 & 0 & -L_{mQ}(\omega - \omega_r) & -L_Q(\omega - \omega_r) \\ 0 & L_d \omega & L_{mD} \omega & 0 & 0 \\ 0 & L_{mD}(\omega - \omega_r) & L_D(\omega - \omega_r) & 0 & 0 \end{bmatrix} \quad (4.24)$$

Where ω is the rotation angular speed of stator, r_s is the resistance on stator windings, r_F , r_D and r_Q are the resistance on rotor windings, L_0 , L_d and L_q are the self inductance on stator windings, L_D and L_Q are the self inductance on rotor windings, L_{mD} is the mutual inductance between stator windings d and D, and L_{mQ} is the mutual inductance between rotor windings q and Q.

The mechanical system equations for induction motors are modeled as (4.25)-(4.26) [72].

$$\frac{\dot{\omega}_r}{\omega_b} = \frac{1}{2H} (T_E - T_L) \quad (4.25)$$

$$\dot{\delta} = \frac{\omega_r}{\omega_b} - 1 \quad (4.26)$$

$$T_E = \lambda_d i_q - \lambda_q i_d \quad (4.27)$$

$$\lambda_d = L_d i_d + L_{mD} i_D \quad (4.28)$$

$$\lambda_q = L_q i_q + L_{mQ} i_Q \quad (4.29)$$

where H is the rotor inertia in seconds, T_L is the load torque, T_E is the electromagnetic torque, i_0 , i_d and i_q are the currents on stator windings, and i_D and i_Q are the currents on rotor windings.

4.3.2.3 Standard Static Load or Line Model

The static load or connecting line is modeled by constant impedance with resistance and inductance connected in series. The static load or line models have voltages on the

load or line as inputs and currents as outputs. \mathbf{x} , \mathbf{u} , \mathbf{A} and \mathbf{B} of the standard static load or line model are shown as (4.30)-(4.33) [72].

$$\mathbf{x} = [i_0 \quad i_d \quad i_q]^T \quad (4.30)$$

$$\mathbf{u} = [v_0 \quad v_d \quad v_q]^T \quad (4.31)$$

$$\mathbf{A} = -(\mathbf{P}\mathbf{L}_L^{-1}\mathbf{P}^{-1})(\mathbf{P}\mathbf{R}_L\mathbf{P}^{-1} + \mathbf{P}\mathbf{L}_L \frac{d\mathbf{P}^{-1}}{dt}) \quad (4.32)$$

$$\mathbf{B} = \mathbf{P}\mathbf{L}_L^{-1}\mathbf{P}^{-1} \quad (4.33)$$

$$\mathbf{R}_L = \begin{bmatrix} r_{aa} & r_{ab} & r_{ac} \\ r_{ba} & r_{bb} & r_{bc} \\ r_{ca} & r_{cb} & r_{cc} \end{bmatrix} \quad (4.34)$$

$$\mathbf{L}_L = \begin{bmatrix} L_{aa} & L_{ab} & L_{ac} \\ L_{ba} & L_{bb} & L_{bc} \\ L_{ca} & L_{cb} & L_{cc} \end{bmatrix} \quad (4.35)$$

$$\frac{d\mathbf{P}^{-1}}{dt} = \omega \begin{bmatrix} -\sin\theta & -\cos\theta & 0 \\ -\sin(\theta - \frac{2\pi}{3}) & \cos(\theta - \frac{2\pi}{3}) & 0 \\ -\sin(\theta - \frac{2\pi}{3}) & \cos(\theta + \frac{2\pi}{3}) & 0 \end{bmatrix} \quad (4.36)$$

where r_{aa} , r_{bb} and r_{cc} is the self resistance on each phase, L_{ab} , L_{bc} and L_{ca} is the mutual inductance between phases, L_{aa} , L_{bb} and L_{cc} is the self inductance on each phase, L_{ab} , L_{bc} and L_{ca} is the mutual inductance between phases, and ω is the angular speed of the reference frame.

4.3.3 Reformulated Component Models

As described earlier, the modeling difficulty with stiffly connected power systems are the incompatibility of interconnection on inductor and resistor buses. In this new generalized method, reformulated component models are adopted to solve the incompatibility and derive bus voltage on inductor and resistor buses. Reformulated

component models keep the physical model of components and reformulate the mathematical format of the component models. In the new modeling method, three types of reformulated component models, reformulated generator models, reformulated line models and linear transformer models were developed.

4.3.3.1 Reformulated Generator Model

In the proposed modeling strategy, the largest synchronous generator in a system is chosen as the reference generator, whose model is reformulated from the standard generator model described in section 4.3.2. The power of the reference generator is the system power base in the per unit system. Instead of using currents as state variables as in standard generator models, flux linkages are used as the state variables for the reformulated generator model. This reformulation will facilitate the derivation of the generator bus voltages in component interconnections.

$$\mathbf{x} = [\lambda_o \quad \lambda_d \quad \lambda_F \quad \lambda_D \quad \lambda_q \quad \lambda_Q]^T \quad (4.37)$$

$$\mathbf{u} = [v_o \quad v_d \quad v_F \quad v_D \quad v_q \quad v_Q]^T \quad (4.38)$$

$$\mathbf{A} = \mathbf{R}_G \mathbf{L}_G^{-1} + \mathbf{P} \frac{d\mathbf{P}^{-1}}{dt} \quad (4.39)$$

$$\mathbf{B} = \text{diag}(1,1,1,1,1,1) \quad (4.40)$$

where \mathbf{x} , \mathbf{u} , \mathbf{A} and \mathbf{B} of the reformulated reference generator model are shown as (4.37)-(4.40). \mathbf{R}_G and \mathbf{L}_G are the same as defined for the standard generator model as (4.10)-(4.11).

4.3.3.2 Reformulated Line Models

In the new modeling method, without shunt capacitance, connecting lines are modeled by pure resistors and inductors in series. Figure 4.3 shows a three-phase connecting cable model. s and r denote the sending and receiving end of the cable. Currents flow through the line from the sending end to the receiving end. The self and

mutual impedance (including resistance and inductance) of the three-phase line model are shown in the figure, respectively.

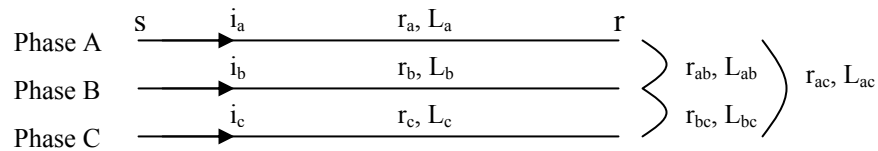


Figure 4.3 A Three-Phase Connecting Line Model

As discussed earlier, the standard line model has voltage differences between sending end and receiving end as inputs and currents flowing from sending end to receiving end as state variables and outputs. The line model is reformulated from the standard line model in section 4.3.2. The reformulated line model, shown as (4.41), has sending end voltages and currents as inputs and receiving end voltages as outputs. In this way, the reformulated line model can help calculate the input voltages of the inductor or resistor bus where the reformulated cable is connected.

$$\mathbf{v}_r = \mathbf{v}_s - (\mathbf{P}\mathbf{R}_L\mathbf{P}^{-1} + \mathbf{P}\mathbf{L}_L\frac{d\mathbf{P}^{-1}}{dt})\mathbf{i} - \mathbf{P}\mathbf{L}_L\mathbf{P}^{-1}\dot{\mathbf{i}} \quad (4.41)$$

$$\mathbf{v}_r = [v_{rq} \quad v_{rd} \quad v_{r0}]^T \quad (4.42)$$

$$\mathbf{v}_s = [v_{sq} \quad v_{sd} \quad v_{s0}]^T \quad (4.43)$$

$$\mathbf{i} = [i_q \quad i_d \quad i_0] \quad (4.44)$$

Subscripts s and r denote the variables associated with the sending and receiving ends of lines. Matrix \mathbf{R}_L includes self and mutual resistances, and \mathbf{L}_L includes the self and mutual inductances of three-phase lines. The matrices are the same as in the standard line model shown in (4.34)-(4.35).

4.3.3.3 Linear Transformer Model

Transformers are connected in a system at primary and secondary sides. The connecting nodes on both primary and secondary sides are inductor buses. Linear transformer models thus should be reformulated to facilitate the voltage derivation on the two nodes.

A three-phase linear transformer is modeled by three single-phase linear transformers, which distribute power to three-phase loads. Each single-phase linear transformer is modeled by a **T** equivalent circuit, which includes a linear magnetizing branch plus winding resistance and leakage inductance in series on primary and secondary sides. The **T** equivalent circuit of a single phase linear transformer is shown in Figure 4.4. Subscripts P and S represent the variables associated with the primary and secondary sides of the transformer. Subscript M represents the variables associated with the magnetizing branch of the transformer.

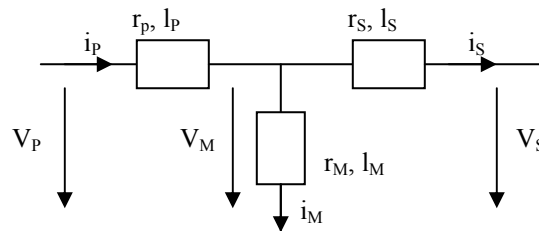


Figure 4.4 A Single Phase Linear Transformer Model

From Figure 4.4, a single-phase linear transformer is modeled with a combination of primary side branch, secondary side branch, and magnetizing branch. The magnetizing branch can be modeled in the same way as a standard constant impedance load shown as (4.30)-(4.36). The primary and secondary sides of the transformer can be modeled as two non-coupled lines as (4.41). The linear transformer model can thus be considered as

a combination of one static load model and two connecting line models. The final mathematical representation of a single-phase linear transformer shown as Figure 4.4 is modeled as (4.45)-(4.62). The magnetizing branch is modeled by (4.45)-(4.48). The primary and secondary side branches are modeled by (4.52) and (4.58), respectively.

$$\mathbf{x} = [i_{M0} \quad i_{Md} \quad i_{Mq}]^T \quad (4.45)$$

$$\mathbf{u} = [v_{M0} \quad v_{Md} \quad v_{Mq}]^T \quad (4.46)$$

$$\mathbf{A} = -(\mathbf{L}_M^{-1})(\mathbf{R}_M + \mathbf{P}\mathbf{L}_M \frac{d\mathbf{P}^{-1}}{dt}) \quad (4.47)$$

$$\mathbf{B} = \mathbf{P}\mathbf{L}_M^{-1}\mathbf{P}^{-1} \quad (4.48)$$

$$\mathbf{R}_M = \text{diag}(r_M, r_M, r_M) \quad (4.49)$$

$$\mathbf{L}_M = \text{diag}(l_M, l_M, l_M) \quad (4.50)$$

$$\frac{d\mathbf{P}^{-1}}{dt} = \omega \begin{bmatrix} -\sin\theta & -\cos\theta & 0 \\ -\sin(\theta - \frac{2\pi}{3}) & \cos(\theta - \frac{2\pi}{3}) & 0 \\ -\sin(\theta - \frac{2\pi}{3}) & \cos(\theta + \frac{2\pi}{3}) & 0 \end{bmatrix} \quad (4.51)$$

$$\mathbf{v}_M = \mathbf{v}_P - (\mathbf{R}_P + \mathbf{P}\mathbf{L}_P \frac{d\mathbf{P}^{-1}}{dt})\mathbf{i}_P - \mathbf{L}_P \dot{\mathbf{i}}_P \quad (4.52)$$

$$\mathbf{R}_P = \text{diag}(r_P, r_P, r_P) \quad (4.53)$$

$$\mathbf{L}_P = \text{diag}(l_P, l_P, l_P) \quad (4.54)$$

$$\mathbf{v}_M = [v_{Mq} \quad v_{Md} \quad v_{M0}]^T \quad (4.55)$$

$$\mathbf{v}_P = [v_{Pq} \quad v_{Pd} \quad v_{P0}]^T \quad (4.56)$$

$$\mathbf{i}_P = [i_{pq} \quad i_{pd} \quad i_{p0}] \quad (4.57)$$

$$\mathbf{v}_S = \mathbf{v}_M - (\mathbf{R}_S - \mathbf{P}\mathbf{L}_S \frac{d\mathbf{P}^{-1}}{dt})\mathbf{i}_S - \mathbf{L}_S \dot{\mathbf{i}}_S \quad (4.58)$$

$$\mathbf{R}_S = \text{diag}(r_S, r_S, r_S) \quad (4.59)$$

$$\mathbf{L}_S = \text{diag}(l_S, l_S, l_S) \quad (4.60)$$

$$\mathbf{v}_S = [v_{Sq} \quad v_{Sd} \quad v_{S0}]^T \quad (4.61)$$

$$\mathbf{i}_s = [i_{sq} \quad i_{sd} \quad i_{s0}] \quad (4.62)$$

4.3.4 Protective Devices

The protective devices, including circuit breakers (CBs), low voltage protections (LVPs), low voltage release (LVRs), automatic bus transfers (ABTs), and manual bus transfers (MBTs), are used in SPS to protect the equipment from overcurrents or low voltages. CBs sense the currents flowing through cables and protect the cables against over currents. The circuit breakers were modeled according to their time current characteristics. LVPs and LVRs sense the terminal voltages of the induction motors and protect the motors against low voltages. The function of automatic pick-up was modeled for LVRs to pick up the protected motors once voltages are recovered. ABTs and MBTs sense bus voltages and protect the loads downstream of the bus transfers against low voltages. The function of automatic transfer was modeled for ABTs to transfer the protected circuit between its normal and alternate paths. Generator switchboard protection logic provides protection for the associated generator/switchboard set. The generator switchboard protection logic consists of under frequency, under voltage, over power and reverse power relays [49]. Under voltage and under frequency relays protect generator/switchboard set from low voltage and low frequency. Over power and reverse power relays sense power out of generators and protect generators from overloading and being motorized [49]. Over power relays can shed some non vital loads and semi vital loads when generators are at 110 percent of rated load [49].

As described in section 2.3.1, an SPS was modeled and simulated in PSAL to provide a platform for studying the transient behavior of SPS [44]. The protective devices mentioned earlier were modeled by their principle functions. The CBs, LVPs, LVRs, ABTs, MBTs and generator switchboard protection logic were modeled based on the functional descriptions of the components in [44][49]. In this dissertation work, each type of protective device mentioned earlier was modeled by a combination of existing modules in Matlab/Simulink. The selective tripping of some non vital and semi vital loads should be studied carefully before over power relays are modeled in SPS,

4.4 COMPONENT INTERCONNECTIONS

The voltages on resistor or inductor buses are necessary to solve system equations. With the line capacitances removed, many buses of an ungrounded stiffly connected power system become resistor or inductor buses. The voltages of these resistor and inductor buses need to be derived artificially. In the new modeling methodology, either a reference generator model or a line model should be reformulated to facilitate component interconnection on each resistor or inductor bus. During component interconnection, the currents of interconnected branches on each bus should satisfy Kirchoff's Current Law (KCL), which states (4.63)

$$\sum_{k=1}^K \mathbf{i}_k = 0 \quad (4.63)$$

where $\mathbf{i}_k = [i_{k0} \ i_{kd} \ i_{kq}]^T$. k denotes the current associated with the k^{th} branch connected to the bus. Each current should be in the same system reference frame.

Figure 4.5 illustrates the interconnection on the reference generator bus. Beside the reference generator, there are k_1 standard generators, k_2 induction motors, k_3 static loads, k_4 reformulated lines, and k_5 standard lines connected to the bus. The reformulated and standard lines connect the reference bus to its neighboring buses. The currents of the motors, static loads, and standard lines are derived from their corresponding component models, and the currents of the reformulated lines are obtained by applying KCL on the neighboring buses. According to (4.41), the reference generator current \mathbf{i} is derived from the summation of the currents of the other interconnected branches. The flux linkage $\boldsymbol{\lambda}$ is derived from the reformulated reference generator model. A set of interconnection equations, shown as (4.64), is then applied to obtain the input voltage \mathbf{v} of the reference generator.

$$\mathbf{v} = -\mathbf{r}_s \mathbf{i} - \dot{\boldsymbol{\lambda}} + \mathbf{P} \frac{d\mathbf{P}^{-1}}{dt} \boldsymbol{\lambda} \quad (4.64)$$

$$\mathbf{r}_s = \text{diag}(r_s, r_s, r_s) \quad (4.65)$$

$$\boldsymbol{\lambda} = \text{diag}(\lambda_q, \lambda_d, \lambda_0) \quad (4.66)$$

where r_s is the stator winding resistance, and λ_q , λ_d and λ_0 are flux linkages on the stator windings.

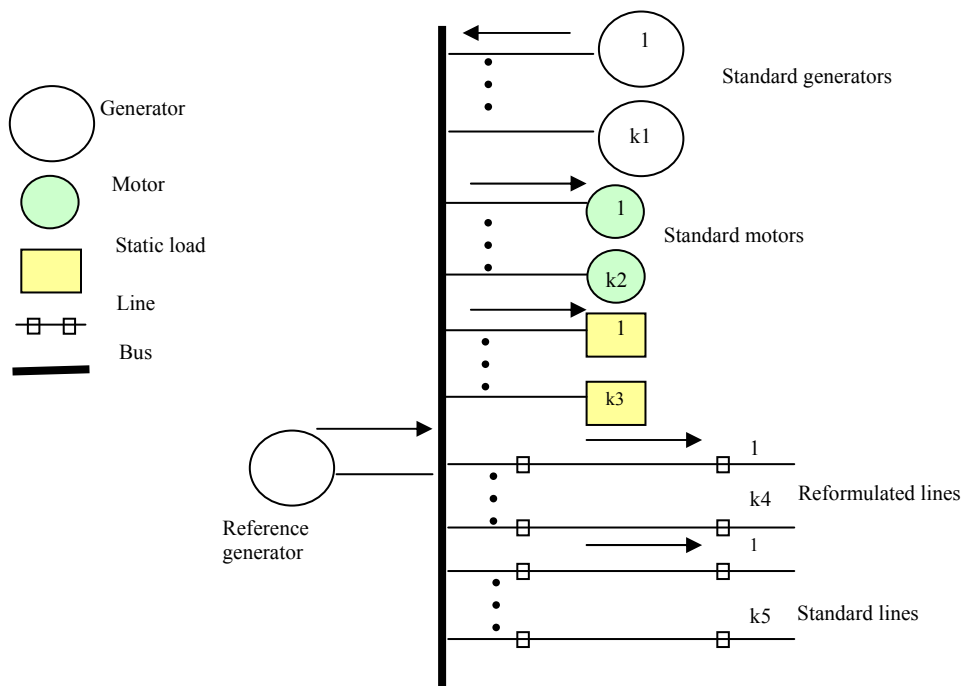


Figure 4.5 Interconnection on a Reference Generator Bus

Figure 4.6 illustrates the interconnection on a typical inductor or resistor bus. Reformulated line 1 connects the typical bus to a bus whose input voltages are already derived. According to (4.63), the currents of reformulated line 1 are equal to the summation of the currents of the other interconnected branches. The input voltages of the typical resistor or inductor bus are then calculated by applying the reformulated line model (4.41) on reformulated line 1.

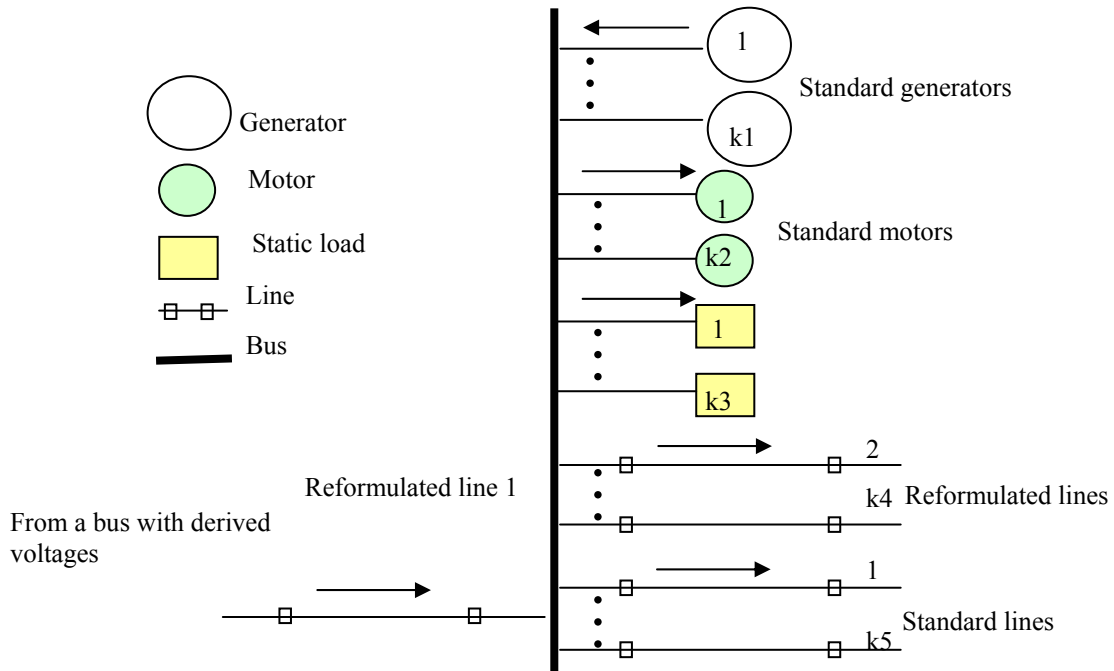


Figure 4.6 Interconnection on a Typical Inductor or Resistor Bus

With (4.41) applied on each reformulated line in Figure 4.5 and Figure 4.6, the input voltages of each resistor or inductor bus are calculated after the input voltages of the reference generator bus are derived. The input voltages of the neighboring buses of the reference generator bus are calculated with the input voltages of the reference generator bus taken as sending end voltages of (4.41). The derived voltages of a bus are then used as sending end voltages to calculate the input voltages of its neighboring buses. The previous procedure is repeatedly applied to each resistor or inductor bus in a modeled system.

System models of ungrounded stiffly connected power systems are formed by interconnecting various component models. The input voltages of all component models can be calculated from either (4.41) or (4.64). These voltage inputs of the component models can be derived according to the interconnection procedures described earlier.

4.5 CASE STUDY

To demonstrate the individual component models and interconnection procedures presented here, a delta-connected reduced SPS, shown in Figure 4.7, was modeled and simulated. Generators 1 and 2 are running in the system, and generator 3 is a back up generator for emergencies. Three generator switchboards are connected in a ring with cables to provide more flexibility of system configuration. This reduced SPS has four buses: generator switchboards 1, 2, 3, and load center 5. Load center 5 is connected downstream of switchboard 2 and upstream of three-phase transformer 1. The transformer is in turn connected upstream of unbalanced static load 5. An induction motor and a static load are connected under each switchboard and load center. The parameters of the reduced SPS can be found in Appendix A.

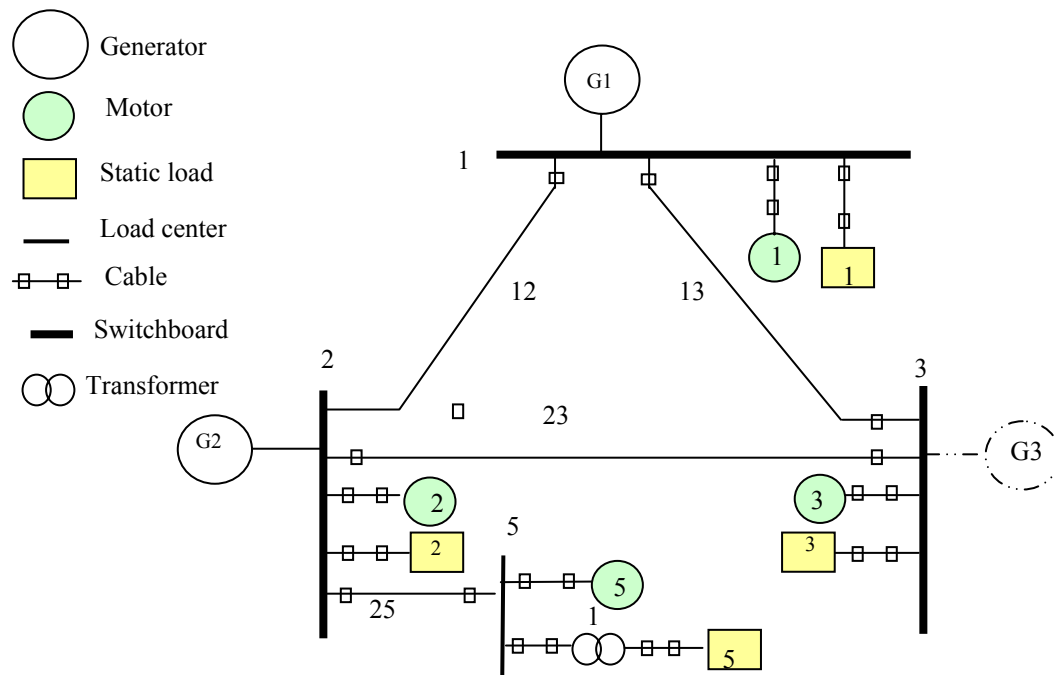


Figure 4.7. A Reduced SPS

The reduced SPS is ungrounded and stiffly connected. Each bus in the system is either an inductor or a resistor bus. According to the method described earlier, generator 1 is taken as the reformulated reference generator, generator 2 uses the standard generator model, cable 12 is modeled with the standard line model, and the other cables are modeled with the reformulated line model.

The simulation for the reduced SPS was conducted in Matlab/Simulink with selected integration algorithm Dormand-Prince ODE5, fixed time step of 0.001 seconds, and automatic error tolerance [73]. The parameters of the components are listed in Appendix A. Without specification, the parameters in per unit are given with V_{base} equal to 450 V (rms, line-to-line) and P_{base} equal to 3125 KVA. Each generator is modeled with a governor with gas turbine and an IEEE Type II Automatic Voltage Regulator (AVR) [18][19]. The block diagrams of the models of AVR controllers and governor with gas turbine are shown as Figure 3.14 and Figure 4.8. The load torque for every induction motor is quadratic modeled as $T_L = \omega^2$, which represents a speed-squared load, as in fans.

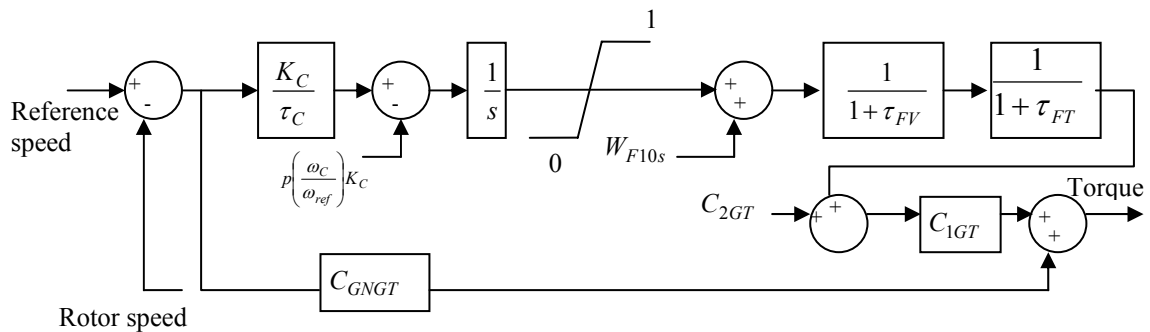


Figure 4.8 Block Diagram of a Governor with Gas Turbine

Figure 4.9-Figure 4.13 show graphs of the representative variables for one simulation case of the system shown in Figure 4.7. In this case, at first, generators 1 and 2 were

running at no-load condition. All static and dynamic loads were then connected into the system at one second. Figure 4.9 and Figure 4.10 are the phase AB and BC voltages of the generator 2. At one second, the voltages decreased due to the large cold load start-up currents from the static and dynamic loads. Due to the function of the governor and voltage regulators on the generators, the voltages are pulled back to the nominal values. Phase AB and BC currents drawn by the unbalanced load 5 are shown as Figure 4.11 and Figure 4.12. As expected, the currents are almost in reverse ratio of the sizes of the single-phase loads on phase AB and BC. Phase AB current of motor 1 is shown in Figure 4.13. This finally settles down to a value below 0.075. This agrees with the ratio of motor demand to system capacity.

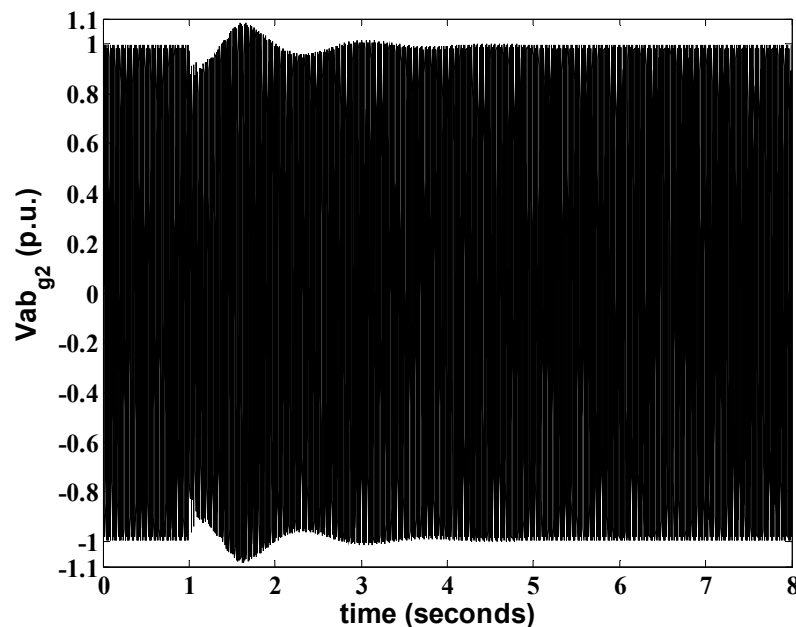


Figure 4.9 Phase AB Voltage of Generator 2

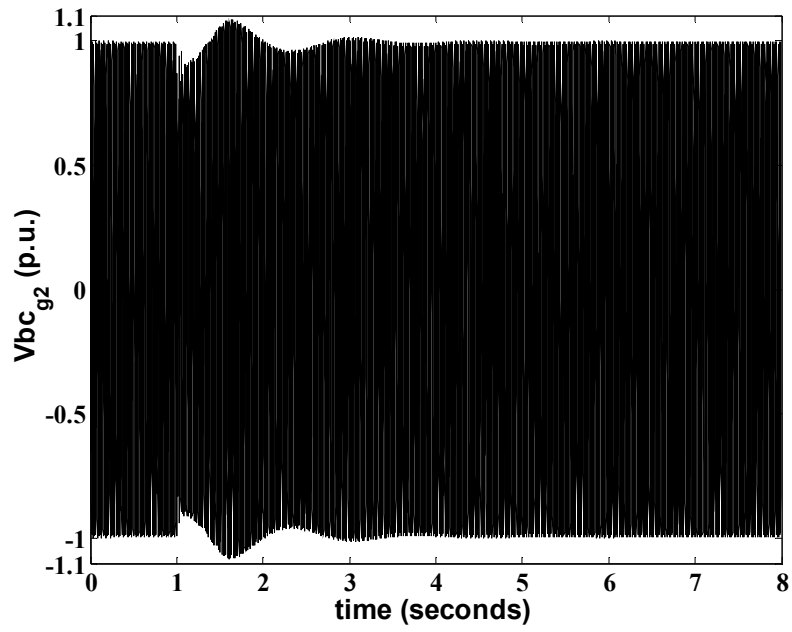


Figure 4.10 Phase BC Voltage of Generator 2

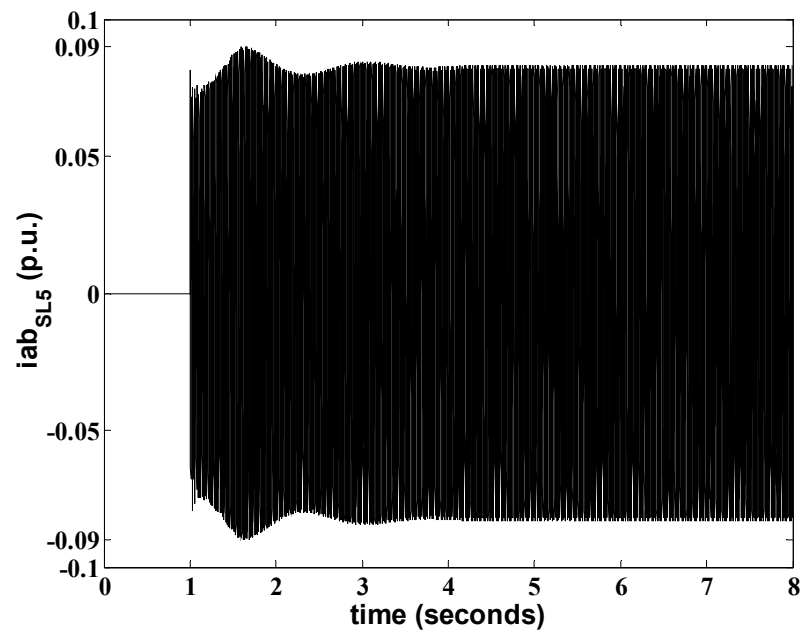


Figure 4.11 Phase AB Current of Static Load 5

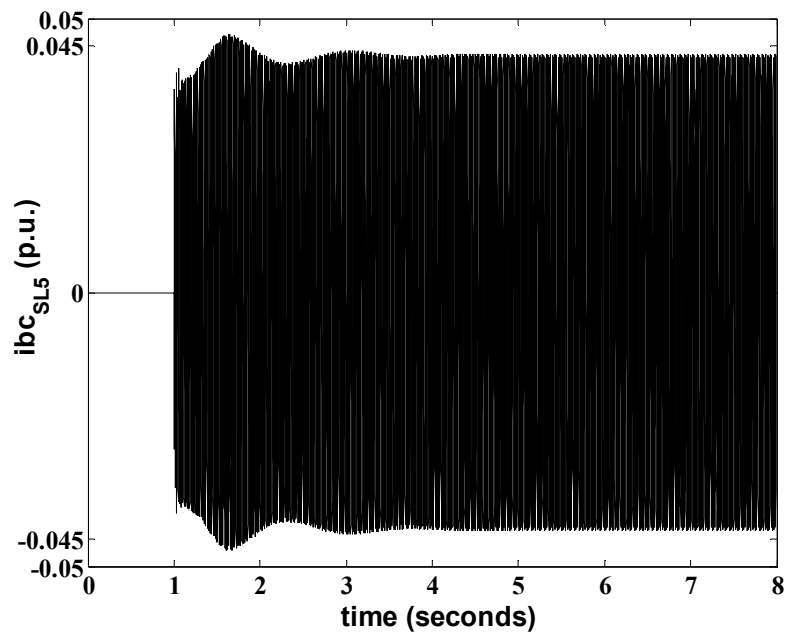


Figure 4.12 Phase BC Current of Load 5

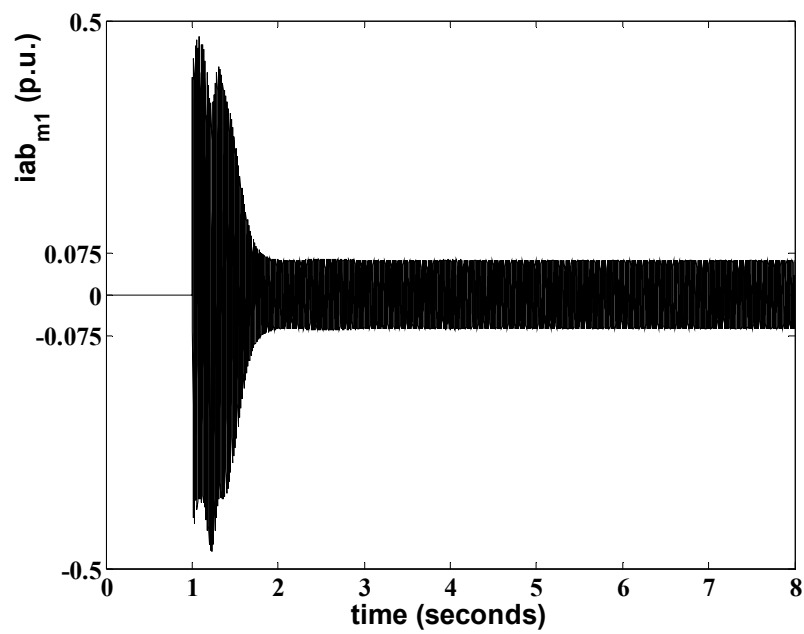


Figure 4.13 Phase AB Current of Induction Motor 1

As described earlier in section 2.3.1, Mayer developed a method based on reformulated component models [18]. Mayer's method reformulates root machines, which could be synchronous or asynchronous machines, to derive the inductor bus voltages. Thus, it is required that there must be at least one root machine connected on each inductor bus. However, in a real power system, it is possible that there are no machines, only inductive components connected on one inductor bus. Mayer's method then could not solve bus voltages for this kind of inductor bus.

In the new modeling methodology for ungrounded stiffly connected power systems, the voltages of both inductor and resistor buses are derived according to the same interconnection procedures. The new method reformulates basic elements of a real power system, generator and lines, to derive input voltages. The new method is thus more generalized than Mayer's method in that it has no limitation on the types of interconnected components on inductor buses. Mayer's method was used to model a one-generator-three-motor SPS [18]. In a paper by the author [74], the same system was modeled and simulated by the new generalized method. The simulation results derived from the new generalized method and from Mayer's method agree with each other. The simulation results of the reduced SPS demonstrate that the new method is a promising modeling methodology for ungrounded stiffly connected power systems.

4.6 A TEST SHIPBOARD POWER SYSTEM

As described earlier, a test SPS having the configuration of an AC radial SPS based on a surface combatant ship was developed in [44]. A new test SPS was designed from the old test SPS for the purpose of stability study. In this section, the new test SPS will be described and the simulation results of the new test SPS at normal operation will be presented.

4.6.1 System Description

A new test SPS developed for the purpose of stability study is shown as Figure 4.14. Each kind of equipment found in the old test system [44] was modeled in the new test system. Generators in both test systems have the same capacity. Table 4.1 lists the components in the test SPS for stability study. The three phase power of motor loads and static loads are shown in Table 4.2 and Table 4.3.

The factors that affect stability were considered in the test system. In the old test system in [44], the percent of the amount of dynamic loads in the total loads was 51.9. The percent was raised to 72.5 in the test system. This percent increase reflects the feature of the predominant amount of induction motors in SPS and facilitates the study of effects of dynamic loads on SPS stability. In order to raise the percent of dynamic loads among the total load in the new test system, several induction motors having large capacity were developed for the new test SPS; their parameters were derived from an auxiliary program named INDMOT from ATP [3]. Several loads having the same characteristics in the old test system in [44] were combined and placed in the new test system. The total capacity of some combined loads was adjusted to maintain the load balance on switchboards. The load torque for every induction motor in the test system was modeled as quadratic torque. The cables in the new test SPS were determined according to capacity of the cables in the old test SPS. Several cables were paralleled for some large loads in the new test SPS.

Table 4.1
Components for Test SPS for Stability Study

Component Name	Components	Ratings
Generators	Generator 1, Generator 2, Generator 3	2.5MW, 0.8 lagging, 60HZ, 450V
Induction Motor loads	L11, L12, L13, L151, L21, L22, L23, L251, L311, L312, L32, L33, L34	Varying from 20 to 300KW, 440V
Three Phase Static Loads	L14, L152, L252, L253, L314, L35	Varying from 60 to 255KW, 440V
Single Phase Static Loads	L153, L24, L36	115V
Transformers	XFM1, XFM2, XFM3	3×25MVA, 450V/120V
Three Phase Cables	C01, C02, C03, C11, C12, C13, C14, C15, C151, C152, C1531, C21, C22, C23, C241, C25, C251, C252, C253, C31, C311, C312, C313, C314, C32, C33, C34, C35, C361, C023, C012, C013, C11a, C12a, C13a, C14a, C151a, C152a, C1531a, C21a, C22a, C23a, C251a, C252a, C311a, C312a, C313a, C314a, C32a, C33a, C35a	450V
Single Phase Cables	C1532, C242, C362,	120V

Table 4.2
Three Phase Power of Induction Motor Loads

Load Name	L11	L12	L13	L151	L21	L22	L23
P (KW)	300	300	100	100	300	240	100
Load Name	L251	L311	L312	L313	L32	L33	L34
P (KW)	240	300	240	20	300	240	100

Table 4.3
Three Phase Power of Static Loads

Load Name	L14	L152	L153	L24	L36
P (KW)	310	60	60	60	60
Load Name	L252	L253	L314	L35	--
P (KW)	115	80	80	255	--

The test system for this stability study had three generators with one for emergency service. The generators were connected to three main switchboards that formed a ring configuration with bus-tie cables. The circuits downstream of the main switchboards were distributed in a radial configuration. The generators were ungrounded delta-connected gas-turbine synchronous machines. There were three load centers downstream of the main switchboards. Load center LC15 was downstream of SB1, LC25 downstream of SB2, and LC31 downstream of SB3. There were fourteen dynamic induction motor loads and nine static loads, fed through main switchboards, load center, and switchboards. The total consumption of this test system was 3.95 MW. Each of the three transformers in the test system was a three-phase transformer bank (three single-phase transformers) in a delta-delta connection. There were 54 power cables to connect various power elements.

A protection scheme was also designed for this test system. The protective devices were circuit breakers for over-current and short-circuit fault protection, ABT and MBT

to provide continuous power supply for vital loads, LVR and LVP to provide low voltage protection for induction motors, and generator switchboard protection logic to provide protection for generator and switchboard group. CBs, ABT, MBT, LVR, and LVP are shown in Figure 4.14. In the figure, the symbols \blacksquare and \square denote a closed and an open circuit breaker, respectively. The symbol $\bullet \times \bullet / \bullet$ denotes a bus transfer unit, in which $\bullet \times \bullet$ indicates a closed position and \bullet / \bullet indicates an open position. An LVP and an LVR in the closed position is denoted by the symbol $\bullet \oplus \bullet$, and the open position is denoted by $\bullet \ominus \bullet$. The ratings and settings of circuit breakers were determined by the rules provided by military document [75]. All circuit breakers in the test SPS were selected from the circuit breakers listed in [76]. The generator switchboard protection logic includes under frequency, under voltage, reverse power and over power relays. These relays were installed on switchboards 1 and 2. The settings of generator switchboard protection logic were determined from the description in [49].

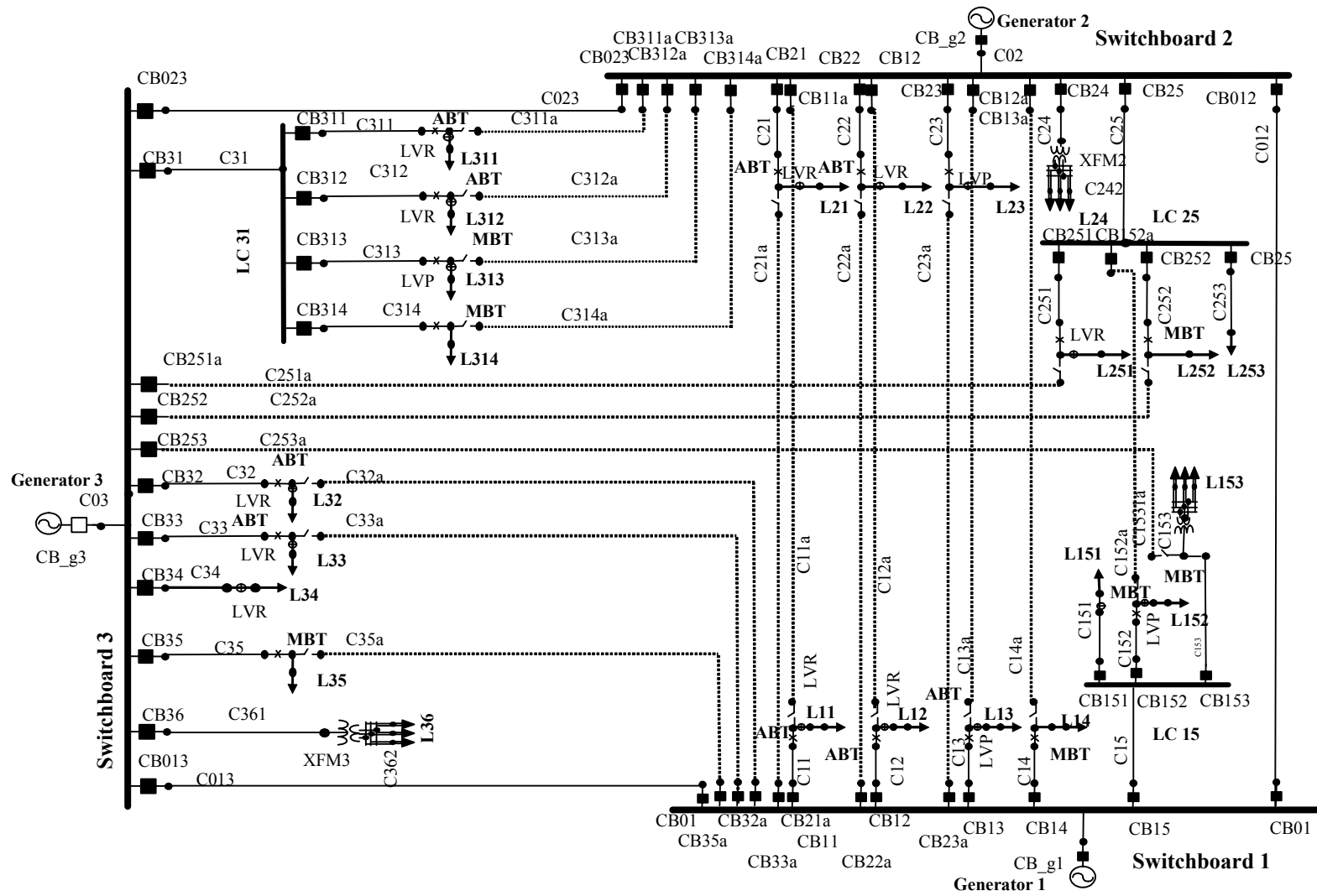


Figure 4.14 A Test SPS for Stability Study

4.6.2 Simulation Results

With the new generalized modeling methodology presented earlier in this chapter, the test system in Figure 4.14 was modeled and simulated in the environment of Matlab/Simulink. The selected integration algorithm was Dormand-Prince ODE5. The simulation was run with a fixed time step of 0.001 seconds and automatic error tolerance.

Figure 4.15-Figure 4.19 shows some representative simulation results of the test SPS at normal operation shown in Figure 4.14. All loads are on their normal paths. The initial condition of generators and loads are set with their steady state values. After a short transient process, the test system settled down to its steady state. Figure 4.15 shows the phase AB voltage of generator 1. Figure 4.16 shows the phase AB voltage of switchboard 3. Figure 4.17 shows the phase A current of induction motor load L11. Figure 4.18 shows the rotor speed of motor load L11. Figure 4.19 shows the phase A current of static load L14. Phase AB voltages of generator 1 and switchboard 3 settle down to a value close to 1.0 p.u.. Current of motor load L11 agrees with the ratio of motor demand to system capacity. Angular speed of motor L11 settles down to a value below 1.0 p.u.. Current of static load L14 agrees with the ratio of static load L14 demand to system capacity. The simulation results at steady state agree with what was expected.

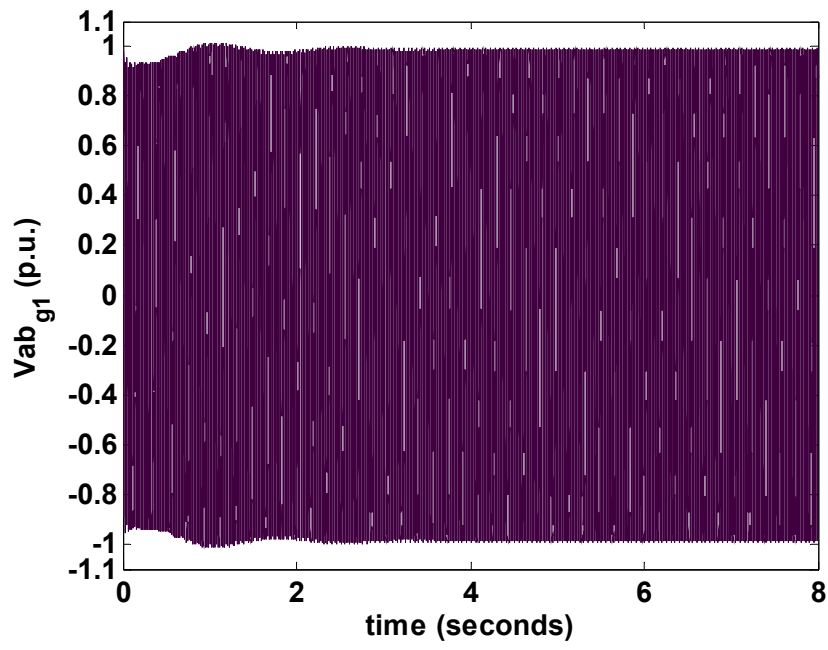


Figure 4.15 Phase AB Voltage of Generator 1

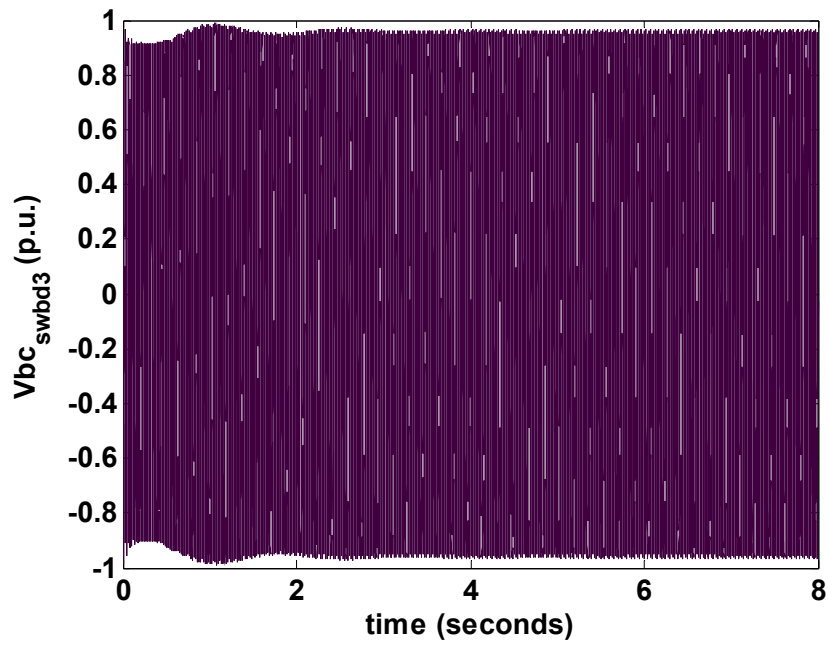


Figure 4.16 Phase BC Voltage on Switchboard 3

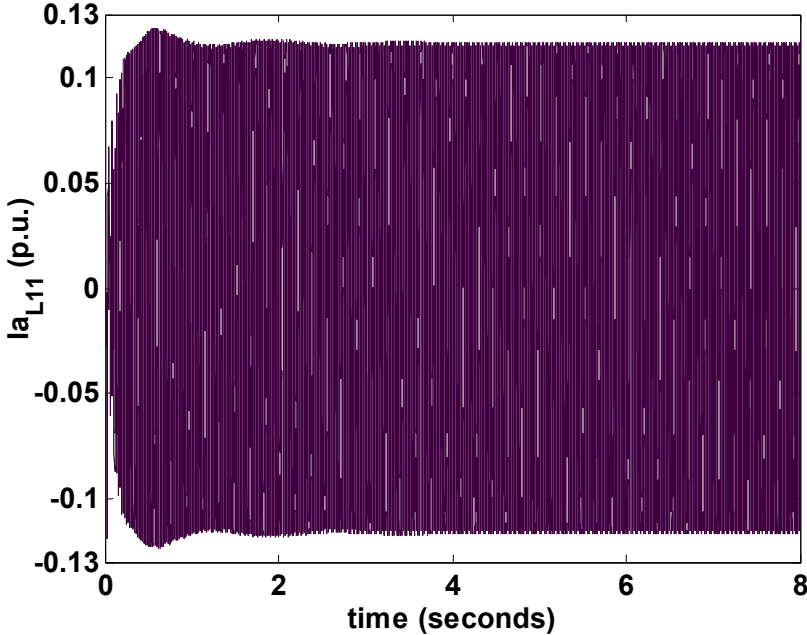


Figure 4.17 Phase A Current of Motor Load L11

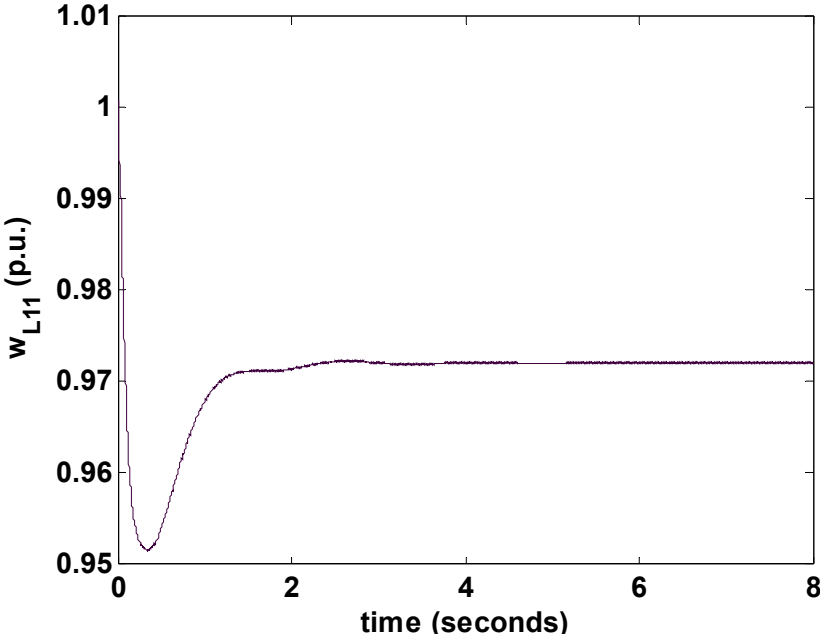


Figure 4.18 Rotor Angular Speed of Motor Load L11

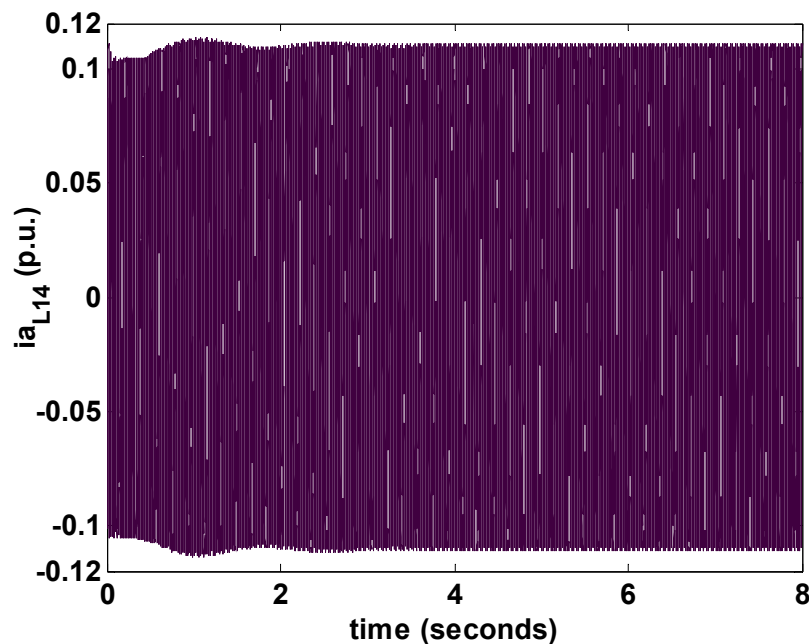


Figure 4.19 Phase A Current of Static Load L14

4.7 CHAPTER SUMMARY

In this chapter, a new generalized modeling methodology for ungrounded stiffly connected power systems was presented. The new method is more generalized than a reformulated model based modeling method reported in the literature by having no limitation on the type of interconnected components on inductor buses. The new method efficiently solves the modeling incompatibility problems on resistor and inductor buses in ungrounded stiffly connected power systems. One reference generator model or line model on each resistor and inductor bus is reformulated from its standard model. A case study shows that the new modeling method is a promising method for ungrounded stiffly connected power systems. A test SPS for the stability study in this dissertation was developed. The test SPS was modeled by the new generalized modeling method. Some representative simulation results of the test SPS at normal operation were shown.

In the next chapter, a new static voltage stability index will be proposed. The new index will be applied for static voltage stability analysis and assessment for the test SPS developed in this chapter.

CHAPTER V

STATIC VOLTAGE STABILITY ANALYSIS

5.1 INTRODUCTION

In order for a power system to maintain system voltage stability after being subjected to a disturbance, equilibrium points of the post disturbance system should exist. The static stability analysis for voltage stability in this dissertation studies whether equilibrium points of post-disturbance systems exist.

In this Chapter, a new static voltage index will be presented. The new index is applied to each cable in a SPS system. The cable with the maximum value of the new index is the weakest cable in the system. The part of SPS below generator switchboards can be taken as a radial distribution system. For the radial part of SPS, the index could indicate the level of stability at each bus. The bus with the maximum value of the new index is thus the most sensitive to voltage instability. In section 5.2, the deduction of the new static voltage stability index will be presented. In section 5.3, the performance of the new index will be compared with the performance of some other voltage stability indices found in the literature. In section 5.4, the index will be applied on the test SPS developed in Chapter IV.

5.2 STATIC VOLTAGE STABILITY INDEX

Figure 5.1 shows a two-bus power system. Sending bus 1 is connected with a source and receiving end bus 2 is connected with a load. The two buses, sending bus 1 and receiving bus 2, are connected by a connecting line L_{21} with impedance Z_{21} . The power flow on the connecting line at the receiving end bus 2 is S_{21} . The current flowing from bus 1 to bus 2 is I_{21} .

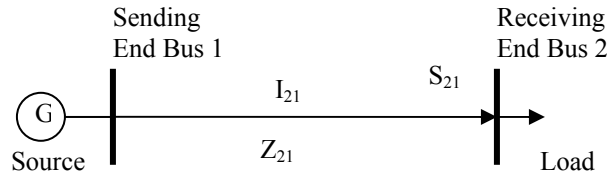


Figure 5.1 A Two-Bus Power System

The power flow on the connecting line S_{21} , the voltages on sending bus V_1 and receiving bus V_2 , and the line impedance Z_{21} are defined as (5.1)-(5.4).

$$S_{21} = P_{21} + jQ_{21} \quad (5.1)$$

$$V_2 = |V_2| \cos \delta_2 + j|V_2| \sin \delta_2 \quad (5.2)$$

$$V_1 = |V_1| \cos \delta_1 + j|V_1| \sin \delta_1 \quad (5.3)$$

$$Z_{21} = R_{21} + jX_{21} \quad (5.4)$$

The real power and reactive power are P_{21} and Q_{21} . The line resistance and reactance are R_{21} and X_{21} . The voltage magnitude and angle are $|V|$ and δ . The subscript 1 and 2 denote variables associated with bus 1 and bus 2.

According to power flow concept in the line, the power flow into the receiving end bus 2 from the sending end bus 1 S_{21} is derived as (5.5).

$$\begin{aligned} S_{21} &= V_2 I_{21}^* = V_2 \left(\frac{V_1 - V_2}{Z_{12}} \right)^* = V_2 \left(\frac{V_1^* - V_2^*}{R_{21} - jX_{21}} \right) = \frac{V_2 V_1^* - |V_2|^2}{R_{21} - jX_{21}} \\ &= \frac{|V_1| |V_2| (\cos \delta_{21} + j \sin \delta_{21}) - |V_2|^2}{R_{21} - jX_{21}} \end{aligned} \quad (5.5)$$

where $\delta_{12} = \delta_2 - \delta_1$, and $\delta_{21} = \delta_1 - \delta_2$. The sign “*” indicates the conjugate of the associated variable.

Separating (5.5) into real and imaginary parts, we have a real power balance equation (5.6) and a reactive power balance equation (5.7).

$$P_{21} = \frac{|V_2||V_1|R_{21} \cos \delta_{21} - |V_2||V_1|X_{21} \sin \delta_{21} - |V_2|^2 R_{21}}{R_{21}^2 + X_{21}^2} \quad (5.6)$$

$$Q_{21} = \frac{|V_2||V_1|X_{21} \cos \delta_{21} + |V_2||V_1|R_{21} \sin \delta_{21} - |V_2|^2 X_{21}}{R_{21}^2 + X_{21}^2} \quad (5.7)$$

Taking the magnitude of the sending end bus voltage as the unknown variable, we can rearrange (5.6) and (5.7) into two quadratic equations (5.8) and (5.9).

$$|V_2|^2 - |V_2||V_1|(\cos \delta_{21} - \frac{X_{21}}{R_{21}} \sin \delta_{21}) + (R_{21} + \frac{X_{21}^2}{R_{21}})P_{21} = 0 \quad (5.8)$$

$$|V_2|^2 - |V_2||V_1|(\cos \delta_{21} + \frac{R_{21}}{X_{21}} \sin \delta_{21}) + (X_{21} + \frac{R_{21}^2}{X_{21}})Q_{21} = 0 \quad (5.9)$$

Subtracting (5.8) from (5.9), we obtain (5.10).

$$|V_2||V_1|(-\frac{R_{21}}{X_{21}} \sin \delta_{21} - \frac{X_{21}}{R_{21}} \sin \delta_{21}) + (X_{21} + \frac{R_{21}^2}{X_{21}})Q_{21} - (R_{21} + \frac{X_{21}^2}{R_{21}})P_{21} = 0 \quad (5.10)$$

Multiplying (5.10) by $R_{21}X_{21}$ and making simplifications, we obtain (5.11) in the form of the sine of the angle difference δ_{21} .

$$\sin \delta_{21} = \frac{-X_{21}P_{21} + R_{21}Q_{21}}{|V_1||V_2|} \quad (5.11)$$

Adding the results of the multiplication of (5.8) by $\frac{X_{21}}{R_{21}}$ and the multiplication of

(5.9) by $\frac{R_{21}}{X_{21}}$, we obtain (5.12).

$$\begin{aligned} & |V_2|^2 \left(\frac{X_{21}}{R_{21}} + \frac{R_{21}}{X_{21}} \right) - |V_2||V_1| \left(\frac{R_{21}}{X_{21}} \cos \delta_{21} + \frac{X_{21}}{R_{21}} \cos \delta_{21} \right) \\ & + (X_{21} + \frac{R_{21}^2}{X_{21}}) \frac{X_{21}}{R_{21}} Q_{21} + (R_{21} + \frac{X_{21}^2}{R_{21}}) \frac{R_{21}}{X_{21}} P_{21} = 0 \end{aligned} \quad (5.12)$$

Multiplying (5.12) by $R_{21}X_{21}$, and making simplifications, we obtain (5.13) in the form of the cosine of the angle difference δ_{21} .

$$\cos \delta_{21} = \frac{|V_2|^2 + X_{21}Q_{21} + R_{21}P_{21}}{|V_1||V_2|} \quad (5.13)$$

Applying the trigonometric identity on (5.11) and (5.13), we derive (5.14).

$$\left(\frac{-X_{21}P_2 + R_{21}Q_{21}}{|V_1||V_2|}\right)^2 + \left(\frac{|V_2|^2 + X_{21}Q_2 + R_{21}P_{21}}{|V_1||V_2|}\right)^2 = 1 \quad (5.14)$$

With $|V_2|$ as the unknown variable, (5.14) can be written as a quadratic equation (5.15).

$$|V_2|^4 + |V_2|^2(2X_{12}Q_2 + 2R_{12}P_2 - |V_1|^2) + X_{12}^2P_2^2 + R_{12}^2Q_2^2 + X_{12}^2Q_2^2 + R_{12}^2P_2^2 = 0 \quad (5.15)$$

There are four solutions for the quadratic equation (5.15). The four solutions are shown as (5.16).

$$|V_2| = \pm \sqrt{\frac{|V_1|^2 - 2X_{21}Q_{21} - 2R_{21}P_{21} \pm \sqrt{(2X_{21}Q_{21} + 2R_{21}P_{21} - |V_1|^2)^2 - 4(X_{21}^2 + R_{21}^2)(P_{21}^2 + Q_{21}^2)}}{2}} \quad (5.16)$$

Two variables a and b are defined as (5.17) and (5.18). (5.15) thus can be written in the form of a and b as (5.19). a and b are two real numbers and b must be positive.

$$a = |V_1|^2 - 2X_{21}Q_{21} - 2R_{21}P_{21} \quad (5.17)$$

$$b = (X_{21}^2 + R_{21}^2)(P_{21}^2 + Q_{21}^2) \quad (5.18)$$

$$|V_2| = \pm \sqrt{\frac{a \pm \sqrt{a^2 - 4b}}{2}} \quad (5.19)$$

Among the four solutions of $|V_2|$, two are positive, the other two are negative. Because voltage magnitude must be a non-negative number, the two negative solutions are not true solutions. Among the two positive solutions, one has a high value and the other a low value. In power systems, voltages must be maintained close to system voltage, which is the base voltage in a per unit system. Voltage magnitude in per unit thus should be high and close to the value of one. The low positive solution is thus not a feasible solution for a real power system.

As described earlier, the voltage magnitude $|V_2|$ must be a positive number in a real system. To derive a positive feasible solution for a real system, the expression under

square root signs of (5.19) should be positive. Therefore, two inequality equations (5.20) and (5.21) must be satisfied to obtain a real and positive solution for (5.15).

$$a \pm \sqrt{a^2 - 4b} \geq 0 \quad (5.20)$$

$$a^2 - 4b \geq 0 \quad (5.21)$$

As defined earlier, b is larger than zero. If a is negative or zero, (5.20) can not be satisfied. Thus, a must be positive. One inequality equation (5.22) is derived as the solution for the inequalities equations (5.20) and (5.21).

$$0 < \frac{2\sqrt{b}}{a} \leq 1 \quad (5.22)$$

From the deduction earlier there exists a feasible solution for a real power system if (5.22) is satisfied. If (5.22) is not satisfied or the inequality equation (5.23) is satisfied, there is no feasible solution for a real system.

$$\frac{2\sqrt{b}}{a} > 1 \quad (5.23)$$

Substituting (5.17) and (5.18) into $\frac{2\sqrt{b}}{a}$, a new voltage static stability index $SVSI_{L21}$ can be defined as (5.24) for the two-bus system in Figure 5.1.

$$SVSI_{L21} = \frac{2\sqrt{(X_{21}^2 + R_{21}^2)(P_{21}^2 + Q_{21}^2)}}{|V_1|^2 - 2X_{21}Q_{21} - 2R_{21}P_{21}} \quad (5.24)$$

$SVSI_{L21}$ is the stability index derived from the power flow on the line between sending bus 1 and receiving bus 2 in the two-bus system. $SVSI_{L21}$ is a real number and indicates whether there are solutions for the two-bus system. $SVSI_{L21}$ indicates the steady state voltage stability of the line and thus can indicate the stability level of the two-bus power system. If the $SVSI_{L21}$ is less than one, there are solutions for (5.15) and the system is stable. If the $SVSI_{L21}$ is equal to one, there are two equal solutions for (5.15) and the system is at stability boundary. If the $SVSI_{L21}$ is larger than one, there is no solution for (5.15). The system becomes unstable or steady-state voltage collapse occurs. The closer to one the value of $SVSI_{L21}$ is, the closer the system is operating to voltage instability.

SVSI_{L21} in a more general sense can be deduced on any line in a power system. Figure 5.2 shows one-line diagram of a line in a power system. In the figure, a line L_{ji} connects two buses i and j in the system with impedance Z_{ji} . This line is connected to other lines to form a network. On the line L_{ji} in the system, the current flowing into bus j from bus i is I_{ji} . The power flow into receiving bus j from line L_{ji} is S_{ji} . If this system is a radial power system, the power transmitted through the line could be the summation of the load demand at the receiving end bus j . At the sending end bus i , according to power flow concept in the line, (5.25) thus is satisfied. The similar procedures to deduce SVSI_{L21} for the two-bus system are applied for (5.25).

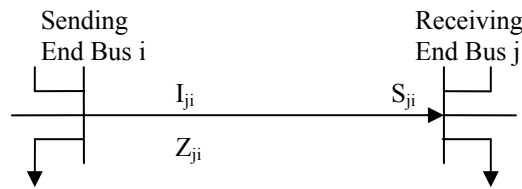


Figure 5.2 One-line Diagram of a Line in a Power System

$$\begin{aligned}
 S_{ji} &= V_j I_{ji}^* = V_j \left(\frac{V_i - V_j}{Z_{ji}} \right)^* = V_j \left(\frac{V_i^* - V_j^*}{R_{ji} - jX_{ji}} \right) = \frac{V_j V_i^* - |V_j|^2}{R_{ji} - jX_{ji}} \\
 &= \frac{|V_i| |V_j| (\cos \delta_{ji} + j \sin \delta_{ji}) - |V_j|^2}{R_{ji} - jX_{ji}}
 \end{aligned} \tag{5.25}$$

Equation (5.26) can be derived from (5.25).

$$\begin{aligned}
 &|V_j|^2 \left(\frac{X_{ji}}{R_{ji}} + \frac{R_{ji}}{X_{ji}} \right) - |V_j| |V_i| \left(\frac{R_{ji}}{X_{ji}} \cos \delta_{ji} + \frac{X_{ji}}{R_{ji}} \cos \delta_{ji} \right) \\
 &+ \left(X_{ji} + \frac{R_{ji}^2}{X_{ji}} \right) \frac{X_{ji}}{R_{ji}} Q_{ji} + \left(R_{ji} + \frac{X_{ji}^2}{R_{ji}} \right) \frac{R_{ji}}{X_{ji}} P_{ji} = 0
 \end{aligned} \tag{5.26}$$

A more generalized static voltage stability index (SVSI_{L,ji}) thus is derived for any line in a power system.

$$SVSI_{ji} = \frac{2\sqrt{(X_{ji}^2 + R_{ji}^2)(P_{ji}^2 + Q_{ji}^2)}}{\left| |V_i|^2 - 2X_{ji}Q_{ji} - 2R_{ji}P_{ji} \right|} \quad (5.27)$$

SVSI_{L_{ji}} is the stability index of any line between two buses in an interconnected power system. SVSI_{L_{ji}} is a real number. If the SVSI_{L_{ji}} is less than one, there are solutions for (5.26). If the SVSI_{L_{ji}} is equal to one, there are two equal solutions for (5.26). The closer to one the value of SVSI_{L_{ji}} is, the lower sustainable load the line is operating with. If the SVSI_{L_{ji}} is larger than one, there is no solution for (5.26). Nonexistence of steady-state of a system agrees with the occurrence of voltage collapse in a system. SVSI_{L_{ji}} thus can be used to study voltage collapse in a system.

In an interconnected power system, SVSI_{L_{ji}} is calculated on all lines in a shipboard power system. If the values of SVSI_{L_{ji}} for all lines in a system are less than one, a system is statically stable. If SVSI_{L_{ji}} of at least one line is equal to one, the whole system is at its stability boundary. If SVSI_{L_{ji}} of at least one line is larger than one, the whole system loses its stability and voltage collapses. In the radial part of a shipboard power system, there is only one line connecting between two buses. SVSI_{L_{ji}} calculated on the line then can indicate the stability level of the receiving end bus of the line. The maximum value of SVSI_{L_{ji}} thus identifies not only the line operating closest to its stability boundary but also the bus closest to voltage collapse.

5.3 COMPARISON OF STATIC VOLTAGE STABILITY INDICES

The performance of the new index is compared with some other indices found in the literature. Three other static voltage stability indices FVSI, LQP, and VSI were proposed by [28], [29], and [30], respectively. They are written as (5.28), (5.29), and (5.30). The static voltage stability index proposed in this dissertation is shown as (5.24).

$$FVSI = \frac{4Z^2 Q_j}{V_i^2 X} \quad (5.28)$$

$$LQP = 4 \left(\frac{X}{V_i^2} \right) \left(\frac{X}{V_i^2} P_i^2 + Q_j \right) \quad (5.29)$$

$$VSI = \frac{S_j}{V_j^2 Y_{jj}} \quad (5.30)$$

Subscripts i and j denote variables related with sending end and receiving end of a line respectively. For all the indices, including the new index $SVSI_{Lji}$, the value of one indicates the stability boundary. Voltage is statically stable when the index value is larger than zero and less than or equal to one. The closer to one the index value is, the closer the system is to voltage instability.

The simple two-bus system shown as Figure 5.1 is used as an example system to compare the three indices and the new index. All variables are expressed as per unit values. The bus voltage at the sending end bus is assumed to be the one in the power flow. The real power of the load at receiving bus 2 increases from zero to 2.4 p.u.. The values of the voltage stability indices were calculated at each load level. The impedance of the line was varied to represent long and short connecting lines (LL and SL). The power factor of the load at the receiving end bus 2 was varied to represent high and low power factors (HPF and LPF). There are four combinations with different line lengths and load factors. They are LL and HPF, LL and LPF, SL and HPF, and SL and LPF. Each of the four combinations represents one situation at which the four voltage indices were compared. The different values of the line impedance and power factors are shown in Table 5.1 and Table 5.2.

Table 5.1
Line Impedance

Line	Impedance
LL	0.17+j0.0205
SL	0.085+j0.01

Table 5.2
Load Power Factors

Power Factor	Value
HPF	0.9
LPF	0.6

Figure 5.3-Figure 5.6 show the performance comparison of the four voltage indices at different situations with different combinations of line length and load factors. The PV curve indicates the change of voltage on bus 2 at the receiving end of the line with the change of real power at bus 2. In each figure, the PV curve at each different situation is drawn. The voltage at bus 2 decreases as real power at bus 2 is increased. At point A of the PV curves, voltage instability occurs. The power at point A is thus the maximum allowable power of the load at bus 2.

Figure 5.3 and Figure 5.4 compare the four indices when the line is short and the power factor of the load is high and low, respectively. All indices increase as the real power of the load increases. When voltage instability occurs, indices $SVSI_{Lji}$ and VSI reach one. The other two indices are below one. LQP is the closer of the two to one. It is found that voltage instability occurs at a lower load level with the low power factor. This is because the load with the low power factor demands more reactive power and draws more current through the line. The voltage drop on the line is larger. Voltage instability with the low power factor thus occurs at a lower load level than that with the high power factor.

Figure 5.5 and Figure 5.6 compare the four indices when the line is long and the power factor of the load is high and low, respectively. The same observations from Figure 5.3 and Figure 5.4 can be made from Figure 5.5 and Figure 5.6. It can also be seen that voltage instability with the long line occurs at a lower load level than that with the short line. The long line has larger line impedance, which causes larger voltage drop

on the line. Voltage instability with long lines thus occurs at a lower load level than with short lines.

Among the three indices found in the literature, LQP neglects the angle difference between sending bus and receiving bus. To improve calculation speed, FVSI neglects line resistance. From the performance of the indices shown in the figures, LQP and FVSI are not as accurate as the new index $SVSI_{Lji}$. VSI gradually approaches the value of one as the load power is increased. However, when the maximum allowable power is reached, VSI begins to decrease. The value of VSI is less than one once the load power is larger than the maximum allowable power and the voltage on bus 2 is unstable. $SVSI_{Lji}$ increases continuously after the voltage on bus 2 enters an unstable region. The value one clearly separates the stable voltage region from the unstable region. From the earlier description, it can be concluded that $SVSI_{Lji}$ has the best performance among the four indices. VSI is second best, LQP is third, and FVSI is fourth.

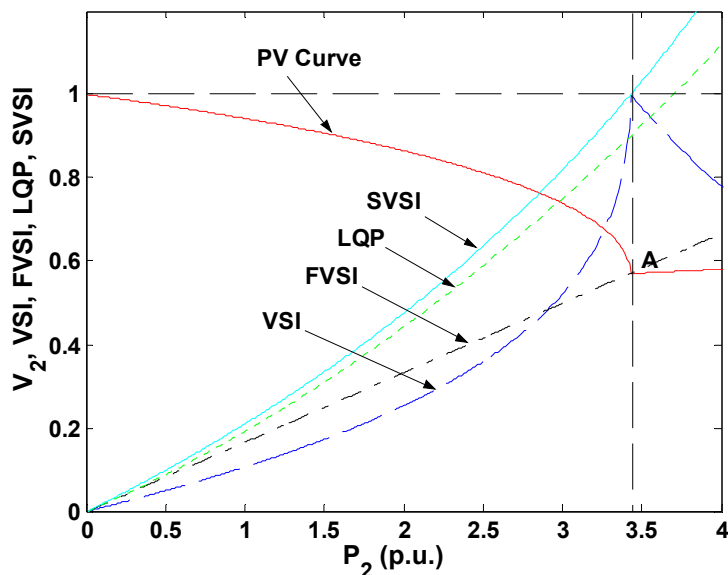


Figure 5.3 Performance Comparison of Various Static Voltage Stability Indices with SL and HPF

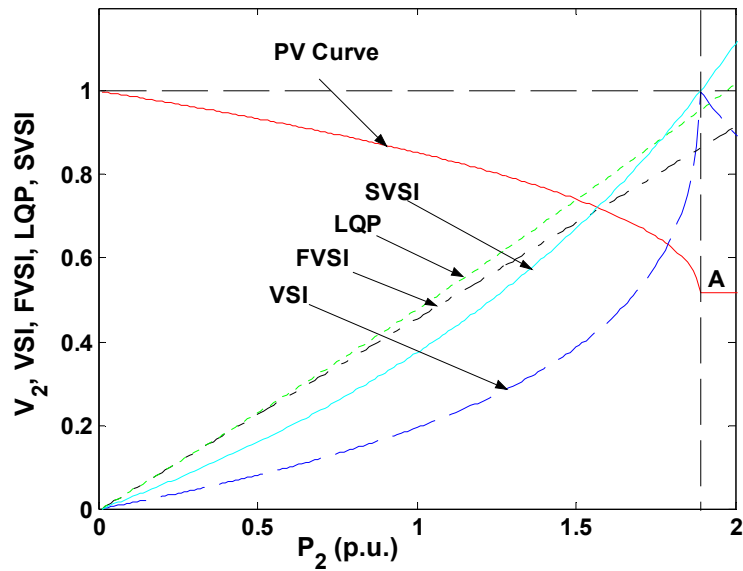


Figure 5.4 Performance Comparison of Various Static Voltage Stability Indices with SL and LPF

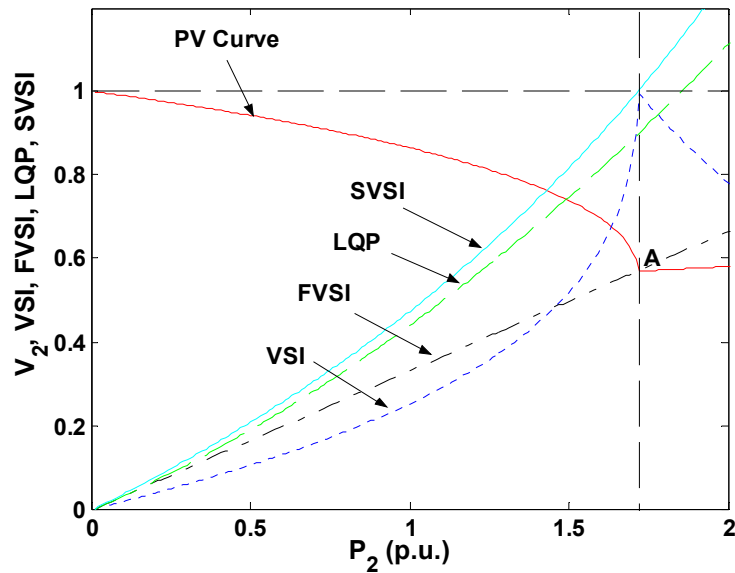


Figure 5.5 Performance Comparison of Various Static Voltage Stability Indices with LL and HPF

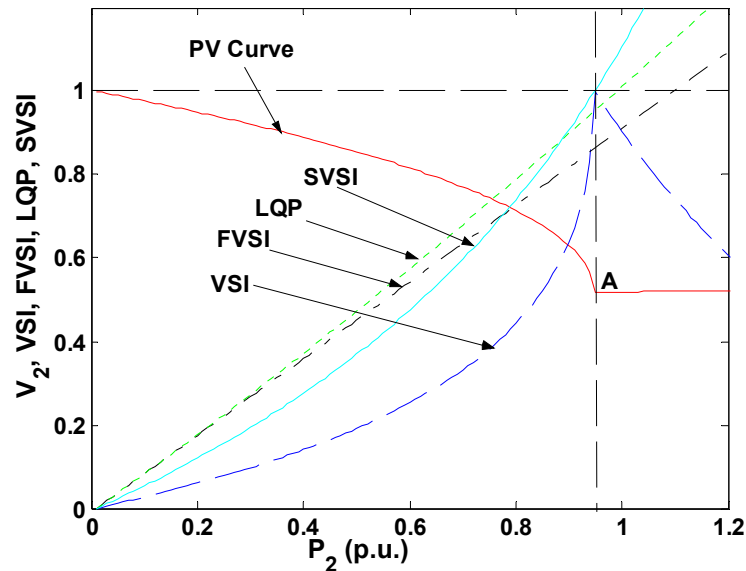


Figure 5.6 Performance Comparison of Various Static Voltage Stability Indices with LL and LPF

5.4 CASE STUDY

The effectiveness of the static voltage stability index ($SVSI_{Lji}$) is demonstrated on the test shipboard power system developed in Chapter IV. The diagram of the test system is shown in Figure 4.14. There are in total 54 cables in the test system. Each transformer in the test SPS is connected between cables. Impedance of transformers and the connected cables were added up and considered as impedance of one cable. Totally 51 cables were studied in the test system for static analysis.

$SVSI_{Lji}$ was calculated for each of the 51 cables in the test system according to (5.24). To calculate $SVSI_{Lji}$ with (5.24), voltage magnitude $|V_2|$, real power P_2 and reactive power Q_2 flowing through the line need to be known. The values of $SVSI_{Lji}$ of the 51 cables were calculated in two ways. One way is through static analysis. The other way is

through the results from time domain simulation. The values of $|V_2|$, P_2 , and Q_2 were calculated in each of the two ways.

Throughout the calculations in static analysis, the output voltages of generators were assumed to be 1.0 p.u. and each load was represented by a constant power load model at nominal rating. With the output voltages of generators assumed to be 1.0 p.u., voltage magnitudes at other buses in the test system were obtained using (5.19). For the radial part of the test system, the power flowing through a cable was calculated as the power summation of loads at the receiving end of the cable. The power flowing through a load cable was calculated as the load power. The power flowing through a load center cable was calculated as the power summation of loads under the load center. It was assumed that each of the two generators supplied half of total load demand in the test system. The loads on switchboards 1 and 2 and were supplied by generators 1 and 2, respectively. The loads on switchboard 3 were supplied by generators 1 and 2 through cables C013 and C023. The power flowing through tie line cables C013 or C023 thus were equal to the half of total load demand minus the load demand on switchboard 1 or 2. At normal operation, the power of all loads was set equal to their nominal values, and all loads having two supplying paths were supplied through their normal path. The SVSI_{L_{ji}} value of each cable at normal operation was calculated and is shown in the second column in Table 5.3.

The test system at normal operation was modeled and simulated in time domain by the methodology described in Chapter IV. From simulation results at steady state, voltage magnitude $|V_2|$, real power P_2 and reactive power Q_2 flowing through cables could be derived. Since time domain simulation results were in the reference frame of 0dq, the voltages and power were calculated by (5.31)-(5.33).

$$|V_2| = \sqrt{V_{d2}^2 + V_{q2}^2} \quad (5.31)$$

$$P_2 = \text{Re}((V_1 - V_2) \cdot I^*) \quad (5.32)$$

$$Q_2 = \text{Im}((V_1 - V_2) \cdot I^*) \quad (5.33)$$

where V is equal to $V_d + jV_q$ and I is equal to $I_d + jI_q$. V_d and V_q are d- and q-axis voltages. Subscripts 1 and 2 denote variables associated with sending and receiving buses of a cable. I is the current flowing through a cable. * denotes the conjugate of a variable. Using the steady state simulation results at normal operation of the test SPS, the $SVSI_{Lji}$ value of each cable were calculated again. The results are shown in the third column in Table 5.3.

From Table 5.3, it can be seen that the $SVSI_{Lji}$ values of all cables in the test system at normal operation are small. The $SVSI_{Lji}$ value of C012 is zero. This is because the voltages on switchboards 1 and 2 were equal at steady state and no current flowed through the tie line C012. Since the alternate cables were not connected in the system at normal operation, their $SVSI_{Lji}$ values are thus shown as zero in the table. $SVSI_{Lji}$ of cable C03, which can connect the back up generator 3 to switchboard, is also zero, since the generator is not connected.

From the comparison of the second and third column of Table 5.3, it can be seen that, using the same calculation equation as (5.24), the $SVSI_{Lji}$ values computed from values calculated in static analysis are larger than the $SVSI_{Lji}$ values computed from values calculated from the simulation results. $SVSI_{Lji}$ is deduced based on static power flow. The assumption of unit voltage at generator output and the usage of constant power load models in static analysis are the reasons for larger $SVSI_{Lji}$ values in static analysis than time domain simulations. Therefore, $SVSI_{Lji}$ derived in static analysis is more conservative in stability assessment than derived from time domain simulations. $SVSI_{Lji}$ in static analysis can be applied to predict the voltage stability level of each cable or each load bus of post-disturbance systems. A $SVSI_{Lji}$ value less than one (such as 0.9) indicates a poor level of stability after a system is disturbed.

Table 5.3
SVSI_{L_{ji}} Values of Cables at Normal Operation

Cable Name	SVSI _{L_{ji}} from Static Analysis	SVSI _{L_{ji}} from Simulation
C01	0.0020	0.0019
C02	0.0020	0.0019
C11	0.0737	0.0699
C12	0.0801	0.0760
C13	0.0473	0.0450
C14	0.0382	0.0374
C15	0.0450	0.0428
C151	0.0205	0.0191
C152	0.0139	0.0132
C1531+C1532+T1	0.0783	0.0716
C21	0.0735	0.0698
C22	0.0931	0.0883
C23	0.0312	0.0298
C241+C242+T2	0.0215	0.0213
C25	0.0792	0.0743
C251	0.0902	0.0813
C252	0.1010	0.0882
C253	0.0151	0.0138
C31	0.0707	0.0660
C311	0.1123	0.1001
C312	0.1883	0.1678
C313	0.0328	0.0295
C314	0.0189	0.0171
C32	0.0557	0.0523
C33	0.0323	0.0304
C34	0.0569	0.0534
C35	0.0581	0.0549
C361+C362+T3	0.1388	0.1255
C023	0.0277	0.0264
C012	0	0

Table 5.3 Continued

C013	0.043	0.0408
C03, C11a, C12a,	0, 0,0,	0, 0,0,
C13a, C14a, C151a,	0, 0,0,	0, 0,0,
C152a, C1531a,	0, 0,0,	0, 0,0,
C21a, C22a, C23a,	0, 0,0,	0, 0,0,
C251a, C252a,	0, 0,0,	0, 0,0,
C311a, C312a,	0, 0,0,	0, 0,0,
C313a, C314a, C32a,	0,0	0,0
C33a, C35a		

In SPS, important loads normally have two paths. These are the normal path and alternate path. To study the $SVSI_{L_{ji}}$ values of alternate cables, all loads having two paths were switched from their normal path to their alternate path. The consumed power of each load was kept at the nominal level. The $SVSI_{L_{ji}}$ values of all cables at this situation are shown in Table 5.4. Due to the different cable lengths, the $SVSI_{L_{ji}}$ values of cables of normal paths and alternate paths were different. As described earlier, the $SVSI_{L_{ji}}$ value of each cable in a radial system indicates the voltage stability level at the receiving end bus of the cable. Therefore, when a load is switched from the normal path to its alternate path, the $SVSI_{L_{ji}}$ values of some buses will increase or decrease. From both the $SVSI_{L_{ji}}$ values in Table 5.3 and the $SVSI_{L_{ji}}$ values in Table 5.4, it can be seen that the voltage stability level at some buses decreased after their loads were switched from their normal path to their alternate path. For example, the $SVSI_{L_{ji}}$ value of cable C23 in Table 5.3 is 0.0312 and the $SVSI_{L_{ji}}$ value of cable C23a in Table 5.4 is 0.1261. The bus corresponding to the terminal of load L23 was thus more sensitive to voltage instability after the load was switched from its normal path to its alternate path.

Table 5.4
SVSI_{L_{ji}} Values of Cables When Loads are on Alternate Paths

Cable Name	SVSI _{L_{ji}}
C01	0.0024
C02	0.0020
C15	0.0221
C151	0.0201
C25	0.021
C253	0.0142
C34	0.0571
C361+C362+T3	0.1394
C023	0.00520
C013	0.0545
C11a	0.019
C12a	0.0423
C13a	0.1444
C14a	0.0418
C151a	0.0201
C152a	0.0659
C1531a+C1532+T1	0.0204
C21a	0.0479
C22a	0.0239
C23a	0.1261
C251a	0.0379
C252a	0.0418
C311a	0.0519
C312a	0.1072
C313a	0.0161
C314a	0.0350
C32a	0.0310
C33a	0.0765
C35a	0.0250

Table 5.4 Continued

C03, C11, C12,	0, 0, 0,
C13, C14, C152,	0, 0,
C1531+C1532+T1,	0,
C21, C22, C23,	0, 0, 0,
C241+C242+T2,	0,
C251, C252, C31,	0, 0, 0,
C311, C312, C313,	0, 0, 0,
C314, C32, C33, C35,	0, 0, 0,0,
C012	0

As described earlier, if a $SVSI_{L_{ji}}$ value is closer to one, a cable is closer to static voltage stability boundary. From Table 5.3 and Table 5.4, it can be seen that, when loads are kept at nominal levels, most $SVSI_{L_{ji}}$ values of the cables in the test system are less than 0.1. The cables in the test SPS are thus far away from the stability boundary. In other words, the cables in the test system are not stressed at all. This is because of the short length of the cables in the test SPS. Among all cables in the test system, four cables in the test system had $SVSI_{L_{ji}}$ values larger than 0.1. From Table 5.3, it is found that the $SVSI_{L_{ji}}$ value of cable C312 is the maximum, which is shaded in Table 5.3. Therefore, among all cables in the test system, cable C312 is the cable most sensitive to voltage instability when the system is at normal operation. The receiving end bus of cable C312, which is connected to load L312, is the critical bus and the most sensitive to voltage instability when the test SPS is at normal operation.

With the other conditions at normal operation unchanged, the real power of load L312 was increased gradually. The relationship between the real power level P_{L312} and the $SVSI_{L_{ji}}$ of cable C312 is shown in Figure 5.7. The $SVSI_{L_{ji}}$ value of C312 increased as the load level of L312 increased, which indicates that cable C312 became more and more stressed as the load level of L312 increased. From the figure, the $SVSI_{L_{ji}}$ value of C312 reached one as P_{L312} is increased to a level around 3.02. For P_{L312} equal to 3.02 p.u., the $SVSI_{L_{ji}}$ values of all cables in the test system at normal operation are shown in

Table 5.5. It is seen in the table that the $SVSI_{L_{ji}}$ of cable C312, shaded in Table 5.5, is larger than one. Voltage instability is thus found on cable C312 by $SVSI_{L_{ji}}$ in this static voltage stability analysis.

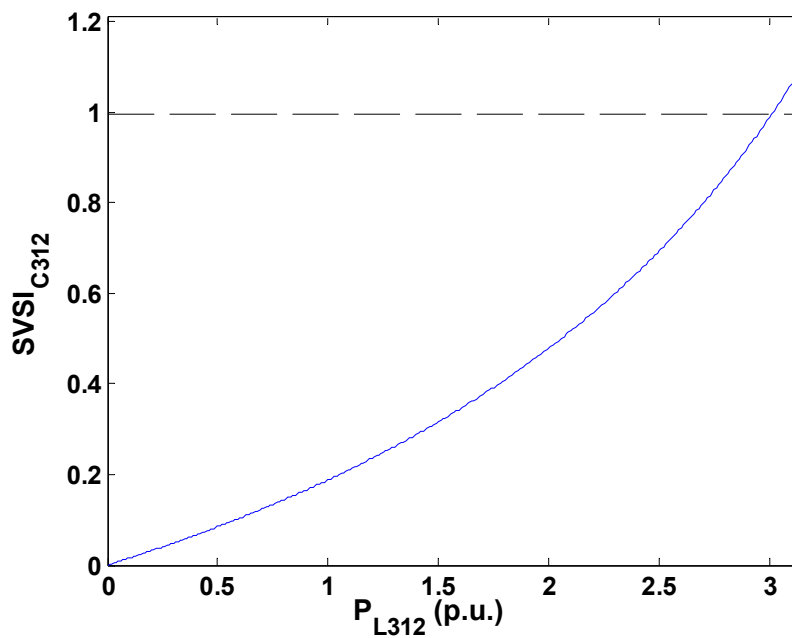


Figure 5.7 The Relationship between $SVSI_{C312}$ and P_{L312}

Table 5.5
SVSI_{L_{ji}} Values When P_{L312}=3.02 p.u.

Cable Name	SVSI _{L_{ji}}		Cable Name	SVSI _{L_{ji}}
C01	0.0023		C251	0.0902
C02	0.0023		C252	0.1010
C11	0.0737		C253	0.0151
C12	0.0802		C31	0.1337
C13	0.0473		C311	0.1209
C14	0.0382		C312	1.0036
C15	0.0450		C313	0.0351
C151	0.0205		C314	0.0202
C152	0.0139		C32	0.0562
C1531+C1532+T1	0.0784		C33	0.0326
C21	0.0735		C34	0.0574
C22	0.0931		C35	0.0586
C23	0.0313		C361+C362+T3	0.1401
C241+C242+T2	0.0215		C023	0.0584
C25	0.0792		C013	0.0365
C03, C012, C11a, C12a, C13a, C14a, C151a, C152a, C1531a, C21a, C22a, C23a, C251a, C252a, C311a, C312a, C313a, C314a, C32a, C33a, C35a	0,0,0, 0,0,0, 0,0, 0,0,0, 0,0,0, 0,0, 0,0,0, 0,0		--	--

SVSI_{L_{ji}} can be implemented in SPS reconfiguration. For each reconfiguration operation, SVSI_{L_{ji}} values of all cables of post-disturbance systems should be calculated. The maximum SVSI_{L_{ji}} at each operation can be used as an indicator of system stability. If there are several reconfiguration operations to choose from, the system stability indicators of different operations should be compared. It is suggested that the operation

with the minimum system stability indicator should be recommended for reconfiguration. In addition, if a reconfiguration operation leads to a poor level of system stability, the reconfiguration operation should be avoided. The value of the level to indicate a poor level of system stability should be chosen according to the situation of a real system.

In static analysis, the largest $SVSI_{L_{ji}}$ value shows the weakest line or bus in a system. However, in static analysis, the dynamics of a system are not considered. A system can be already unstable during its dynamic process before the system is evolved to the point where instability is indicated in static analysis. In this sense, $SVSI_{L_{ji}}$ is more useful for contingency ranking, which chooses the cases most likely to be unstable among many cases. The maximum $SVSI_{L_{ji}}$ of each contingency is used to determine system stability level. These $SVSI_{L_{ji}}$ values are ranked in contingency ranking. Voltage instability is more likely to occur in these contingencies with the largest $SVSI_{L_{ji}}$ values. In this chapter, it was shown that cable C312 is the weakest cable for voltage instability in the test system at normal operating point (loads at 1.0 p.u. and on normal paths). In the dynamic stability analysis in the next chapter, the dynamic instability caused by the load increase of L312 will be studied.

5.5 CHAPTER SUMMARY

In this chapter, based on the solvability of load flow equations, a new static voltage stability index ($SVSI_{L_{ji}}$) was deduced. The performance of the new index was compared with other static voltage stability indices in the literature. The new index was determined to indicate voltage instability more accurately. $SVSI_{L_{ji}}$ was applied on the test system developed in Chapter III. The $SVSI_{L_{ji}}$ values were calculated and indicated the voltage stability level of each cable or bus in the test system. It was shown that cable C312 in the test system was the most sensitive to voltage instability when loads were at nominal levels and all loads having two paths were supplied power from normal and alternate paths. The load L312 is thus the critical load in the test system at this operating point.

In the next chapter, a new dynamic voltage stability index will be presented. The new dynamic index will be applied to analyze and assess voltage stability of the test SPS developed in Chapter IV.

CHAPTER VI

DYNAMIC VOLTAGE STABILITY ANALYSIS

6.1 INTRODUCTION

In Chapter V, a static voltage stability index was presented for static analysis. Static analysis can only detect voltage stability for a statically modeled system. With dynamics modeled by differential equations, dynamic analysis can provide more accurate results in voltage stability studies. In dynamic analysis, bifurcations of a dynamic system including both saddle node bifurcation and Hopf bifurcation are detected where instability occurs.

In this Chapter, using the techniques of eigenvalue decomposition (ED) and singular value decomposition (SVD), a new dynamic voltage stability index (DVSI) will be deduced to detect bifurcations in a dynamic power system. In section 6.2, the eigenvalue decomposition (ED), singular value decomposition (SVD) and their application to bifurcation detection will be introduced. Based on ED and SVD, a new dynamic voltage stability index (DVSI) will be deduced in section 6.3. In section 6.4, the results of bifurcation detection from the new index will be compared with the results derived from AUTO, an existing software package for bifurcation analysis. In section 6.4, the index will be applied to the test SPS developed in Chapter IV.

6.2 EIGENVALUE DECOMPOSITION AND SINGULAR VALUE DECOMPOSITION

As described in Chapter III, a reduced Jacobian matrix, \mathbf{J}_r , describes a linear system and approximates a dynamic nonlinear system around its equilibrium points. In voltage stability studies, a reduced Jacobian matrix is thus studied for the local bifurcations of a power system. Eigenvalues and singular values of a reduced Jacobian matrix will be used for developing a new voltage stability index to detect local bifurcations in this

chapter. In this section, some basic knowledge of eigenvalue decomposition (ED) and singular value decomposition (SVD) will be introduced. The related applications of ED and SVD on bifurcation detection will also be described.

6.2.1 Eigenvalue Decomposition

The eigenvalue decomposition for a reduced Jacobian matrix \mathbf{J}_r , assuming that is diagonalizable, can be written as (6.1) [2].

$$\mathbf{J}_r = \sum_n \mu_n \mathbf{u}_n \mathbf{v}_n^T \quad (6.1)$$

where μ_n is the n^{th} eigenvalue. \mathbf{u}_n and \mathbf{v}_n are the n^{th} left and right eigenvectors. \mathbf{u}_n and \mathbf{v}_n are defined as non zero vectors. A zero eigenvalue or a pair of pure imaginary eigenvalues emerges when a saddle node bifurcation or a Hopf bifurcation occurs.

According to the eigenvalue decomposition shown as (6.1), the linearized system modeled by \mathbf{J}_r can be decomposed into several modes [2]. Each mode has an eigenvalue and right and left eigenvectors associated with it. A mode represents a transient behavior with a single time constant or a single damping and frequency [2]. The system behavior is the result of many modes acting at once. For a monotonically growing or decaying mode, the associated eigenvalue μ_n is a real positive or negative number, which describes modal damping. For an oscillatory mode, the associated eigenvalue μ_n is a complex number, which describes modal damping and frequency. Right eigenvector \mathbf{v}_n gives mode shapes or relative activities of state variables when the n^{th} mode is excited. The magnitude of the right eigenvectors of different eigenvalues show the extent of the activities and the angles show the phase displacements of the activities. Left eigenvector \mathbf{u}_n weighs the contribution of these activities to the n^{th} mode. The maximum entry in the right eigenvector corresponds to the critical state variable in a system, and the maximum entry in the left eigenvector pinpoints the most sensitive direction for change of the system [2].

6.2.2 Singular Value Decomposition

Any matrix can be decomposed by an orthonormal singular value decomposition (SVD). The singular decomposition of a reduced Jacobian matrix \mathbf{J}_r is shown as (6.2) [69].

$$\mathbf{J}_r = \mathbf{U} \mathbf{\Sigma} \mathbf{V}^T = \sum_{n=1}^N \sigma_n \mathbf{u}_n \mathbf{v}_n^T \quad (6.2)$$

where U and V are N by N orthonormal matrices. \mathbf{u}_n and \mathbf{v}_n are the n^{th} left and right singular vectors and n^{th} columns of matrices U and V . \mathbf{u}_n and \mathbf{v}_n are non zero vectors. Σ is a diagonal matrix and can be written as (6.3) [69].

$$\mathbf{\Sigma}(\mathbf{J}_r) = \text{diag}\{\sigma_n(\mathbf{J}_r)\} \quad (6.3)$$

where $\sigma_n(\mathbf{J}_r)$ is the n^{th} singular value of matrix J_r . σ_n is a non negative real number.

If the matrix \mathbf{J}_r is singular, then there must be at least one zero singular value among all singular values [69]. Therefore, there must be at least one zero singular value at saddle node bifurcations. Since singular values are non negative numbers, the minimum singular value of the system Jacobian matrix $\sigma_{\min}(\mathbf{J}_r)$ is equal to zero at a saddle node bifurcation. When a system is near a singular point, the minimum singular value of the system Jacobian matrix is close to zero. In power systems, the minimum singular value indicates the distance between an operating point and a saddle node bifurcation point [6]. The application of singular value decomposition on voltage stability analysis thus focuses on monitoring the smallest singular value up to the point when it becomes zero. The minimum singular value is a relative measure of how close the system is to a singular point.

6.3 DYNAMIC VOLTAGE STABILITY INDEX

A new dynamic voltage stability index is deduced based on the eigenvalue decomposition and singular value decomposition described in the previous section. From the eigenvalue decomposition, the n^{th} complex eigenvalue of a reduced system Jacobian

matrix \mathbf{J}_r can be defined as (6.4). Subscripts R and I indicate the real and imaginary parts of the eigenvalue.

$$\mu_n = \mu_{Rn} + j \cdot \mu_{In} \quad (6.4)$$

The corresponding right eigenvector \mathbf{v} for the complex eigenvalue is (6.5).

$$\mathbf{v}_n = [\mathbf{v}_{Rn} + j \cdot \mathbf{v}_{In}] \quad (6.5)$$

For the n^{th} right eigenvector and eigenvalue of a matrix, (6.6) is satisfied [2].

$$\mathbf{J}_r \cdot \mathbf{v}_n = \mu_n \cdot \mathbf{v}_n \quad (6.6)$$

Substituting the n^{th} complex eigenvalue and right eigenvector defined by (6.4) and (6.5) into (6.6), we obtain (6.7).

$$\mathbf{J}_r \cdot [\mathbf{v}_{Rn} + j \cdot \mathbf{v}_{In}] = (\mu_{Rn} + j \cdot \mu_{In}) \cdot [\mathbf{v}_{Rn} + j \cdot \mathbf{v}_{In}] \quad (6.7)$$

Arranging (6.7) into real and imaginary parts, we can derive (6.8) and (6.9).

$$(\mathbf{J}_r - \mu_{Rn} \cdot \mathbf{I}) \cdot \mathbf{v}_{Rn} + \mu_{In} \cdot \mathbf{v}_{In} = \mathbf{0} \quad (6.8)$$

$$(\mathbf{J}_r - \mu_{Rn} \cdot \mathbf{I}) \cdot \mathbf{v}_{In} - \mu_{In} \cdot \mathbf{v}_{Rn} = \mathbf{0} \quad (6.9)$$

Equations (6.8) and (6.9) can be rewritten in the format of (6.10) with \mathbf{v}_{Rn} and \mathbf{v}_{In} as unknown variables.

$$\begin{bmatrix} \mathbf{J}_r - \mu_{Rn} \cdot \mathbf{I} & \mu_{In} \cdot \mathbf{I} \\ -\mu_{In} \cdot \mathbf{I} & \mathbf{J}_r - \mu_{Rn} \cdot \mathbf{I} \end{bmatrix} \cdot \begin{bmatrix} \mathbf{v}_{Rn} \\ \mathbf{v}_{In} \end{bmatrix} = \mathbf{0} \quad (6.10)$$

Since eigenvectors of any matrix are defined as nonzero vectors, (6.11) should be satisfied. Equation (6.12) can be derived from (6.11).

$$\begin{bmatrix} \mathbf{J}_r - \mu_{Rn} \cdot \mathbf{I} & \mu_{In} \cdot \mathbf{I} \\ -\mu_{In} \cdot \mathbf{I} & \mathbf{J}_r - \mu_{Rn} \cdot \mathbf{I} \end{bmatrix} = \mathbf{0} \quad (6.11)$$

$$\begin{bmatrix} \mathbf{J}_r & \mu_{In} \cdot \mathbf{I} \\ -\mu_{In} \cdot \mathbf{I} & \mathbf{J}_r \end{bmatrix} = \begin{bmatrix} \mu_{Rn} \cdot \mathbf{I} & \mathbf{0} \\ \mathbf{0} & \mu_{Rn} \cdot \mathbf{I} \end{bmatrix} \quad (6.12)$$

Among all eigenvalues of the system Jacobian matrix, an eigenvalue whose absolute value of its real part is the smallest is selected. This eigenvalue is defined as μ_{\min} by (6.13).

$$\mu_{\min} = \mu_{R\min} + j \cdot \mu_{I\min} \quad (6.13)$$

Substituting (6.13) into (6.12), we define a matrix A as (6.14). A new dynamic voltage stability index DVSI thus is defined as (6.15). $\sigma_{\min}(\mathbf{A})$ is the minimum singular value of the matrix A .

$$\mathbf{A} = \begin{bmatrix} \mathbf{J}_r & \mu_{I_{\min}} \cdot \mathbf{I} \\ -\mu_{I_{\min}} \cdot \mathbf{I} & \mathbf{J}_r \end{bmatrix} \quad (6.14)$$

$$DVSI = \sigma_{\min}(\mathbf{A}) \quad (6.15)$$

Hopf bifurcations are characterized by a pair of purely imaginary eigenvalues $\mu_{HB1,2}$, which are defined as (6.16) and (6.17).

$$\mu_{HB1,2} = \mu_{RHB} \pm j \cdot \mu_{IHB} \quad (6.16)$$

$$\mu_{RHB} = 0 \quad (6.17)$$

Since the real parts of this pair of purely imaginary eigenvalues are equal to zero, their absolute real parts are the smallest. μ_{\min} thus is equal to μ_{HB1} or μ_{HB2} . At Hopf bifurcation, the matrix A is written as (6.18). According to (6.12), substituting the zero real parts of $\mu_{HB1,2}$ into the right hand side of (6.12), we derive (6.19). Therefore, A is equal to zero or singular at Hopf bifurcations.

$$\mathbf{A} = \begin{bmatrix} \mathbf{J}_r & \pm \mu_{IHB} \cdot \mathbf{I} \\ \mp \mu_{IHB} \cdot \mathbf{I} & \mathbf{J}_r \end{bmatrix} \quad (6.18)$$

$$\mathbf{A} = \begin{bmatrix} \mu_{RHB} \cdot \mathbf{I} & \mathbf{0} \\ \mathbf{0} & \mu_{RHB} \cdot \mathbf{I} \end{bmatrix} = \begin{bmatrix} \mathbf{0} \cdot \mathbf{I} & \mathbf{0} \\ \mathbf{0} & \mathbf{0} \cdot \mathbf{I} \end{bmatrix} \quad (6.19)$$

Saddle node bifurcations are characterized by at least one zero eigenvalue μ_{SNB} , which is defined as (6.20)-(6.22).

$$\mu_{SNB} = \mu_{RSNB} + j \cdot \mu_{ISNB} \quad (6.20)$$

$$\mu_{RSNB} = 0 \quad (6.21)$$

$$\mu_{ISNB} = 0 \quad (6.22)$$

Since the real part of μ_{SNB} is equal to zero, μ_{\min} is equal to μ_{SNB} at saddle node bifurcations. At saddle node bifurcation, the matrix A is written as (6.23). The matrix A

is equal to the right hand side of (6.12). Substituting the zero real parts of μ_{SNB} into the right hand side of (6.12), we derive (6.24). Therefore, A is equal to zero or singular at saddle node bifurcations.

$$\mathbf{A} = \begin{bmatrix} \mathbf{J}_r & \mu_{ISNB} \cdot \mathbf{I} \\ \mu_{ISNB} \cdot \mathbf{I} & \mathbf{J}_r \end{bmatrix} = \begin{bmatrix} \mathbf{J}_r & \mathbf{0} \\ \mathbf{0} & \mathbf{J}_r \end{bmatrix} \quad (6.23)$$

$$\mathbf{A} = \begin{bmatrix} \mu_{RSNB} \cdot \mathbf{I} & \mathbf{0} \\ \mathbf{0} & \mu_{RSNB} \cdot \mathbf{I} \end{bmatrix} = \begin{bmatrix} \mathbf{0} \cdot \mathbf{I} & \mathbf{0} \\ \mathbf{0} & \mathbf{0} \cdot \mathbf{I} \end{bmatrix} \quad (6.24)$$

In summary, according to (6.19) and (6.24), the matrix A is equal to zero or singular at either saddle node bifurcations or Hopf bifurcations. In practical applications, DVSI is calculated at each point on the system trajectory along with the change of a bifurcation parameter. At saddle node bifurcations or Hopf bifurcations, DVSI will be equal to zero. At the other points, DVSI will be larger than zero.

The minimum singular value of the Jacobian matrix $\sigma_{\min}(\mathbf{J}_r)$ has been used in a stability method to analyze voltage stability [6]. This minimum singular value shown in (6.25) is called DVSI1 in this dissertation.

$$DVSI1 = \sigma_{\min}(\mathbf{J}_r) \quad (6.25)$$

The development of DVSI and DVSI1 uses the technique of singular value decomposition. The minimum singular values are critical singular values and can detect bifurcations. In applications of the minimum singular values on bifurcation detection in real power systems, the masking effect on critical singular values of small and slowly changing singular values was observed [33]. Several small singular values can be obtained in real power systems with the change of bifurcation parameters. These small singular values are almost constant with the change of bifurcation parameters. The small singular values indicate the relationship between the local area in voltage stability studies and the other areas of a system [33]. However, these small singular values do not indicate the stability level of a system. The critical singular value decreases as bifurcation parameters change, but not enough to be included in the group of small singular values being computed. The critical singular value is thus masked by those small and slowly changing singular values. These small singular values are not the

critical singular values to reflect voltage stability and should be filtered out. In this dissertation work, the singular values are calculated with the change of bifurcation parameters. Small, almost constant singular values are deleted to derive the critical singular value.

The bifurcations of a system can be detected by calculating DVSI during dynamic analysis. When DVSI is close to zero, the system is closer to voltage instability. Using both DVSI and DVSI1, the types of bifurcations can be determined. A zero value of DVSI of (6.23) means that either saddle node bifurcation or Hopf bifurcation occurs in a system. If the value of DVSI of (6.23) is equal to zero and DVSI1 of (6.25) is not equal to zero, the detected bifurcation is a Hopf bifurcation. If both the values of DVSI of (6.23) and the DVSI1 of (6.25) are equal to zero, the detected bifurcation is a saddle node bifurcation. It should be noted that in theoretical studies the zero values of DVSI indicate where bifurcations occur. However, a perfect zero value is not practical in real situations. We believe that a small value, such as $10e^{-4}$, is small enough as the threshold for finding bifurcations.

6.4 COMPARISON OF BIFURCATION DETECTION

The new dynamic voltage stability index (DVSI) presented earlier is based on ED and SVD on Jacobian matrices. As described earlier, a Jacobian matrix is derived from the linearization of a nonlinear system. A Jacobian matrix thus can represent the local behavior of the nonlinear system around its equilibrium points, but not exactly the same behavior as the original nonlinear system. As described earlier in section 2.2.6.2, a software package called AUTO can be used directly to analyze bifurcations in dynamic nonlinear systems [35]. AUTO uses predictor-corrector algorithms as well as specialized continuation methods for following equilibriums and periodic orbits to detect locations and types of bifurcations of a nonlinear system. In this section, with a small power system, the results of bifurcation detection by the new DVSI will be compared with the results of bifurcation detection by AUTO.

A small two-generator-one-motor power system shown in Figure 6.1 is used for comparison of bifurcation detection between the new DVSI and AUTO. There are three buses in the system and the three buses are connected in a ring configuration. One generator is connected on each of buses 1 and 2. An induction motor load is connected on bus 3. The parameters of the system can be found in Appendix B.1 [77].

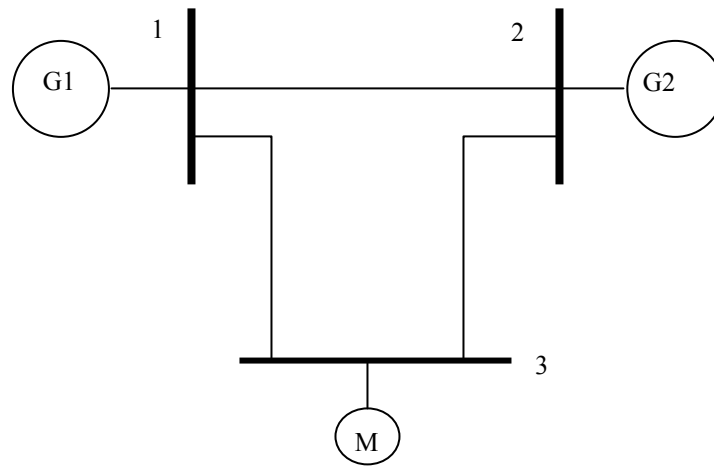


Figure 6.1 A Two-Generator-One-Motor Power System

As described earlier, differential-algebraic equations are used to model power systems in dynamic analysis. The induction motor in the system was modeled by a differential equation shown as (6.26), where the mechanical torque was a quadratic function of the motor speed.

$$\frac{d\omega_m}{dt} = T_E - T_M \quad (6.26)$$

$$T_M = K\omega_m^2 \quad (6.27)$$

where T_e and T_M are the electrical and mechanical torque of the motor, respectively. ω_m is the motor speed. K is the load torque at synchronous speed. The value of K is slowly changed to simulate changes of the mechanical load of the induction motor. K

thus indicates the changes in the load power demand of the motor. K is used as the bifurcation parameter. The component models of the system can be found in Appendix B.2 [77].

A time domain simulation was conducted on the system shown in Figure 6.1 in the environment of Matlab. The simulation results of the motor speed ω and the voltage on bus 3 V_3 with the change of the mechanical load level of K are shown in Figure 6.2 and Figure 6.3, respectively. From the figures, the responses of the motor speed ω and the voltage V_3 monotonically decrease after a certain mechanical load level is reached. Since it has quadratic torque, the motor does not stop completely. The motor eventually moves to a stable equilibrium corresponding to a low rotor speed and the voltage V_3 decreases to a low level.

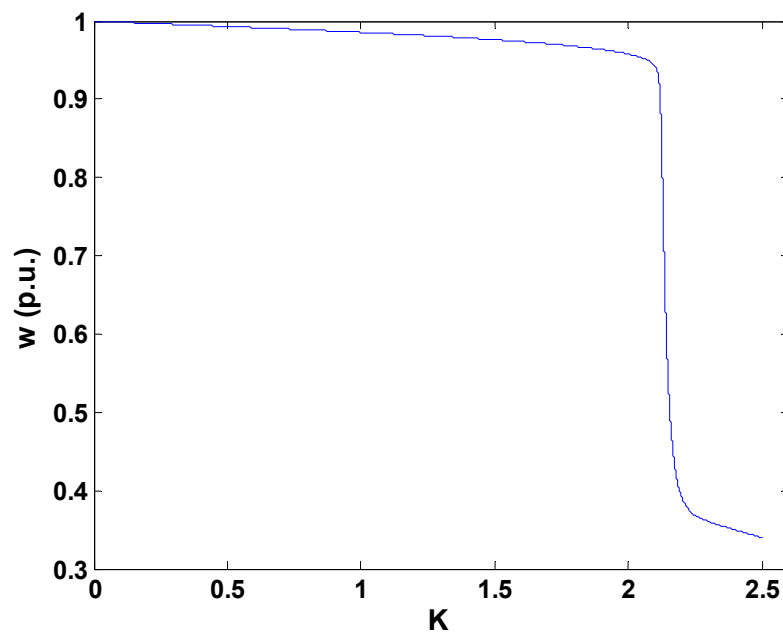


Figure 6.2 Motor Speed with Change of K

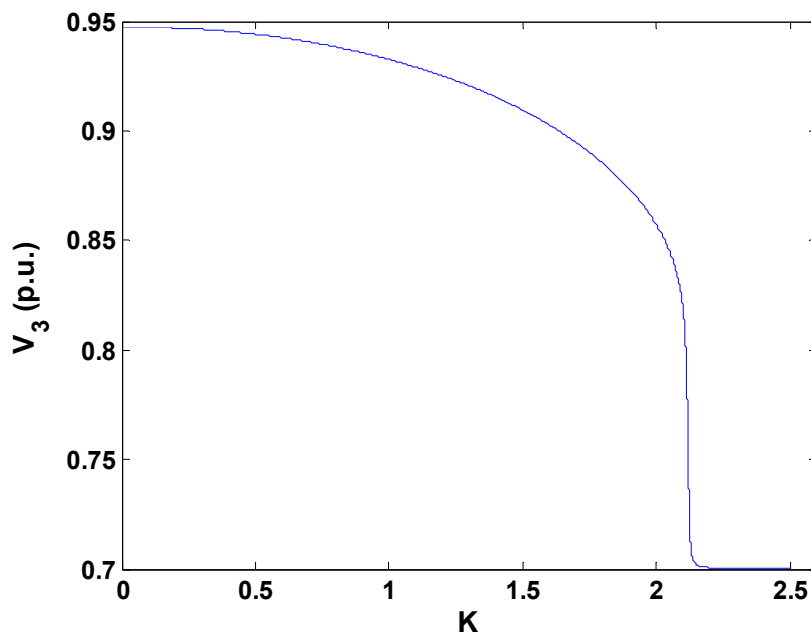


Figure 6.3 Voltage on Bus 3 with Change of K

The Jacobian matrix of the test system was derived from the simulation results at each mechanical load level K . D VSI was calculated from the Jacobian matrix. Figure 6.4 shows the values of D VSI with the continuous change of K . The values of D $VSI1$ with the continuous change of K are shown in Figure 6.5. From Figure 6.4, three bifurcations are detected before the system becomes unstable. As described earlier, the types of bifurcations can be determined from the values of D VSI and D $VSI1$. From Figure 6.5, the values of D $VSI1$ at the first two bifurcations are not equal to zero, and the value of D $VSI1$ is equal to zero at the third bifurcation. Therefore, the first two bifurcations are Hopf bifurcations and the third bifurcation is a saddle node bifurcation. The system begins to oscillate after the first Hopf bifurcation and begins to collapse at the saddle node bifurcation. The value of the mechanical load level K at each bifurcation point is shown in Figure 6.4 and Figure 6.5. They are 0.555 p.u. at the first Hopf bifurcation HB1, 1.396 p.u. at the second Hopf bifurcation HB2, and 2.089 p.u. at the saddle node bifurcation SNB.

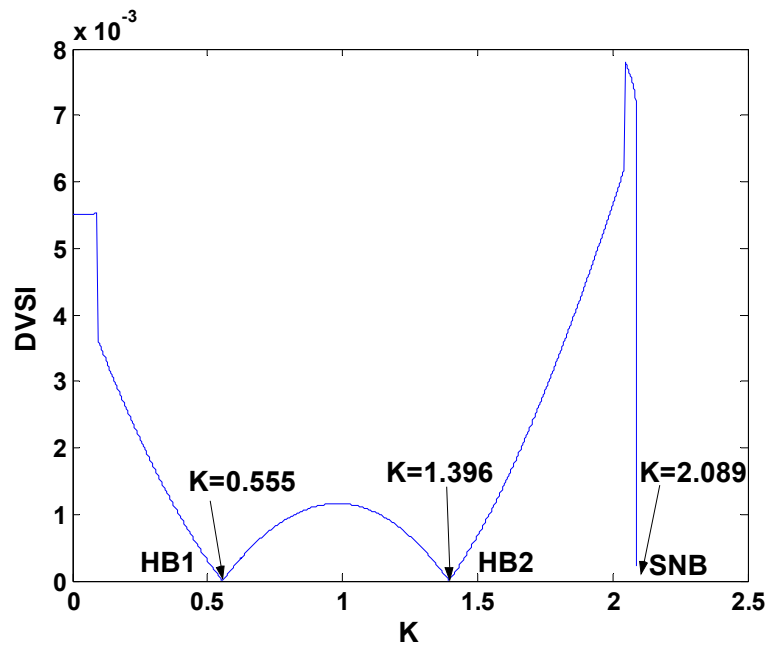


Figure 6.4 DVSI with Change of K

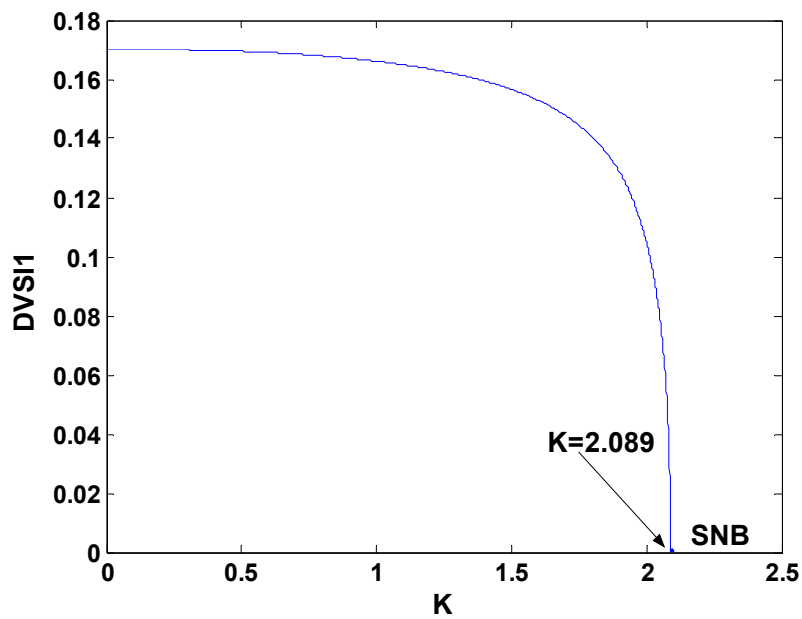


Figure 6.5 DVSI1 with Change of K

Some AUTO calculation results of bifurcation analysis for the system in Figure 6.1 are shown in Table 6.1. Each row in the table is a point on the system trajectory. The point number is listed in the PT column. The system trajectory can be separated into different branches. The branch number is listed in BR column. TY indicates the type of solution, which can be a normal start, end point, or a bifurcation point. EP represents the normal start or end point of a branch. The start point is input manually and the point where AUTO begins calculation. The end point is solved by AUTO. HB and LP indicate Hopf bifurcation and saddle node bifurcation, respectively. Each row is also a solution of the studied system. The solutions are labeled in the LAB column. PAR(0) is the first bifurcation parameter in an array of bifurcation parameters and is the mechanical load level K in this study. The first four state variables are $U(1)$, $U(2)$, $U(3)$, and $U(4)$. $U(1)$, $U(2)$ and $U(3)$ are voltage magnitude on bus 1, voltage magnitude and angle on bus 2, respectively. $U(4)$ is bus voltage V_3 .

Four bifurcations were detected for the system by AUTO. The four rows that list the four bifurcations are shaded in Table 6.1. The first three bifurcations agree with HB1, HB2, and SNB detected by DVSI. As described in section 2.2.6.2, with the continuation method, AUTO can detect bifurcations even after a saddle node bifurcation is met where a system collapses in time domain simulation. The fourth bifurcation occurs after the two-generator-one-motor system collapses and thus can not be detected from the simulation results.

Table 6.1
 AUTO Results for the System in Figure 6.1

BR	PT	TY	LAB	PAR(0)	U(1)	U(2)	U(3)	U(4)
1	1	EP	1	1.000000 E-03	9.597185 E-01	9.597179 E-01	7.270550 E-02	9.473133 E-01
1	23	HB	2	5.545999 E-01	9.591953 E-01	9.589629 E-01	5.300364 E-02	9.433852 E-01
1	30	--	3	8.890904 E-01	9.575954 E-01	9.573059 E-01	4.154264 E-02	9.360759 E-01
1	41	HB	4	1.396167 E+00	9.528676 E-01	9.526007 E-01	2.471077 E-02	9.157948 E-01
1	60	--	5	2.037438 E+00	9.371377 E-01	9.370515 E-01	5.650223 E-02	8.482893 E-01
1	66	LP	6	2.089189 E+00	9.305440 E-01	9.304543 E-01	5.843056 E-02	8.189627 E-01
1	90	--	7	1.432063 E+00	9.091803 E-01	9.088130 E-01	4.582237 E-02	7.194150 E-01
1	96	LP	8	1.254447 E+00	9.062433 E-01	9.059371 E-01	6.248649 E-02	7.061909 E-01
1	120	--	9	2.363920 E+00	9.048103 E-01	9.046232 E-01	7.531930 E-02	7.004532 E-01
1	150	EP	10	3.860729 E+00	9.046726 E-01	9.045054 E-01	7.696452 E-02	6.999715 E-01

The complete bifurcation diagram of the system, or the trajectory of the bus voltage V_3 changing with the mechanical load level K of the induction motor, was generated by AUTO. The diagram is shown in Figure 6.6. The first three bifurcation points detected by AUTO are indicated in the bifurcation diagram. The straight dot dashed lines in the figure indicate the mechanical load levels at which bifurcations occur. With the complete bifurcation diagram, the situation of the solution for the system can be shown. The number of intersections between the KV_3 curve and mechanical load level K changes first from one to three, then from three to one as K increases eventually. Each intersection represents one equilibrium point in the system. The upper part of the KV_3 curve always represents the feasible solutions of the system. With the change in mechanical load level K , the system moves along the upper part of the KV_3 curve until SNB is met. When K increases further, V_3 decreases to a low level and is almost unchanged after SNB.

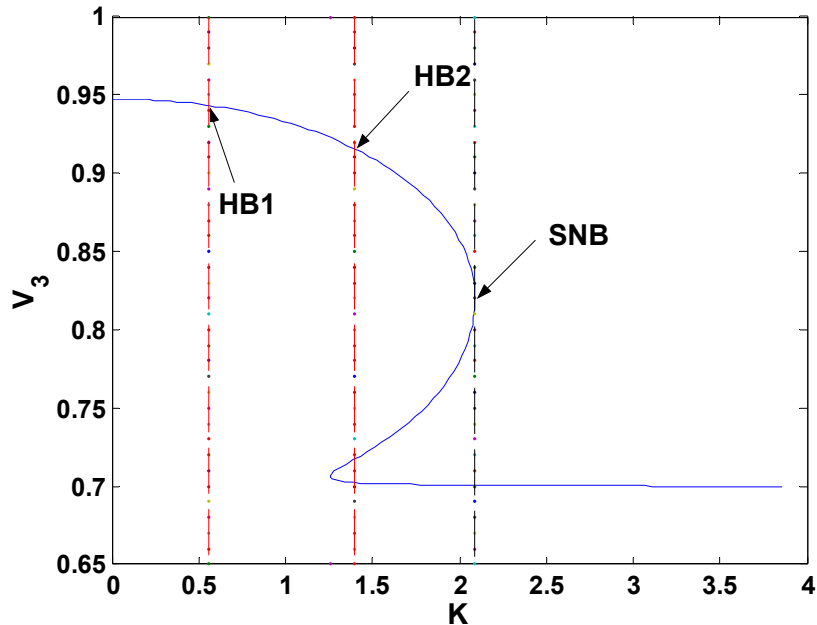


Figure 6.6 Complete Bifurcation Diagram from AUTO

The bifurcation detection results of the new index DVSI agree with the results of AUTO. AUTO can detect the exact positions and types of bifurcations in a nonlinear system. However, power systems are normally large and may comprise a large number of differential equations and algebraic equations. The algebraic variables must be substituted explicitly before AUTO can be applied to detect bifurcations in a nonlinear system [35]. This significantly limits the ability of AUTO to solve bifurcations for large power systems. The calculation of DVSI is based on time domain simulations. However, as described in section 3.4.3.1, the Jacobian matrix can be obtained by numerical differentiation. The explicit solutions of algebraic equations are not required by the calculation of DVSI, which makes it easier to use DVSI to detect bifurcations in large power systems.

It is noted that two Hopf bifurcations were detected in the system in Figure 6.1. To better explain the behavior of the system after Hopf bifurcations, the eigenvalues with the change of mechanical load level K in the nonlinear system are shown in Figure 6.7. In areas A and B in Figure 6.7, the first and second Hopf bifurcations occur. Eigenvalues in area A and area B are conjugates to each other. Either of them can thus be used to show the system behavior between the two Hopf bifurcations. Area A is enlarged and shown in Figure 6.8. It is seen from Figure 6.8 that a pair of eigenvalues first crosses the imaginary axis from negative plane to positive plane and then from positive plane to negative plane. At the first crossing, the first Hopf bifurcation HB1 is detected. At the second crossing, the second Hopf bifurcation HB2 is detected. The system is in stable operation before the first Hopf bifurcation point. The system then becomes oscillatory unstable between the first and the second Hopf bifurcation. However, the oscillation magnitude is too small to be observed from the simulation results shown in Figure 6.2 and Figure 6.3. The system becomes stable again after the second Hopf bifurcation until the saddle node bifurcation is reached where the system begins to collapse.

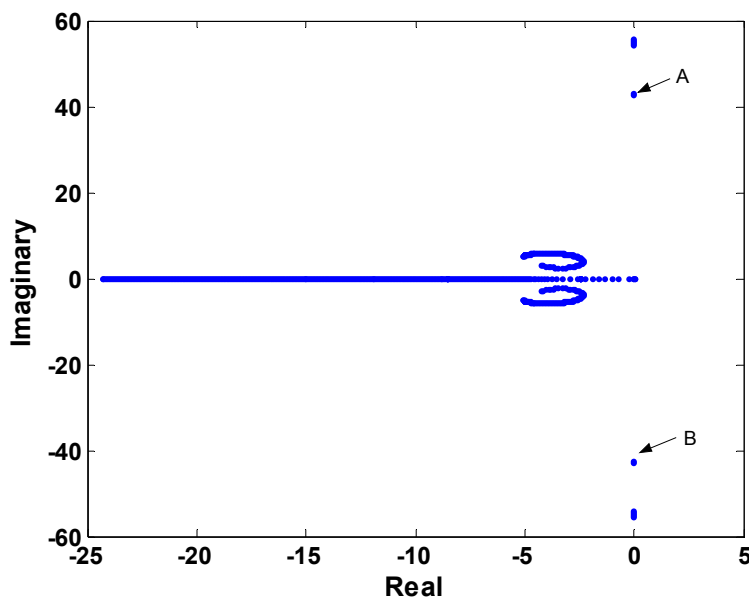


Figure 6.7 Root Locus of the Power System in Figure 6.1 for Stability Study

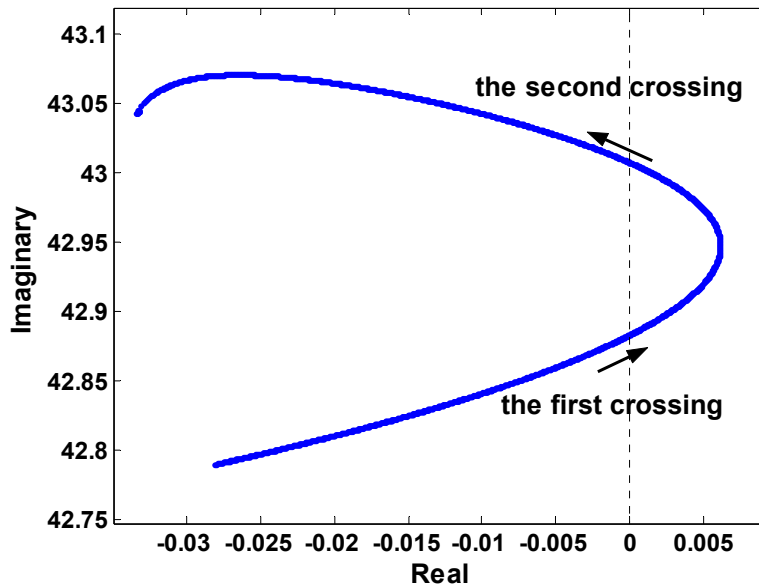


Figure 6.8 Enlarged Root Locus of Area A in Figure 6.7

The Jacobian matrix derived from the linearization can represent the local behavior of a nonlinear system. From the results shown earlier, the bifurcations detected by DVSI agree with the bifurcations detected with AUTO. The new voltage stability index DVSI can thus be used to detect local bifurcations in a nonlinear system.

6.5 COMPARISON OF QSS AND SIMULATION

As described earlier in section 3.4.2.2, the QSS method can be used in voltage stability studies. In the QSS method used in this study, the differential and algebraic equations of the system in Figure 6.1 were solved as a set of algebraic equations with the bifurcation parameter K increased successively. After the saddle node bifurcation, QSS could no longer be solved due to the singularity of the system Jacobian matrix.

The KV_3 curves derived from time domain simulation and QSS are compared in Figure 6.9. Some details of the KV_3 curves away from and close to the saddle node

bifurcation are enlarged and shown in Figure 6.10 and Figure 6.11. When the system is away from the saddle node bifurcation with K changed from 1.0118 p.u. to 1.0228 p.u., the results from QSS and time domain simulations are close. When the system is closer to the saddle node bifurcation with K changed from 2.03 p.u. to 2.012 p.u., the differences between the results are larger. The range of K from 1.0118 p.u. to 1.0228 p.u. is between the two Hopf bifurcations HB1 and HB2. As described earlier, the magnitude of the unstable oscillation between the two Hopf bifurcations are small. Therefore, the results of QSS and time domain simulations are close. However, if the oscillation magnitudes are large, the results after Hopf bifurcations from QSS and time domain simulations would not be as close as shown in Figure 6.10.

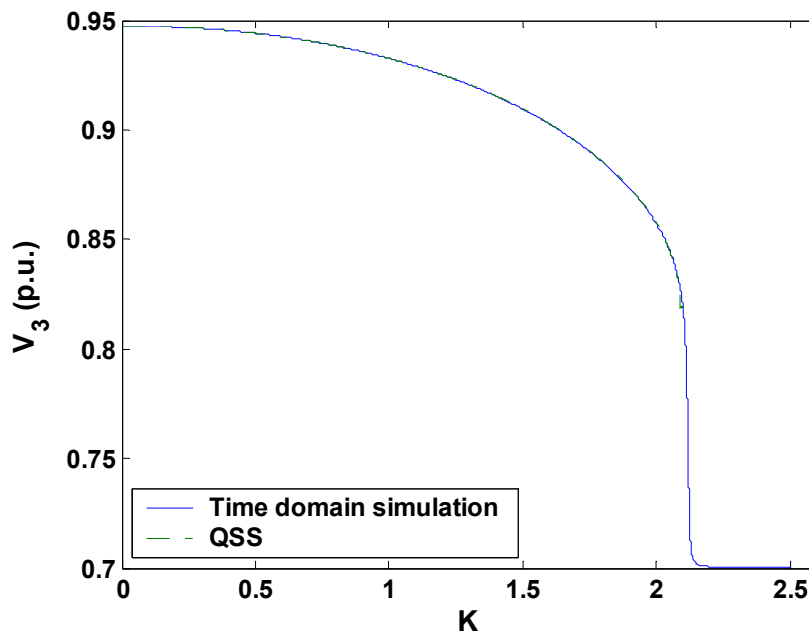


Figure 6.9 Results of Comparison between Simulation and QSS

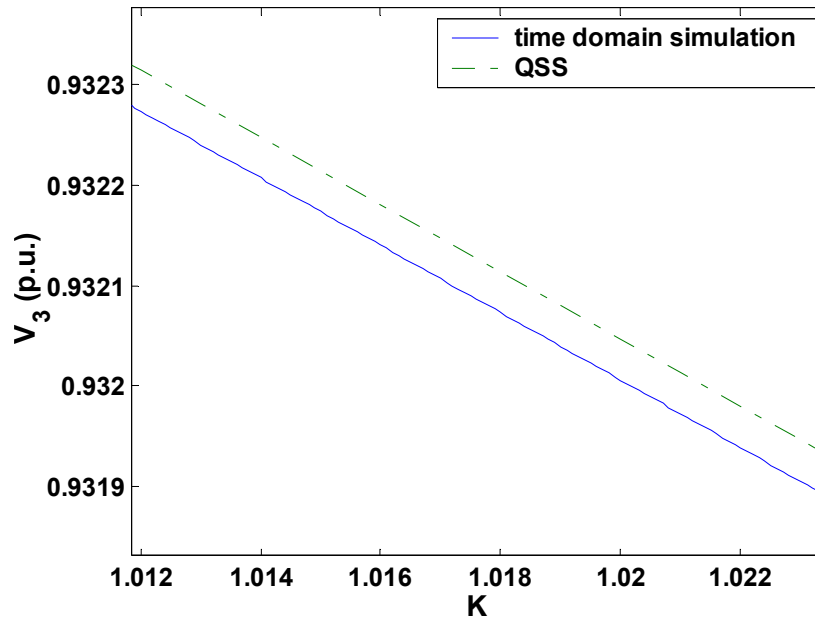


Figure 6.10 Results of Comparison between Simulation and QSS ($K=1.0118\sim 1.0228$)

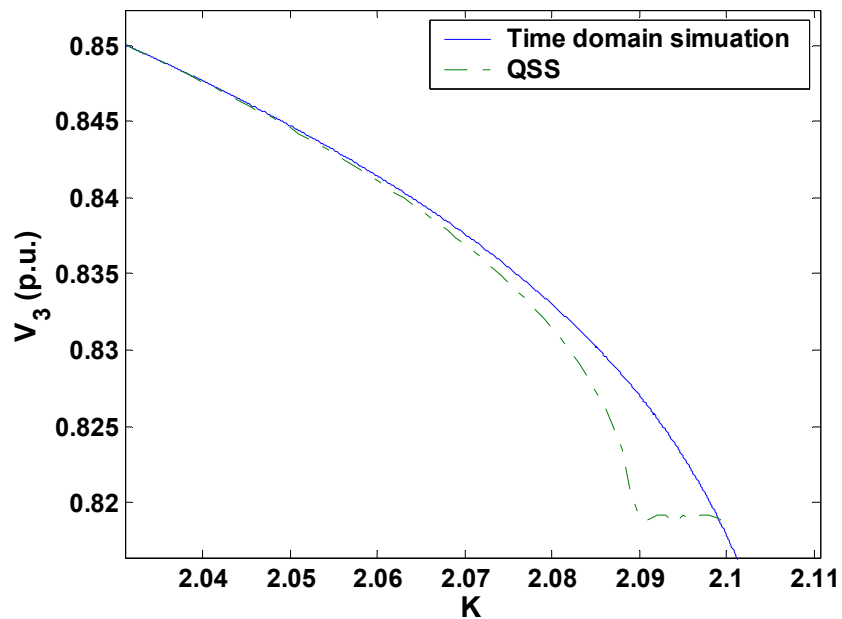


Figure 6.11 Results of Comparison between Simulation and QSS ($K=2.03\sim 2.102$)

The biggest advantage of the QSS method is that QSS requires much less time to solve a system than do time domain simulations. QSS can thus replace time domain simulations when a system is not close to bifurcations. In the case study shown later, QSS and time domain simulations will be used complementarily to analyze bifurcations. The QSS method is first applied and the approximate positions of bifurcations are detected. Time domain simulations are then conducted around these approximate locations to find the exact location of bifurcations. In this way, a large amount of time that would be spent on time domain simulations can be saved and the system trajectory is accurate enough for bifurcation detection.

6.6 CASE STUDIES

In this section, two cases are studied on the test shipboard power system developed in Chapter IV. The diagram of the test system was shown in Figure 4.14. The first case studies voltage stability with load L312 increased in the test system. In Chapter V, static analysis detected voltage instability when the mechanical load level of load L312 was increased to 3.02 p.u.. However, in dynamic analysis, voltage instability can possibly occur before L312 is increased to 3.02 p.u.. As described earlier in section 3.3, when load torque increases on an induction motor, motor stalling or local voltage instability can occur. This voltage instability occurs during dynamic processes and will be assessed by dynamic indices DVSI and DVSI1. The second case studies voltage stability with the system load level increased in the test system. As discussed in section 3.4.4.4, the parameters of voltage controllers may no longer be appropriate after loads are increased. The interaction of loads and voltage controllers can cause voltage instability. The voltage instability caused by this interaction will also be assessed by dynamic indices DVSI and DVSI1.

To achieve the objectives of saving time and deriving accurate results simultaneously, QSS and time domain simulations were complementarily employed to conduct dynamic analysis. At first, a bifurcation parameter, such as the mechanical load level of L312 was

increased successively. At each level of a bifurcation parameter, time domain simulations were run until the system reaches steady state. The simulation results at different steady states were used as the results of QSS. From QSS analysis, bifurcations were detected approximately. Time domain simulations were then run around the approximate bifurcations with a bifurcation parameter increased continuously. From time domain simulations, bifurcations were detected accurately.

The first case study studies voltage stability induced by motor stalling with the mechanical load level of L312 increased. In this dynamic analysis, differential equations were used to model the dynamic load L312. The rotor dynamics of induction motors were modeled by (6.28). T_E and T_M represent electrical and mechanical torque of motor L312, respectively. ω_m is the speed of motor L312.

$$\frac{d\omega_m}{dt} = T_E - T_M \quad (6.28)$$

In practical applications, the mechanical torque of an induction motor operates in one of three categories. These categories are constant torque, linear torque, and quadratic torque. The constant torque is independent of the motor speed. It has many applications in many kinds of loads, such as air condition (AC) compressors, gear shift, anchor windlass, cranes, crabs, and belt conveyors for load transportation. The linear torque and quadratic torque are dependent on the motor speed. The demanded torque on the rotor increases as the speed increases. Examples of loads with linear torques are electric wood saw, planers, and piston pumps. Examples of loads with the quadratic torques include fans and pumps. The three types of mechanical torque are modeled as (6.29)-(6.31).

$$T_M = K \quad (6.29)$$

$$T_M = K\omega_m \quad (6.30)$$

$$T_M = K\omega_m^2 \quad (6.31)$$

where K is the load torque at synchronous speed. The value of K is slowly changed to simulate changes of the mechanical load of the induction motor and indicates the changes in the load power demand of the motor. K is the bifurcation parameter in this case study. In section 4.6.2, the mechanical torque of all motor loads was modeled as

quadratic torque to demonstrate the simulation results of the test system at normal operation. However, the three types of mechanical loads have different effects on voltage stability [23]. In this case study, the mechanical torque of motor load L312 is modeled by the three different types of mechanical torques respectively, and voltage stability for various mechanical torque models with the change of mechanical load level K of motor L312 is studied.

The simulation results of the motor terminal voltage V_{L312} and the motor speed with the change of bifurcation parameter K for various load torques are shown in Figure 6.12 and Figure 6.13. The motor terminal voltage was computed by (6.32).

$$v = \sqrt{v_d^2 + v_q^2} \quad (6.32)$$

where v_d and v_q are voltages on the d- and q-axis of motor L312. From these figures, it can be seen that, with the same system and motor data, different situations arise if the mechanical load torque is modeled differently. With constant load torque, the voltage collapses and motor stalling occurs after the mechanical load level K was increased to 2.19 p.u.. With linear torque, the voltage and motor speed drops to low values after the mechanical load level K was increased to 2.6 p.u.. With quadratic torque, the voltage continuously changes and the motor continuously works at all mechanical load levels.

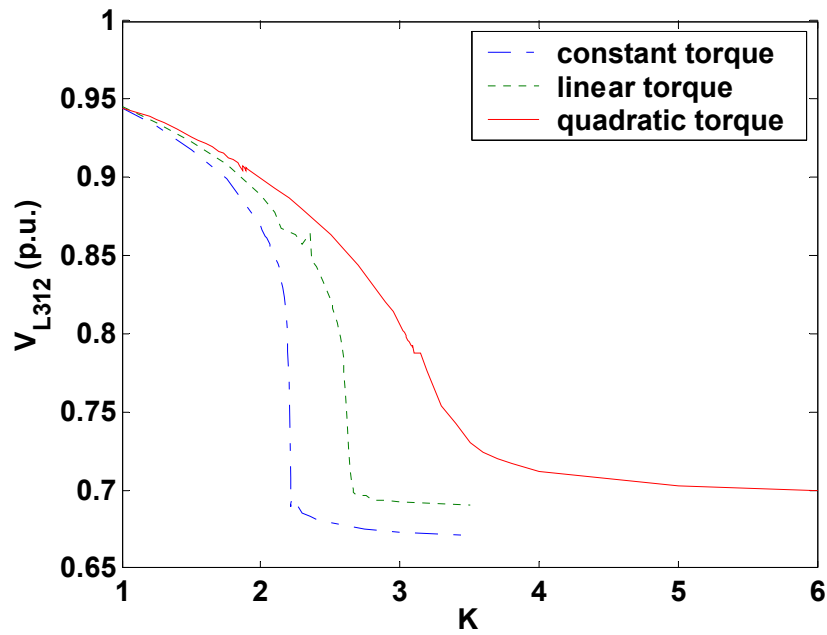


Figure 6.12 Voltage VL312 with Change of K for Various Load Torques

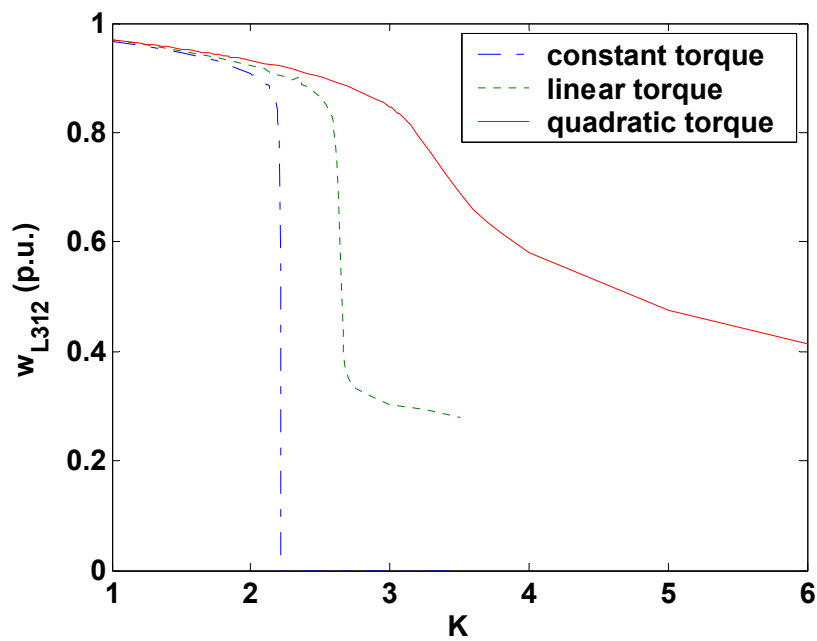


Figure 6.13 Motor Speed WL312 with Change of K for Various Load Torques

The values of DVSI and DVSI1 with mechanical load level of L312 increased were calculated from the results from QSS and time domain simulations. In this case study, the masking effect described in section 6.3 was observed during the calculation of the minimum singular values for DVSI and DVSI1. Four small and slowly changing singular values were found from calculating DVSI and two small and slowly changing singular values were found from calculating DVSI1. These small singular values were not critical singular values reflecting voltage stability and were thus filtered out for deriving the final values of DVSI and DVSI1.

After the masking singular values were filtered out, the critical singular values indicating voltage stability with various load torques is shown. Figure 6.14 shows the values of DVSI and DVSI1 with the change in mechanical load level K when the mechanical load torque was constant. Figure 6.15 shows the values of DVSI and DVSI1 when the mechanical load torque was linear. Figure 6.16 shows the values of DVSI and DVSI1 when the mechanical load torque was quadratic. DVSI and DVSI1 have the same values in Figure 6.14-Figure 6.16. Thus, only saddle node bifurcations occurred in the system. When the mechanical load was constant, the mechanical load level where the saddle bifurcation occurred was around 2.19 p.u.. When the mechanical load was linear, the mechanical load level was around 2.6 p.u.. No bifurcation was detected when the mechanical torque was quadratic.

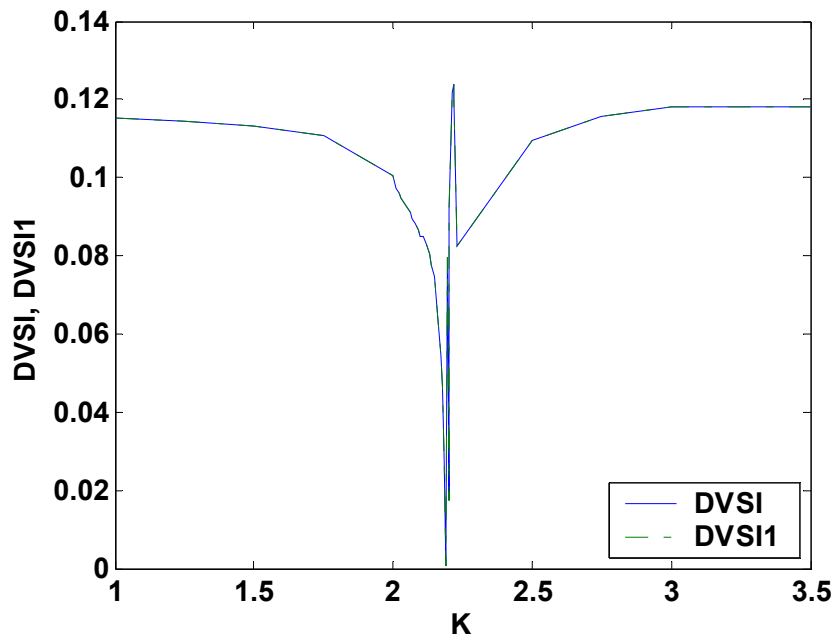


Figure 6.14 DVSI and DVSI1 with Constant Mechanical Torque

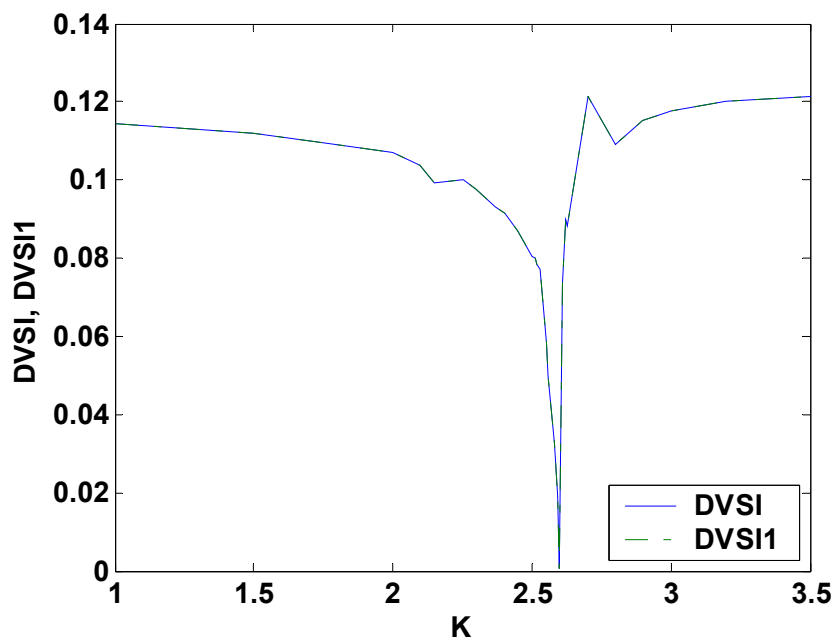


Figure 6.15 DVSI and DVSI1 with Linear Mechanical Torque

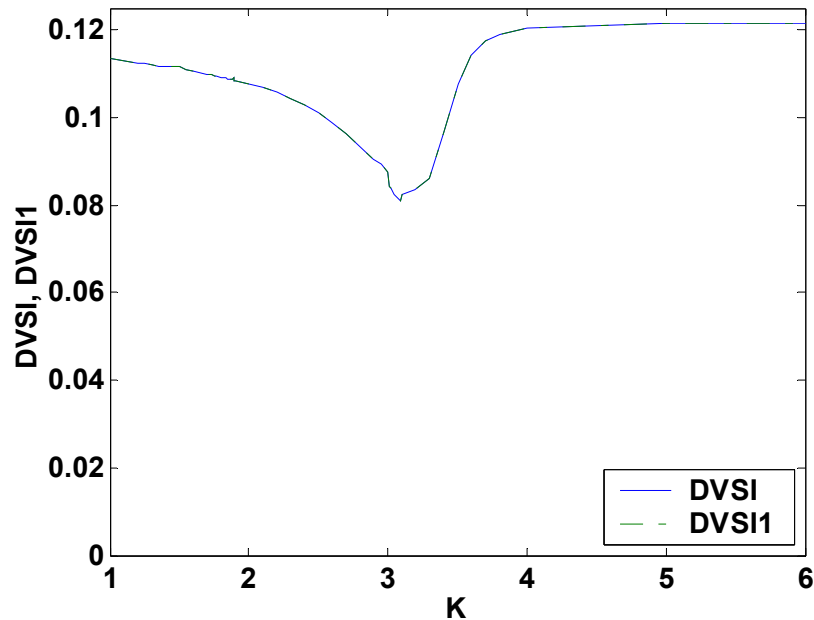


Figure 6.16 DVS1 and DVS11 with Quadratic Mechanical Torque

From Figure 6.14-Figure 6.16, the three different types of mechanical load torques have different effects on voltage stability. The most vulnerable situation occurred when the motor operated under constant load torque. The saddle node bifurcation point occurred at a higher voltage level and at higher speed than when the load torque was speed dependent. In the case of constant torque, values of the load torque above the bifurcation value imply motor stalling and eventually voltage collapse at terminal voltage of motor L312. However, the instability may be alleviated if the load torque is dependent on speed. The voltage and motor speed decreased at the saddle node bifurcation when the load torque was linear. If a system is strong, the stable operation may be maintained even after the voltage is low and the motor speed significantly decreases. The situation is even less critical when the load torque is a quadratic. Figure 6.12 and Figure 6.13 indicate that the bus voltage remains stable even though the motor operates at an unacceptable low speed if the load torque is quadratic.

The second case study examines the voltage instability induced by inappropriate parameter settings of voltage controllers when the load level of a system is increased. For the test SPS shown in Figure 4.14, at normal operation, all loads were operated at nominal power. A system load level parameter was used on all loads in the test system. This load level parameter K_L , as a coefficient, was used to adjust the output currents of each load, whose summation is the input of generators. In this case study, the system load level K_L was the bifurcation parameter. This load level parameter K_L was assumed to be one at normal operation. QSS and time domain simulations were complementarily applied as discussed earlier. K_L was increased successively in QSS and continuously in time domain simulations. When the system load level K_L increased, the voltage at generator terminals decreased. The voltage controllers on the generators in the test system responded to the low terminal voltage and adjusted the terminal voltage as close to 1.0 p.u. as possible. However, when the system load level K_L increased to a certain level, voltage drop was out of the adjustment range of the voltage controllers of the generators or the settings of the voltage controller were not appropriate for the increased system load level K_L . Voltage in the test SPS thus became unstable. In this case, voltage oscillations were caused by a Hopf bifurcation before voltage collapse was caused by a saddle node bifurcation.

Figure 6.17 shows the terminal voltage of generator 1 $V_{t_{g1}}$ with the change of system load level K_L . Similar behavior occurred for generator 2. The generator terminal voltage $V_{t_{g1}}$ was derived according to (6.32), with v_d and v_q being the d- and q-axis voltages of generator 1. It can be seen that when load level K_L was increased to a value around 2.3, the generator terminal voltage decreased suddenly to almost zero. Since generators were the only power suppliers in the test system, the system thus collapsed. The dynamic behavior of the terminal voltage at the range of K_L from 1.3 to 2.3 is enlarged and shown in Figure 6.18. It can be seen that the terminal voltage of generator 1 oscillated before the system finally collapsed.

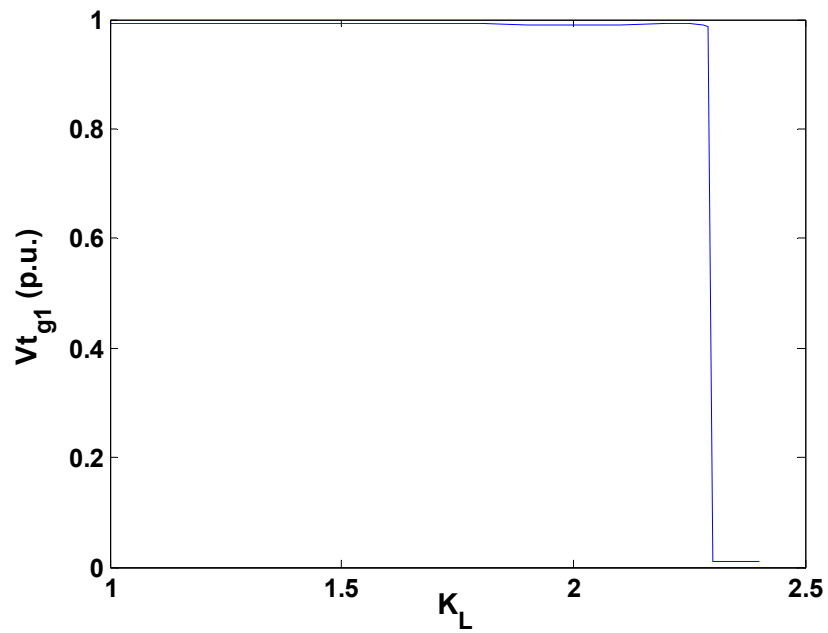


Figure 6.17 Terminal Voltage $V_{t_{g1}}$ with Change of System Load Level K_L

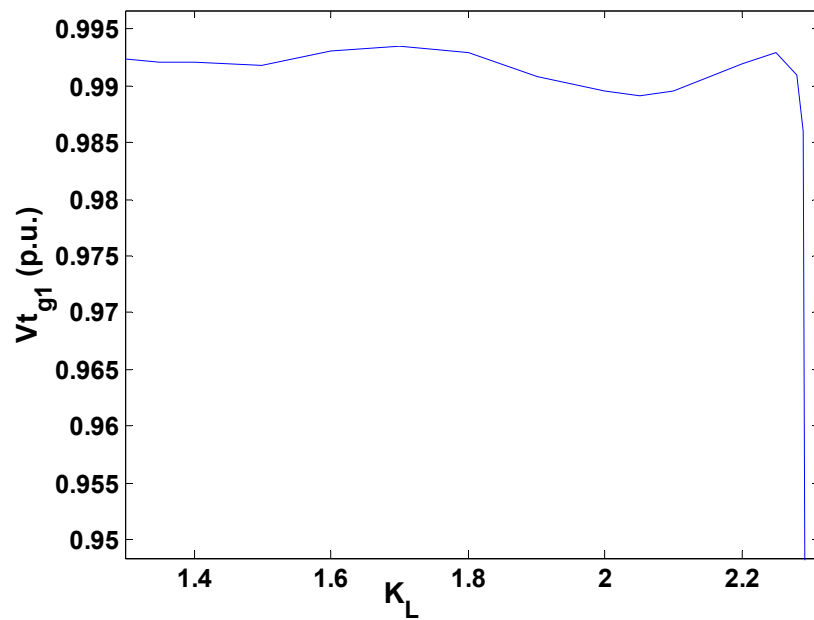


Figure 6.18 Terminal Voltage $V_{t_{g1}}$ with Change of System Load Level K_L ($K_L=1.3\sim 2.3$)

DVSI and DVSI1 were computed to detect bifurcations for the dynamic process when system load level K_L was increased. In this case study, the masking effect on critical singular values was also observed. When system load level K_L was increased, four small and slowly changing singular values were found from calculating DVSI and two small and slowly changing singular values were found from calculating DVSI1. These small singular values were not critical singular values and were thus filtered out for deriving the final values of DVSI and DVSI1.

After this masking effect was removed, Figure 6.19 shows the change of DVSI and DVSI1 when the system load level increased from 1.0 to 2.4. From the DVSI values, it can be seen that two bifurcations occurred in the system. The first bifurcation occurred when the load level was around 1.4. The second bifurcation occurred when the load level was around 2.3. Between the two bifurcations, the DVSI values were smaller than the DVSI1 values. Using both the DVSI and the DVSI1 values, the first bifurcation is identified as a Hopf bifurcation and the second one is identified as a saddle node bifurcation. In the range of K_L from 1.3 to 2.3 shown, some oscillations were observed from the complementary results of QSS and time domain simulations in Figure 6.18. These oscillations are also reflected in the values of DVSI and DVSI1 in Figure 6.19. The system trajectory between the Hopf bifurcation and the saddle node bifurcation consisted of a large amount of points. To save bifurcation analysis time, not all points between the Hopf bifurcation and saddle node bifurcation were analyzed by DVSI and DVSI1. The oscillations in Figure 6.19 are thus not as smooth as those shown in Figure 6.18. However, the trends in the changes of DVSI and DVSI1 can still be observed.

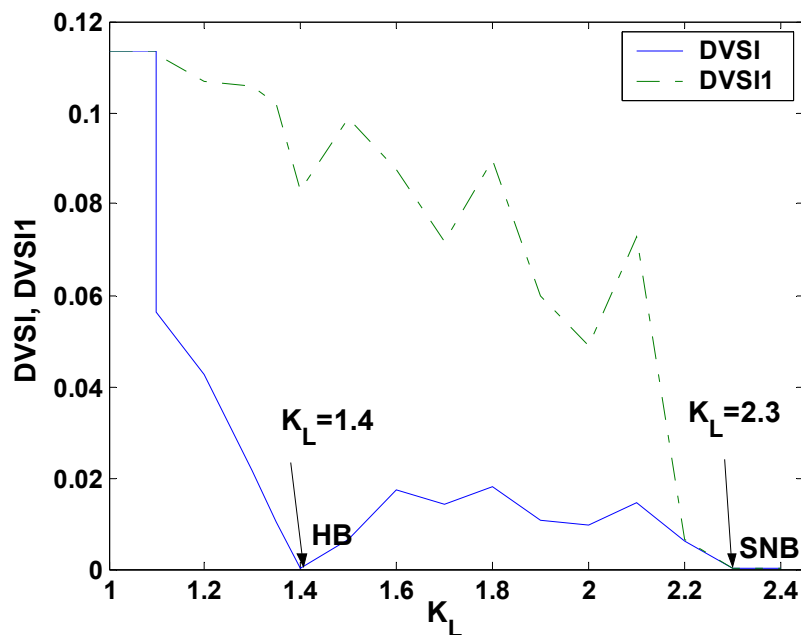


Figure 6.19 DVSI and DVSII with Change of System Load Level K_L

6.7 CHAPTER SUMMARY

In this chapter, a new dynamic voltage stability index (DVSI) was deduced with the techniques of eigenvalue decomposition and singular value decomposition. The new index DVSI can detect local bifurcations in a dynamic power system, including both Hopf bifurcations and saddle node bifurcations. Another index DVSII was used to detect only saddle node bifurcations. The results of bifurcation detection for a two-generator-one-motor system by DVSI and DVSII were compared with those by AUTO, an existing bifurcation detection software package. The results of the indices and AUTO agreed with each other. DVSI and DVSII were also applied on the test system developed in Chapter IV. DVSI and DVSII detected the bifurcations in the test system while the dynamic process of the mechanical load level of the motor load L312 increased gradually. The results confirmed that the factor of the motor stalling affects voltage stability, which was discussed in Chapter III. DVSI and DVSII indicated a Hopf and a

saddle node bifurcation for the test system when the system load level was increased. The results in turn confirmed that the interaction of loads and voltage controllers is a factor affecting voltage stability in SPS, which was also discussed in Chapter III.

In the next chapter, conclusions and future work will be discussed.

CHAPTER VII

CONCLUSIONS AND FUTURE WORK

7.1 SUMMARY

Researchers in the Power System Automation Lab at TAMU have developed methods for performing SPS reconfiguration. Reconfiguration operations change the status of open/closing of switches in an SPS before or after a weapon hit to reduce the damage to the system. As one critical aspect of system reliability, stable operations must be maintained during SPS reconfiguration. When the stability margin is small, the topology changes and dynamics of equipments due to reconfiguration might cause voltage instability, such as progressive voltage fall or voltage oscillation. SPS stability thus should be assessed to ensure the stable operation during reconfiguration. In this dissertation, methods for analyzing and assessing stability during reconfiguration were developed and implemented on AC shipboard power systems.

Time domain simulations provide valuable information for stability studies. Shipboard power systems studied in this dissertation were ungrounded and stiffly connected. Detailed models were used to simulate the accurate dynamics of shipboard power systems. Due to the negligible effects on dynamics, line capacitances were ignored to improve simulation speeds. Inductor buses and resistor buses emerge in ungrounded stiffly connected power systems. Interconnection incompatibility is thus induced when only voltages-in-currents-out component models are interconnected at resistor or inductor buses. A new generalized modeling and simulation methodology was discussed in this dissertation for effectively modeling ungrounded stiffly connected power systems. This new methodology reformulated the mathematical equations of certain component models to solve interconnection incompatibility problems. Generally, to model a system, one reference generator model or cable model on each resistor or inductor bus is reformulated from its standard model. This method was implemented in the environment of Matlab/Simulink for modeling and simulating ungrounded shipboard

power systems. Simulation results showed that the new methodology is promising for modeling and simulating ungrounded stiffly connected power systems.

A test shipboard power system model was designed and developed for stability studies. This test system was comprised of three synchronous generators, three transformers, nine constant impedance loads, 14 induction motor loads, 54 cables, and various protective devices. A protection scheme was designed and implemented for this test system. The factors affecting shipboard power system stability studies, such as system stress and dynamic loads, were studied for the test SPS. The new generalized modeling and simulation methodology was implemented on the test SPS. The simulation results from the test system were used for stability analysis and assessment.

The stability problems of shipboard power systems, especially during reconfiguration operations, were formulated. Shipboard power systems are special power systems. Salient features of SPS include finite inertia and capacity, short connecting lines, predominant dynamic loads, and fast response controllers. Effects of these salient features on SPS stability were discussed. The time frames of dynamics classified stability problems in SPS into the categories of dynamic stability, transient stability and long-term stability. Due to large disturbances and the involvement of slow response equipment, stability problems occurring during SPS reconfiguration were extended beyond the areas of dynamic and transient stability to long-term stability. Stability problems are generally classified into angle stability and voltage stability according to the nature of the stability problems. Due to the tight interconnection and the parallel operation of generators, strong synchronism or angle stability is maintained in SPS. In this dissertation, voltage stability during SPS reconfiguration was studied.

Four factors affecting voltage stability in SPS during reconfiguration/restoration were identified. These factors were loading condition, motor stalling, windup limit in voltage controllers, and interactions between loads and voltage controllers. Loads are transferred from one bus to another bus during SPS reconfiguration. Voltage stability limits could be violated if the load at a bus increases or the power factor of the load decreases. Induction motors are the predominant type of loads in SPS. An induction motor could

lose its stability when the mechanical torque is increased or the motor is exposed to low voltage for a long time. Motor instability may even induce system-wide voltage instability. Voltage stability is maintained by reactive power in power systems, which is mainly supplied by synchronous generators in SPS. When the windup limits of the voltage controllers are encountered, the inner voltage of the generators becomes constant. A part of reactive power is consumed by the inner reactance of generators. The reactive power supplied to SPS is reduced and the shortage of reactive power may thus cause voltage instability. In SPS, synchronous generators are installed with voltage controllers to control voltages within certain limits. When additional equipment is installed on a ship, the settings of voltage controllers may no longer be appropriate. This interaction between voltage controllers and loads may be harmful to the system and induce unstable oscillatory voltage in SPS. Considering static or dynamic effects on voltage stability, the four factors affecting voltage stability were analyzed in static or dynamic voltage stability.

A new static voltage stability index ($SVSI_{Lji}$) was deduced for static voltage stability analysis based on power flow concept in lines. If $SVSI_{Lji}$ is larger than zero and less than one, voltage stability is satisfied. If $SVSI_{Lji}$ is equal to one, voltage instability occurs. $SVSI_{Lji}$ indicates the voltage stability level of a line in a power system. If a $SVSI_{Lji}$ is closer to one, the corresponding line is operating closer to its stability boundary. The minimum $SVSI_{Lji}$ indicates the line operating closest to voltage instability. Compared with three existing indices [28]-[30] for a two-bus power system, $SVSI_{Lji}$ assessed voltage stability more accurately. $SVSI_{Lji}$ studies the existence of steady state of a power system. $SVSI_{Lji}$ is the stability index for each line connecting two buses in a power system. If at least one $SVSI_{Lji}$ exceeds one, voltage instability, more specifically voltage collapse, occurs. $SVSI_{Lji}$ was performed on the test SPS developed for stability studies. $SVSI_{Lji}$ was calculated for all cables in the test system. When all loads operated at their nominal values on either normal or alternate paths, the cable that was operating closest to stability boundary was identified. When the load connected to the cable was increased above 3.02 p.u., voltage instability occurred.

With the techniques of eigenvalue decomposition (ED) and singular value decomposition (SVD), a new dynamic voltage stability index (DVSI) was deduced for detecting local bifurcations, including saddle node and Hopf bifurcations, in dynamic systems. DVSI can analyze and assess voltage stability for dynamic voltage stability analysis. When DVSI is equal to zero, local bifurcations are detected and voltage instability occurs. A comparison of results of bifurcation detections for a small power system by DVSI and AUTO [35], a conventionally used bifurcation analysis software package, agreed with each other. Also DVSI was performed on the test system SPS. QSS (Quasi-Steady-State) and time domain simulations were used complementarily to determine the parameters required by DVSI. This combination improved the accuracy and speed of bifurcation detection. The voltage stability of a dynamic process, during which the mechanical load of one motor was increased gradually, was assessed by DVSI. Three different types of mechanical torque were modeled for the motor load and their effects on voltage stability were studied. Bifurcations were detected for constant and linear mechanical torques at mechanical load levels around 2.19 p.u. and 2.6 p.u., respectively. No bifurcation was detected for quadratic mechanical torque. The voltage stability of another dynamic process, during which system load level was increased, was also assessed by DVSI. Two types of bifurcations were detected. The first bifurcation was a Hopf bifurcation occurring at the system load level of 1.4. The second bifurcation was a saddle node bifurcation occurring at the system load level of 2.3.

7.2 CONCLUSIONS

Two new voltage stability indices $SVSI_{L_{ji}}$ and DVSI were discussed in this dissertation. $SVSI_{L_{ji}}$ is suitable for static voltage stability analysis and DVSI for dynamic voltage stability analysis. Compared with some existing indices on the line of a detailed two-bus system, $SVSI_{L_{ji}}$ is a better index for static voltage stability analysis. DVSI detects bifurcations in dynamic voltage stability analysis. Considering the singularity of a matrix at local bifurcations, DVSI can detect both saddle node bifurcation and Hopf bifurcation in dynamic systems.

Results of voltage stability assessment by $SVSI_{Lji}$ are conservative. This is because $SVSI_{Lji}$ is deduced from power flow formulations. In static voltage stability analysis, static component models are used. While in dynamic voltage stability analysis, dynamic component models are used. Since the dynamics of a system are not modeled in static analysis, voltage instability during a dynamic process can only be detected in dynamic analysis. A system can become unstable during a dynamic process before the system is developed to the point where instability is indicated in static analysis. Dynamic voltage stability analysis can thus be more accurate than static voltage stability analysis. In the static voltage stability analysis discussed in Chapter V, with the real power of a static load model increased to a certain level, voltage instability in the statically modeled test system was detected by $SVSI_{Lji}$. In the dynamic stability analysis discussed in Chapter VI, the instability occurring during the increase of that load in the dynamically modeled test system was analyzed by DVSI. Each type of mechanical torques for the load was studied. Voltage instability caused by the stalling of the motor load occurred during the dynamic process of increasing load L312 with constant or linear mechanical torque. The load levels where voltage instability, caused by motor stalling during the dynamic process of increasing the load, occurred in dynamic analysis were lower than the load level where voltage instability occurred in static analysis.

$SVSI_{Lji}$ and DVSI can be used together for stability assessment. Several reconfiguration operations are possible for a shipboard power system. The $SVSI_{Lji}$ value of each cable in the system is calculated for each possible reconfiguration operation first. The maximum $SVSI_{Lji}$ value of one reconfiguration operation is used to indicate the system stability level for the corresponding reconfiguration operation. All possible reconfiguration operations are ranked by sorting the maximum $SVSI_{Lji}$ values in ascending order. The smallest maximum $SVSI_{Lji}$ value indicates the operation with the highest stability level. DVSI then is calculated for the first reconfiguration operation to find whether there is any instability during the dynamic process of the reconfiguration. If there is not any instability, this operation is thus selected as the appropriate reconfiguration operation. If there is any instability during the dynamic process, the first

reconfiguration operation should not be selected. Alternatively, the second reconfiguration operation is assessed by DVSI. The same procedure of assessing stability by DVSI is applied on the ranked reconfiguration operations until a stable operation is found or until all ranked possible reconfiguration operations are assessed and the search is exhaustive.

Among the four factors discussed in Chapter III as affecting voltage stability for SPS reconfiguration, three factors were confirmed by the two new indices, $SVSI_{L,ji}$ and DVSI. The factor of windup limits in voltage controllers could not be confirmed. Windup limits could limit the reactive power supplied by generators. If the windup limit is reached, the stability limit is reduced and voltage instability can be induced. However, the mechanisms causing voltage instability after windup limits are reached are not well understood. Voltage instability caused by windup limits were thus not able to be created in time domain simulations for the test system. The effect of windup limits in voltage controllers on SPS voltage stability could not be justified.

7.3 FUTURE WORK

A new methodology was developed for modeling and simulating ungrounded stiffly connected power systems, such as shipboard power systems. For small-scale shipboard power systems, the simulation speed is fast and predictable. However, with large-scale shipboard power systems, such as the test system developed for stability studies, the simulation is slow. The modeling and simulation method were realized in Matlab/Simulink. In the future work, some advanced measures in Matlab/Simulink to enhance the speed of simulating dynamic systems, such as real time workshop, should be investigated. Proper measures could thus improve the speed of SPS simulation with the new modeling methodology.

A test shipboard power system was designed for stability studies. In Chapter IV, the mechanical torque of all induction motor loads was modeled as a quadratic function of motor speed. However, the type of induction motor loads in a real SPS varies. Mainly, there are three types of mechanical torques for induction motors in SPS. The three types

are constant, linear, and quadratic, which can have different effects on voltage stability. In future studies, the mechanical torque for each induction motor in the test SPS should be modeled according to its actual load type. For example, a steering gear in SPS should be modeled with constant mechanical torque.

In static voltage stability analysis, component models are static. Dynamic loads, or induction motors, were thus modeled by static models having constant power and a fixed power factor. For induction motors, the real power and power factor of an induction motor are not constant and change at different equilibrium points. The conservative assessment of voltage stability by $SVSI_{Lji}$ is partly due to the constant power models of induction motors. An induction motor at steady state can be represented by an equivalent circuit of constant impedance. The constant impedance in the equivalent circuit is based on the motor speed at steady state, which is different at different equilibrium points. A more accurate model for induction motors at steady state should thus be investigated for more accurate results of $SVSI_{Lji}$ in static voltage stability analysis.

REFERENCES

- [1] J. V. Amy Jr., “Composite System Stability Methods Applied to Advanced Shipboard Electric Power Systems”, Ph.D. dissertation, Massachusetts Institute of Technology, Cambridge, MA, 1992.
- [2] P. Kundur, *Power System Stability and Control*. New York, NY: McGraw-Hill, 1994.
- [3] H. Dommel, *Electromagnetic Transients Program Reference Manual (EMTP Theory Book)*. Portland, OR: Bonneville Power Administration, 1986.
- [4] Hydro-Quebec, TransEnergie, *SymPowerSystems for Use with Simulink*. Natick, MA: The Mathworks Inc, July 2002.
- [5] Mathworks Inc., *Simulink – Dynamic System Simulation for Matlab*. Natick, MA: The Mathworks Inc, Nov. 2000.
- [6] IEEE Power Engineering Society Power System Stability Subcommittee, *Voltage Stability Assessment: Concepts, Practices and Tools*. Piscataway, NJ: Aug. 2002.
- [7] M. A. Pai, *Power System Stability*. New York, NY: North-Holland Publishing Company, 1981.
- [8] M. A. Pai, *Energy Function Analysis for Power System Stability*. Boston, MA, Kluwer Academic Publishers, 1989.
- [9] D. R. Davidson, D. N. Ewart, and L. K. Kirchmayer, “Long-term Dynamic Response of Power Systems: An Analysis of Major Disturbances”, *IEEE Trans. on Power Systems*, vol. PAS-94, pp. 819-825, May/June 1975.
- [10] K. Hemmaplardh, J. N. Manke, W. R. Pauly and J. W. Lamont, “Consideration for a Long-term Dynamics Simulation Program”, *IEEE Trans. on Power Systems*, vol. 1, no. 1, pp.129-135, Feb. 1986.
- [11] R. D. Dunlop and D. N. Ewart, “Use of Digital Computer Simulations to Assess Long-term Power System Dynamic Response”, *IEEE Trans. on Power Systems*, vol. PAS-94, no. 3, pp. 850-857, May/Jun. 1975.

- [12] N. J. Balu and H. W. Mosteller, "Lotdys Analysis of August 1973 Gulf Coast Area Power System Disturbance", in *Proc. of 1979 Power Industry Computer Applications Conference*, Cleveland, OH, May 1979, pp. 365-373.
- [13] R. K. Varma, R. M. Mathur, G. J. Rogers, and P. Kundur, "Modeling Effects of System Frequency Variation in Long-Term Stability Studies", *IEEE Trans. on Power Systems*, vol. 11, no. 2, pp. 827-832, May 1986.
- [14] M. Stubbe, A. Bihain, J. Deuse, and J. C. Baader, "Stag – A New Unified Software Program for the Study of the Dynamic Behavior of Electrical Power Systems", *IEEE Trans. on Power Systems*, vol. 4, no. 1, pp. 129-138, Feb. 1989.
- [15] O. Fillatre, C. Evrard, D. Paschini, A. Bihain, K. Karoui, and J. P. Antoine, "A Powerful Tool For Dynamic Simulation of Unbalanced Phenomena", in *Proc. 1997 4th International Conference on Advances in Power System Control, Operation and Management*, Hong Kong, China, Nov. 1997, pp. 526-531.
- [16] J. L. Sancha, M. L. Llorens, B. Meyer, J. F. Vernotte, and W. W. Price, "Application of Long-term Simulation Programs for Analysis of System Islanding", *IEEE Trans. on Power Systems*, vol. 12, no. 1, pp. 189-197, Feb. 1997.
- [17] J. F. Vernotte, P. Panciatici, B. Meyer, J. P. Antoine, J. Deuse, and M. Stubbe, "High Fidelity Simulation of Power System Dynamics", *IEEE Computer Application in Power*, vol. 8, no. 1, pp. 37-41, Jan. 1995.
- [18] J. S. Mayer and O. Wasynczuk, "An Efficient Method of Simulating Stiffly Connected Power Systems With Stator and Network Transient Included", *IEEE Trans. on Power Systems*, vol. 6, no. 3, pp. 922-929, Aug. 1991.
- [19] J. G. Ciezki and R. W. Ashton, "The Resolution of Algebraic Loops in the Simulation of Finite-Inertia Power Systems", in *Proc. 1998 IEEE International Symposium on Circuits and Systems*, Monterey, CA, May 1998, pp. 342-345.
- [20] C. W. Taylor, *Power System Voltage Stability*. New York, NY: McGraw-Hill, 1994.

- [21] M. K. Pal, "Voltage Stability Conditions Considering Load Characteristics". *IEEE Trans. on Power Systems*, vol. 7, no. 1, pp. 243-249, Feb. 1992.
- [22] IEEE Task Force on Load Representation for Dynamic Performance, "Load Representation for Dynamic Performance Analysis", *IEEE Trans. on Power Systems*, vol. 8, no. 2, pp. 472-482, May 1993.
- [23] D. H. Popovic, I. A. Hiskens, and D. J. Hill, "Stability Analysis of Induction Motor Network", *International Journal of Electric Power and Energy Systems*, vol. 20, no. 7, pp. 475-487, 1998.
- [24] M. N. Gustafsson, N. U. Krantz, and J. E. Daalder, "Voltage Stability: Significance of Load Characteristics and Current Limiter", *IEE Proc. Generation Transmission and Distribution*, vol. 144, no. 3, pp. 257-262, May 1997.
- [25] M. A. Pai, P. W. Sauer, and B. C. Lesieutre, "Static and Dynamic Nonlinear Loads and Structural Stability in Power Systems", *Proceedings of the IEEE*, vol. 83, no. 11, pp.1562-1572, Nov.1995.
- [26] F. P. de Mello and J. W. Feltes, "Voltage Oscillatory Instability Caused By Induction Motor Loads", *IEEE Trans. on Power Systems*, vol. 11, no. 3, pp. 1279-1284, Aug. 1996,.
- [27] C. A. Canizares, "Conditions for Saddle Node Bifurcations in AC/DC Power Systems", *International Journal of Electrical Power and Energy Systems*, vol. 17, no. 1, pp 61-68, 1995.
- [28] A. Mohamed and G.B. Jasmon, "Voltage Contingency Selection Technique for Security Assessment", *IEE Proc. Generation, Transmission, and Distribution*, vol. 136, no. 1, pp. 24-28, Jan. 1989.
- [29] I. Musirin and T. K. A. Rahman, "Estimating Maximum Loadability for Weak Bus Identification Using FVSI", *IEEE Power Engineering Review*, vol. 22, no. 11, pp. 50-52, Nov. 2002.
- [30] G. Huang and L. Zhao, "Measurement based Voltage Stability Monitoring of Power Systems", Power Systems Engineering Research Center, University of

Wisconsin, Madison, WI, 2001. [Online] Available:

<http://www.pserc.wisc.edu/ecow/get/publicatio/2001public/indicator.pdf>

- [31] G. B. Jasmon and L. Lee, "Distribution Network Reduction for Voltage Stability Analysis and Load Flow Calculation", *International Journal of Electrical Power and Energy Systems*, vol. 13, no. 1, pp 9-13, 1991.
- [32] F. Gubina and B. Strmcnik, "A Simple Approach to Voltage Stability Assessment in Radial Network", *IEEE Trans. on Power Systems*, vol. 12, no. 3, pp. 1121-1128, 1997.
- [33] J. Barquin, T. Gomez and E. L. Pagola, "Estimating The Loading Limit Margin Taking Into Account Voltage Collapse Areas", *IEEE Trans on Power Systems*, vol. 10, no. 4, pp. 1952-1962, Nov. 1995.
- [34] C. A., Canizares and F. L Alvarado, *UWPFLOW Continuation and Direct Methods to Locate Fold Bifurcation in AC/DC/FACTS Power Systems*. Waterloo, ON: University of Waterloo, 1999.
- [35] E. J. Doedel, R. C. Paffenroth, A. R. Champneys, T. F. Fairgrieve, Y. A. Kuznetsov, B. Sandstede, and X. J. Wang, *AUTO 2000: Continuation and Bifurcation Software For Nonlinear Differential Equations (with HomCont)*. Pasadena, CA: California Institute of Technology, 2001.
- [36] H. O. Wang, E. H. Abed, and A. M. A. Hamdan, "Bifurcations, Chaos, and Crises in Voltage Collapse of a Model Power System", *IEEE Trans. on Circuits and Systems*, vol. 41, no. 3, pp. 294-302, Mar. 1994.
- [37] H. B. Ross, N. Zhu, J. Giri, and B. Kindel, "An AGC Implementation for System Islanding and Restoration Conditions", *IEEE Trans. on Power Systems*, vol. 9, no. 3, pp.1399-1410, Aug. 1994.
- [38] C. Concordia, L.H. Fink, and G Poullikkas, "Load Shedding on an Isolated System", *IEEE Trans. on Power Systems*, vol. 10, no. 3, pp. 1467-1472, Aug. 1995.

- [39] J. O'Sullivan, M. Power, M. Flynn, and M. O'Malley, "Modeling of Frequency Control in an Island System", in *Proc. 1999 IEEE Power Engineering Society Winter Meeting*, New York, NY, Jan 1999, pp. 574-579.
- [40] G. N. Kariniotakis, and G. S. Stavrakakis, "A General Simulation Algorithm for the Accurate Assessment of Isolated Diesel-wind Turbines Systems Interaction. Part I. A General Multimachine Power System Model", *IEEE Trans. on Energy Conversion*, vol. 10, no. 3, pp. 584-590, Sep. 1995.
- [41] C. Sharma, "Modeling of an Island Grid", *IEEE Trans. on Power Systems*, vol. 13, no. 3, pp. 971-978, Aug. 1998.
- [42] N. R. Fahmi and R. C. Johnson, "Phase Co-ordinate Model for Analysis of Isolated Power Systems", *IEE Proc. Generation Transmission Distribution*, vol. 140, no. 2, pp.123-130, Mar. 1993.
- [43] P. Murray, J. J. Graham, and C. L. Halsall, "Modeling Strategy for Isolated Power Systems Employing Synchronous Motor Drives", in *Proc. 1997 4th conference on Advances in Power System Control, Operation and Management*, Hong Kong, China, Nov. 1997, pp. 354-359.
- [44] A. Adediran, H. Xiao, and K. L. Butler-Purry, "The Modeling and Simulation of a Shipboard Power System in APT", in *Proc. 2003 International Conference on Power System Transients*, New Orleans, LA, Sep. 2003, pp. 15/1-15/6.
- [45] Naval Sea Systems Command, Engineering Directorate, Electrical Engineering Group, "NAVSEA design practice and criteria manual for electrical systems for surface ships, Chapter 300", NAVSEA T9300-AF-PRO-020, Naval Sea Systems Command, Arlington, VA, Dec. 1992.
- [46] C. R. Petry and J.W. Rumberg, "Zonal Electrical Distribution Systems: an Affordable Architecture for the Future", *Naval Engineers Journal*, pp. 45-51, May 1993.
- [47] J. G. Ciezki and R. W. Ashton, "A Technology Overview for A Proposed Navy Surface Combatant DC Zonal Electric Distribution System", *Naval Engineers Journal*, pp. 59-69, May 1999.

- [48] K. L. Butler, N.D. R. Sarma, C. Whitcomb, H. D. Carmo, and H. Zhang, "Shipboard Systems Deploy Automated Protection", *IEEE Computer Application on Power System*, pp. 31-36, April 1998.
- [49] "Engineering Systems 3 Study Guide: USS Thorn (DD 988)", Jan. 1994. (Personal Collection, K. L. Butler-Purry)
- [50] T. Ericson and A. Tucker, "Power Electronics Building Blocks and Potential Power Modulator Application", in *Proc. 1998 Power Modulator Symposium*, Rancho Mirage, CA, Jun. 1998, pp. 12-15.
- [51] P. W. Sauer, and M. A. Pai, *Power System Dynamics and Stability*. Upper Saddle River, NJ: Prentice Hall, 1998.
- [52] "Military Specification: Frequency Changer, Solid State (Naval Shipboard)", MIL-F-24122C (SH), Aug. 1990. (Personal Collection, K. L. Butler-Purry)
- [53] T. A. Lipo, D. M. Divan, W. E. Brumsickle, A. L. Julian, and B. H. Kenny, "Considerations for PEBB-based Systems and Medium-Power PEBB Applications", Navy PEBB Project Report. [Online]. Available: http://www.ece.umn.edu/links/power/Energy_Course/energy/Pow_electronics/pebb/wis01.html [Accessed Oct. 2004]
- [54] Central Station Engineers of the Westinghouse Electric Corporation, *Electrical Transmission and Distribution Reference Book*. East Pittsburgh, PA: Westinghouse Electric Corporation, 1964.
- [55] IEEE Subsynchronous Resonance Working Group of the System Dynamic Performance Subcommittee, "Reader's Guide to Subsynchronous Resonance", *IEEE Trans. on Power Systems*, vol. 7, no. 1, pp.150-157, Feb. 1992.
- [56] K. R. Padiyar, *Analysis of Subsynchronous Resonance in Power System*. Boston, MA: Kluwer Academic Publishers, 1999.
- [57] P. W. Sauer and M. A. Pai, *Power System Dynamics and Stability*, Upper Saddle River, NJ, Prentice Hall, 1998.

- [58] P. M. Anderson and B. L. Agrawal, *Subsynchronous Resonance in Power Systems*. New York, NY: IEEE Press, 1990.
- [59] G. Gates, D. Shipp, and W. Vilcheck, "Electrical Distribution System Analysis for Off-shore Oil Production Facilities", in *Proc. 1998 Petroleum and Chemical Industry Conference*, Indianapolis, IN, Sep. 1998, pp.129-137.
- [60] R. Billinton and R. Karki, "Capacity Planning in Small Isolated Power Systems Using Probabilistic Methods", *IEE Proc. Generation Transmission Distribution*, vol. 146, no. 1, pp. 61-64, Jan 1999.
- [61] S. B. Griscom, W. A. Lewis, and W. R. Ellis, "Generalized Stability Solution for Metropolitan Type Systems", *Trans. American Institute of Electrical Engineering*, pp. 363-374, June 1932.
- [62] T. McCoy, "Dynamic Simulation of Shipboard Electric Power Systems", M.S. thesis, Massachusetts Institute of Technology, Cambridge, MA, 1993.
- [63] C. D. Vournas and G. A. Manos, "Modeling of Stalling Motors During Voltage Stability Studies", *IEEE Trans. on Power Systems*, vol. 13, no. 3, pp. 775-781, Aug. 1998.
- [64] Y. Sekine and H. Ohtsuki, "Cascaded Voltage Collapse", *IEEE Trans. on Power Systems*, vol. 5, no. 1, pp. 250-256, Feb. 1990.
- [65] E. W. Kimbark, *Power System Stability, Vol. 1, Elements of Stability Calculations*. New York, NY: John Wiley & Sons Inc., 1948.
- [66] L. Dreller, "The Fundamental of Parallel Operation of Direct and Alternating Current Generators", *Journal of the American Society of Naval Engineers*, vol. 49, no. 3, pp. 273-306, Aug. 1937.
- [67] V. Venkatasubramanian, H. Schattler, J. Zaborszky, "Analysis of Local Bifurcation Mechanisms in Large Differential-Algebraic Systems such as the Power System", in *Proc. 1993 32nd Conference on Decision and Control*, San Antonio, TX, Dec. 1993, pp. 3727-3733.
- [68] F. Colonius and L. Grüne, *Dynamics, Bifurcations, and Control*. New York, NY: Springer-Verlag Inc., 2002.

- [69] P. A. Lof, T. Smed, G. Anderson, D. J. Hill, "Fast Calculation of a Voltage Stability Index", *IEEE Trans. on Power Systems*, vol. 7, no. 1, pp. 54-64, Feb. 1992.
- [70] P. M. Anderson and A. A. Fouad, *Power System Control and Stability*. Piscataway NJ: IEEE Press, 1993.
- [71] V. Venkatasubramanian, H. Schattler, and J. Zaborszky, "Voltage Dynamics: Study of a Generator with Voltage Control, Transmission, and Matched MW Load," *IEEE Trans. Automatic Control*, vol. 37, no. 11, pp. 1717-1733, Nov. 1992.
- [72] P. C. Krause, *Analysis of Electric Machine*. New York, NY: McGraw-Hill, 1986.
- [73] L. Qi and K. L. Butler-Purry, "Reformulated Model Based Modeling and Simulation of Ungrounded Stiffly Connected Power Systems", in *Proc. 2003 IEEE Power Engineering Society General Meeting*, Toronto, ON, Canada, July 2003, pp 725-730.
- [74] L. Qi and K. L. Butler-Purry, "A New Modeling Strategy for Finite Inertia Power Systems based on Reformulated Reference Generator Model," in *Proc. 2002 34th Annual North American Power Symposium*, Tempe, AZ, Oct. 2002, pp. 280-287.
- [75] "Design Data Sheet, Fault Current Calculations and Protective Device Coordinations for 60 and 400 Hz Power Systems Supplied by Rotating Machinery DDS 300-2", Naval Sea Systems Command, Washington Navy Yards, Washington, DC, May 1995.
- [76] "Military Specification: Circuit Breakers, Low Voltage, Electric Power, Air, Open Frame, Removable Construction", MIL-C-17587B (SH), April 1983. (Personal Collection, K. L. Butler-Purry)
- [77] G. A. Manos and C. D. Vournas, "Bifurcation Analysis of a Generator-Motor System", in *Proc. 1996 4th IEEE Mediterranean Symposium on New Directions in Control and Automation*, Maleme, Krete, Greece, Jun. 1996, pp. 250-255.

APPENDIX A

PARAMETERS OF A REDUCED SPS

A reduced shipboard power system shown as Figure 4.7 consists of generators, voltage controllers, governor with gas turbine, induction motors, static loads, cables, and linear transformers. The parameters of each type of component are shown as follows.

Table A.1 Synchronous Generator Parameters

Parameters	r_s (p.u.)	r_{kq}' (p.u.)	r_{fd}' (p.u.)	r_{kd}' (p.u.)	I_s (p.u.)	I_{lkq}' (p.u.)
Value	0.00515	0.0613	0.0011	0.02397	0.08	0.3298
Parameters	I_{fd}' (p.u.)	I_{kd}' (p.u.)	I_{mq} (p.u.)	I_{md} (p.u.)	H (s)	--
Value	0.13683	0.33383	1.0	1.768	2.137	--

Table A.2 Parameters for IEEE Type II Voltage Controller

Parameters	K_A	T_A	W_{RMAX}	V_{RMIN}	K_F	T_{F1}
Value	400	0.01	8.4	0	0.01	0.15
Parameters	T_{F2}	K_E	T_E	A	B	T_R
Value	0.06	1	0.1	0.1	0.3	0

Table A.3 Parameters for Governor with Gas Turbine

Parameters	K_C	T_C	T_{FV}	T_{FT}	W_{F10S}
Value	22.5	0.55	0.01	0.05	0.23
Parameters	C_{2GT}	C_{1GT}	C_{GNGT}	W_{MAX}	--
Value	0.251	1.3523	0.5	1.0	--

Table A.4 Parameters for Induction Motors

Parameters	P_{base} (KW)	V_{base} (KV)	r_s (p.u.)	I_{is} (p.u.)
Value	192.6	0.44	0.0198	0.06
Parameters	I_m (p.u.)	r_r' (p.u.)	I_{lr}' (p.u.)	H (s)
Value	2.7963	0.0531	0.0529	0.98

Table A.5 Parameters for Static Loads

Load Name	Parameters	Value	Unit
SL1	R _{aa} ,R _{bb} ,R _{cc}	10,10,10	Per unit
SL3	R _{aa} ,R _{bb} ,R _{cc}	8,8,8	Per unit
	L _{aa} ,L _{bb} ,L _{cc}	6,6,6	Per unit
SL5	R _{aa} ,R _{bb} ,R _{cc}	10,20,10	Per unit

Table A.6 Parameters for Cables

Parameters	Value (p.u.)
R _{aa} ,R _{bb} ,R _{cc}	0.0205
R _{aa} ,R _{bb} ,R _{cc}	0.005478
L _{aa} ,L _{bb} ,L _{cc}	0.169
L _{aa} ,L _{bb} ,L _{cc}	0.1607

Table A.7 Parameters for Linear Transformers

Parameters	N (KV/KV)	R₁ (p.u.)	L₁ (p.u.)	R₂ (p.u.)
Value	0.45/0.115	0.3477	0.002478	0.024691
Parameters	L₂ (p.u.)	R_m (p.u.)	L_m (p.u.)	--
Value	1.25.	6380.81	24.91	--

APPENDIX B

PARAMETERS AND MODELS OF A TWO-GENERATOR-ONE-MOTOR POWER SYSTEM

A two-generator-one-motor power system shown as Figure 6.1 consists of generators, voltage controllers, motors and lines. The parameters of each type of component are shown in the tables of section B.1. The mathematical representations of the component models are shown in section B.2.

B.1 PARAMETERS

Table B.1 Generator Parameters

Parameters	x_d (p.u.)	x_q (p.u.)	x_d' (p.u.)	T_{d0}' (s)
Value	0.8958	0.8645	0.1198	6

Table B.2 Line Parameters

Parameters	X_e (p.u.)
Value	0.1

Table B.3 AVR Parameters

Parameters	K_E (p.u.)	T_E (p.u.)
Value	30	0.5

Table B.4 Induction Motor Parameters

Parameters	X_{1m} (p.u.)	R_{1m}, R_{2m} (p.u.)	X_{2m} (p.u.)	X_m (s)	H (s)
Value	0.8958	0.8645	0.1198	6	1.5

B.2 MATHEMATICAL MODELS

Generators G1 and G2 in the two-generator-one-motor system were modeled as a set of differential equations as (B.1)-(B.8).

$$T_{d01} \frac{dE'_{q1}}{dt} = \frac{x_{d1} - x'_{d1}}{x_{d1}} V_1 \cos(\delta_1 - \theta_1) + E_{fd1} - \frac{x_{d1}}{x'_{d1}} E'_{q1} \quad (\text{B.1})$$

$$T_{A1} \frac{dE_{fd1}}{dt} = -E_{fd1} - K_{A1} (V_1 - V_{ref1}) \quad (\text{B.2})$$

$$2H_1 \frac{d\omega_1}{dt} = P_{GM1} - \frac{V_1}{x_{d1}} E'_{q1} \sin(\delta_1 - \theta_1) \quad (\text{B.3})$$

$$\frac{d\delta_1}{dt} = (\omega_1 - 1)\omega_0 \quad (\text{B.4})$$

$$T_{d02} \frac{dE'_{q2}}{dt} = \frac{x_{d2} - x'_{d2}}{x_{d2}} V_2 \cos(\delta_2 - \theta_2) + E_{fd2} - \frac{x_{d2}}{x'_{d2}} E'_{q2} \quad (\text{B.5})$$

$$T_{A2} \frac{dE_{fd2}}{dt} = -E_{fd2} - K_{A2} (V_2 - V_{ref2}) \quad (\text{B.6})$$

$$2H_2 \frac{d\omega_2}{dt} = P_{GM2} - \frac{V_2}{x_{d2}} E'_{q2} \sin(\delta_2 - \theta_2) \quad (\text{B.7})$$

$$\frac{d\delta_2}{dt} = (\omega_2 - 1)\omega_0 \quad (\text{B.8})$$

where E'_q is the generator voltage on q axis. T_{d0} is transient time constant on d axis. x_d is reactance on d axis. x'_d is transient reactance on d axis. V is the voltage magnitude on a bus. E_{fd} is the excitation field voltage. T_A is the time constant of exciter. K_A is the gain of exciter. P_{GM1} is the mechanical power from prime mover. H is the generator inertia. ω is the rotor angular speed. ω_0 is the system base angular speed. δ is the rotor angle. θ is the angle of voltage on a bus. The subscripts 1 and 2 of the generator variables represent variables associated with generator G1 and generator G2. The subscripts 1, 2, or 3 of variable V denote variables associated with bus 1, 2 or 3. Induction motor M in the system were modeled as a differential equation as (B.9).

$$\frac{ds_m}{dt} = K(1 - s_m)^2 - T_m \quad (\text{B.9})$$

Where s_m is the motor slip. T_m is the mechanical torque. K is the mechanical load level of the motor.

The algebraic equations at bus 1 are shown as (B.10) and (B.11)

$$\frac{V_1}{x_d} E'_{q1} \sin(\delta_1 - \theta_1) - V_1 V_2 b_{12} \sin \theta_{12} - V_1 V_3 b_{13} \sin \theta_{13} = 0 \quad (\text{B.10})$$

$$\frac{V_1}{x_d} (E'_{q1} \cos(\delta_1 - \theta_1) - V_1) + V_1^2 b_{11} + V_1 V_2 b_{12} \cos \theta_{12} + V_1 V_3 b_{13} \cos \theta_{13} = 0 \quad (\text{B.11})$$

The algebraic equations at bus 2 are shown as (B.12) and (B.13).

$$\frac{V_2}{x_d} E'_{q2} \sin(\delta_2 - \theta_2) - V_2 V_1 b_{21} \sin \theta_{21} - V_2 V_3 b_{23} \sin \theta_{23} = 0 \quad (\text{B.12})$$

$$\frac{V_2}{x_d} (E'_{q2} \cos(\delta_2 - \theta_2) - V_2) + V_2^2 b_{22} + V_2 V_1 b_{21} \cos \theta_{21} + V_2 V_3 b_{23} \cos \theta_{23} = 0 \quad (\text{B.13})$$

where b is the susceptance of a line between two buses. The subscripts of b denote the number of the two buses. The algebraic equations at bus 3 are shown as (B.14) and (B.15).

$$-\frac{R_{2m} / s_m}{(R_{1m} + R_{2m} / s_m)^2 + (X_{1m} + X_{2m})^2} V_3^2 - V_1 V_2 b_{12} \sin \theta_{12} - V_1 V_3 b_{13} \sin \theta_{13} = 0 \quad (\text{B.14})$$

$$-\frac{X_{1m} + X_{2m}}{(R_{1m} + R_{2m} / s_m)^2 + (X_{1m} + X_{2m})^2} V_3^2 + V_1^2 b_{11} + V_1 V_2 b_{12} \cos \theta_{12} + V_1 V_3 b_{13} \cos \theta_{13} = 0 \quad (\text{B.15})$$

where R_m and X_m are resistance and reactance of a motor. The subscripts 1 and 2 represent the variables associated with the stator and rotor of the motor.

VITA

Li Qi was born in Xi'an, People's Republic of China. She received a Bachelor of Engineering degree in electrical engineering in 1994 from Xi'an Jiaotong University in China. She received a Master of Science degree in electrical engineering in 1997 from Zhejiang University, China. She received her Ph.D. degree in electrical engineering at Texas A&M University in December 2004. She was a research assistant in the Power System Automation Laboratory at Texas A&M University.

She is a student member of IEEE. She was the President of IEEE-PES-IAS-PELS, joint student chapter at Texas A&M University from the fall of 1999 through the spring of 2000 and the Vice-President from the fall of 2000 through the spring of 2001. She can be contacted at eeql@hotmail.com. Her permanent address is 2-34-515, Xian Jiaotong University, Xi'an, 710049, People's Republic of China.